JAERI-M
90-154

A REVIEW OF JAERI R&D ACTIVITIES ON THE NEGATIVE-ION-BASED NEUTRAL BEAM INJECTION SYSTEM

August 1990

Yoshihiro OHARA, Masato AKIBA, Masanori ARAKI
Masayuki DAIRAKU, Masaya HANADA, Takashi INOUE
Hiroaki KOJIMA*, Masaaki KURIYAMA, Yasuhiro MATSUDA**
Mamoru MATSUOKA, Makoto MIZUNO, Yoshikazu OKUMURA
Masahiro SEKI, Shigeru TANAKA, Kazuhiro WATANABE
and Kenji YOKOYAMA

日本原子力研究所
Japan Atomic Energy Research Institute

JAERI-Mレポートは，日本原子力研究所が不定期に公刊している研究報告書です。
入手の問合わせは，日本原子力研究所技術情報部情報資料課（〒319-11茨城県那珂郡東海村）あて，お申しこしください。なお，このほかに財団法人原子力弘済会資料センター（〒319-11 茨城県那珂郡東海村日本原子力研究所内）で複写による実費頒布をおこなっております。

JAERI-M reports are issued irregularly.
Inquiries about availability of the reports should be addressed to Information Division Department of Technical Information, Japan Atomic Energy Research Institute, Tokai-mura, Naka-gun, Ibaraki-ken 319-11, Japan.

編集兼発行　日本原子力研究所
印　　刷　いばらき印刷㈱

JAERI-M 90-154

A Review of JAERI R&D Activities on the Negative-Ion-Based Neutral Beam Injection System

Yoshihiro OHARA, Masato AKIBA, Masanori ARAKI, Masayuki DAIRAKU
Masaya HANADA, Takashi INOUE, Hiroaki KOJIMA*, Masaaki KURIYAMA+
Yasuhiro MATSUDA**, Mamoru MATSUOKA+, Makoto MIZUNO+, Yoshikazu OKUMURA
Masahiro SEKI, Shigeru TANAKA, Kazuhiro WATANABE and Kenji YOKOYAMA

Department of Thermonuclear Fusion Research
Naka Fusion Research Establishment
Japan Atomic Energy Research Institute
Naka-machi, Naka-gun, Ibaraki-ken

(Received August 14, 1990)

R&D efforts to realize a negative-ion-based neutral beam injection system have been made intensively at JAERI for the past several years. Concerning a high current negative ion source which is one of the most important R&D items, a 10 A, 50 keV negative hydrogen ion beam has been produced successfully. The negative ion beam current and the current density correspond already to the value required for the negative-ion-based NBI system. In order to increase the beam energy further, a 350 keV, 0.1 A test stand has been constructed, and the test of a high energy negative ion accelerator has started.

Concerning a high energy acceleration power supply, an inverter type power supply which has a high speed AC switch was proposed and applied to the 100 kV, 5 A power supply for JAERI Electron Beam Irradiation Stand. The reliable operation indicates that the concept of this system can be applied for a MV class acceleration power supply. As one of the promising candidates for a beam dump cooling element, an externally-finned

---

+ Department of JT-60 Facility

* Hitachi Ltd.

** Nissin Electric Co. Ltd.

swirl tube was proposed and tested to have a high burnout heat flux of 4.1kW/cm^2, which is high enough for the next NBI system.

The R&Ds on the negative-ion-based NBI system have made great progress at JAERI in recent years. The construction of a 500 keV class NBI system has become realistic from the engineering point of view.

Keywords: Negative Ion Beam, Neutral Beam Injection System, R&Ds, Negative Ion Source, High Current, Negative Hydrogen, Accelerator, Acceleration Power Supply, Inverter, Beam Dump Cooling Element, Burnout

原研における負イオンを用いた中性粒子入射装置に関するR＆Dの概要

日本原子力研究所那珂研究所核融合研究部
小原　祥裕・秋場　真人・荒木　政則・大楽　正幸
花田磨砂也・井上多加志・小島　啓明*・栗山　正明+
松田　恭博**・松岡　　守+・水野　　誠+・奥村　義和
関　　昌弘・田中　　茂・渡辺　和弘・横山　堅二

（1990年8月14日受理）

過去数年にわたり，負イオンを用いた中性粒子入射装置を実現するための研究開発を強力に実施してきた。特に，最も重要な開発項目である大電流負イオン源に関しては，50 keVで10 Aの水素負イオンを生成することに成功した。得られた負イオンビーム電流及び電流密度は，すでに負イオンNBIシステムで必要とされる値に達している。ビームエネルギーをさらに増大するために，350 keV，0.1 Aのテストスタンドを建設し，高エネルギー負イオン加速器の試験を開始した。

高エネルギー加速電源に関しては，インバータに基づいた高速交流スイッチング方式を提案し，電子ビーム照射装置用の100 kV，5 A加速電源として実用化した。この開発により，次期装置用に必要とされるMV級加速電源に本方式を適用できる可能性を示した。一方，高熱流束ビームに晒されるビームダンプの冷却エレメントとして，外部フィン付スワールチューブを提案しその試験を行った。その結果，4.1 kW/cm^{2}という高いバーンアウト熱流束が得られ，ビームダンプ用に使用できることを示した。

以上のように，負イオンを用いた中性粒子入射装置に関するR＆Dはここ数年で大きな進歩を遂げた。現在，500 keV級NBIシステムの建設は技術的に可能となりつつある。

那珂研究所：〒311－01　茨城県那珂郡那珂町大字向山801－1
＋ JT－60試験部
＊（株）日立製作所
＊＊ 日新電機（株）

CONTENTS

目　　次

1. INTRODUCTION

A high energy NBI system which can deliver a 1 MeV class neutral deuterium beams is considered to be the primary heating and current drive system for the next fusion machine, and expected to play an important role to obtain a steady-state burning plasma. In order to achieve a high neutralization efficiency at this high energy region, negative ion beams must be utilized instead of the positive ion beams which are used in the present NBI systems. However, it is not easy to develop a high current negative ion source, on which much efforts have been concentrated in many laboratories so far[1,2,3].

We have started to develop a high current negative ion source in 1984, just after having finished the developmental work of the JT-60 NBI system based on the positive ion beams. Since then, the negative ion beam power has been increased step by step using the volume production type ion sources [4]. In our recent experiments using a newly-designed multi-ampere negative ion source, a world record on the negative ion production has been established successfully, namely, a hydrogen ion beam of 50keV, 10A, 0.1s was produced [5]. This negative ion current is close to the value required for the next NBI systems. However, the beam energy is still low compared to the value required for the next NBI systems. Therefore, we are concentrating our efforts on high energy negative ion acceleration, using a 350 keV, 0.1 A test stand.

In parallel to the development of the negative ion source, we are developing intensively a high voltage acceleration power supply system and beamline components such as an ion beam dump. A new concept of the acceleration power supply system, namely, an inverter type DC power supply which has an AC switch instead of a conventional DC switch, has been successfully demonstrated at an electron beam irradiation test stand constructed in 1989 [6]. Concerning a beam dump exposed to a high heat flux beam, an externally-finned swirl tube has been tested and turned out to be able to handle a heat flux up to 4.1 kW/cm^2[7].

Due to these recent progresses on the negative ion sources and related technologies, we are now in a position to construct a 500 keV class negative-ion-based NBI system. In the present paper, R&D results on the negative-ion-based NBI system obtained at JAERI for the past few years are reviewed.

References

1. K.N. Leung, K.W. Ehlers, and R.V. Pyle ; Rev. Sci. Instrum. 56(3), pp.364-368, March 1985.
2. A.J.T. Holmes ; Proc. of the Int. Conf. on Ion Sources, Berkeley, June 10-14 (1989) pp.389-391.
3. Y. Okumura, et al.; IAEA Technical Committee Meeting on Negative Ion Beam Heating, Culham Lab. July 15-17 (1987).
4. M. Bacal and G.W. Hamilton ; Phys. Rev. Lett. 42, 1538 (1979).
5. H. Kojima, M. Hanada, T. Inoue, Y. Matsuda, Y. Ohara, Y. Okumura, H. Oohara, M. Seki, and K. Watanabe ; Proc. of the 13th Symp. on Ion Sources and Ion-Assisted Technology, Tokyo, June 4-6, pp.145-148 (1990).
6. M. Mizuno, M. Dairaku, Y. Ohara, A. Ozaki, S. Tanaka, T. Uede, K. Watanabe, Y. Yamashita, and K. Yokoyama ; Proc. of the 13th Symp. on Fusion Engineering, Knoxville, Oct.2-6 (1989)pp.574-577.
7. M. Araki, M. Dairaku, T. Inoue, M. Komata, M. Kuriyama, S. Matsuda, M. Ogawa, Y. Ohara, M. Seki, and K. Yokoyama ; Fusion Engineering and Design 9, 231-236 (1989).

2. R&D STRATEGY

2.1 R&D Steps of Negative Ion Beams

We have three programs about the negative-ion-based neutral beam injectors. The first program is to develop a 500 keV deuterium beam injection system for the JT-60 Upgrade tokamak (JT-60U). In the JT-60U High Performance Experiment (3) starting in 1993, a high density current drive experiment using a negative-ion-based NBI system is planned [1]. In this experiment, deuterium neutral beams of 500 keV, 10 MW are injected tangentially with two beamlines [2].

The second program is to develop a 1 MeV class NBI system for the Fusion Experimental Reactor in Japan (FER) and/or the International Thermonuclear Experimental Reactor (ITER), which will be built at the beginning of the next century. This NBI system is considered to be the primary current drive and heating system and is required to deliver a 50 - 75 MW neutral deuterium beam at 0.5 - 1.3 MeV to sustain a long pulse D-T burning plasma.

The third program is to develop a 2 MeV class NBI system for the Steady State Tokamak Reactor (SSTR) which is expected to be constructed around 2020. The SSTR originally proposed by Kikuchi at JAERI makes use of both the bootstrap current and the beam driven plasma current to demonstrate a steady state electrical power generation of 1,000 MW [3]. This NBI system is required to inject a 80 MW neutral deuterium beam with a total power efficiency higher than 50 %.

The major specifications of the above three NBI systems are shown in Table 2.1-1. The long range R&D strategy depends on the above three programs. In the first step, a 500keV NBI system will be developed for JT-60U. In the second step, a 1MeV class test facility will be constructed to develop the NBI system for ITER/FER. The physics and technology data base obtained in the first step will be helpful and utilized in the design of the 1MeV NBI system. In the third step, aggressive technologies such as a plasma neutralizer will be developed and applied for the 2MeV class NBI system with high system efficiency. The R&D steps are illustrated in Fig.2.1-1.

Besides the above three programs, we are interested in developing a 2-5 MeV lithium or oxygen beam injection system for measuring the ion temperature and the plasma current profile in a burning plasma [4]. The specifications of this system are also indicated in Table 2.1-1.

References

1. JT-60 Team presented by H. Kishimoto ; Proceedings of the 12th Int. Conf. on Plasma Physics and Controlled Nuclear Fusion Research, Nice, Oct.12-19 (1988) IAEA-CN-50/A-I-4.
2. Y. Ohara, et al.; Proc. of the 13th Symp. on Fusion Engineering, Knoxville, Oct.2-6 (1989)pp.284-287.
3. M. Kikuchi ; Nuclear Fusion, 30, 265-276 (1990).
4. Y. Kusama, K. Tobita, Y. Ohara, Y. Okumura, M. Nemoto, H. Kimura, H. Takeuchi and JT-60 Team : IAEA Technical Committee Meeting on Alpha Particle Confinement and Heating, Kiev, Oct.23-26 (1989).

Table 2.1-1 R&D Steps for Negative-Ion-Based NBI Systems at JAERI

	HEATING AND CURRENT DRIVE			DIAGNOSTICS
	1st STEP	2nd STEP	FINAL TARGET	
TARGET MACHINE	JT-60 U	FER / ITER	SSTR	JT-60 U
TO BE OPERATIONAL	1994	2005	2020	1996
BEAM SPECIES	D^- / H^-	D^- / H^-	D^-	Li^- / O^-
INJECTION POWER	10 MW	50 / 75 MW	80 MW	20 mA
BEAM ENERGY	500 keV	0.5 - 1.3 MeV	2 MeV	2 - 5 MeV
PULSE DURATION	10 s	1000 s / 2 weeks	CW	CW
INJECTION PORT	2	2 / 3	2	1
BEAMLINES / PORT	1	3	1	1
SOURCES / BEAMLINE	2	1	10	1
BEAM CURRENT / SOURCE	12 A	18 A	3.5 A	100 mA
SOURCE TYPE	Volume-Surface	Volume-Surface	Volume-Surface	Volume
ACCELERATOR TYPE	ES 3-stages	ES or ESQ 6-stages	ES or ESQ 10-stages	ES Cockcroft
NEUTRALIZER TYPE	Gas Neutralization D_2	Gas Neutralization D_2	Plasma Neutralization	Gas Neutralization H_2
TOTAL POWER EFFICIENCY	30 %	40 %	50 % <	—
Footnotes Q-Values	0.1	20	40	

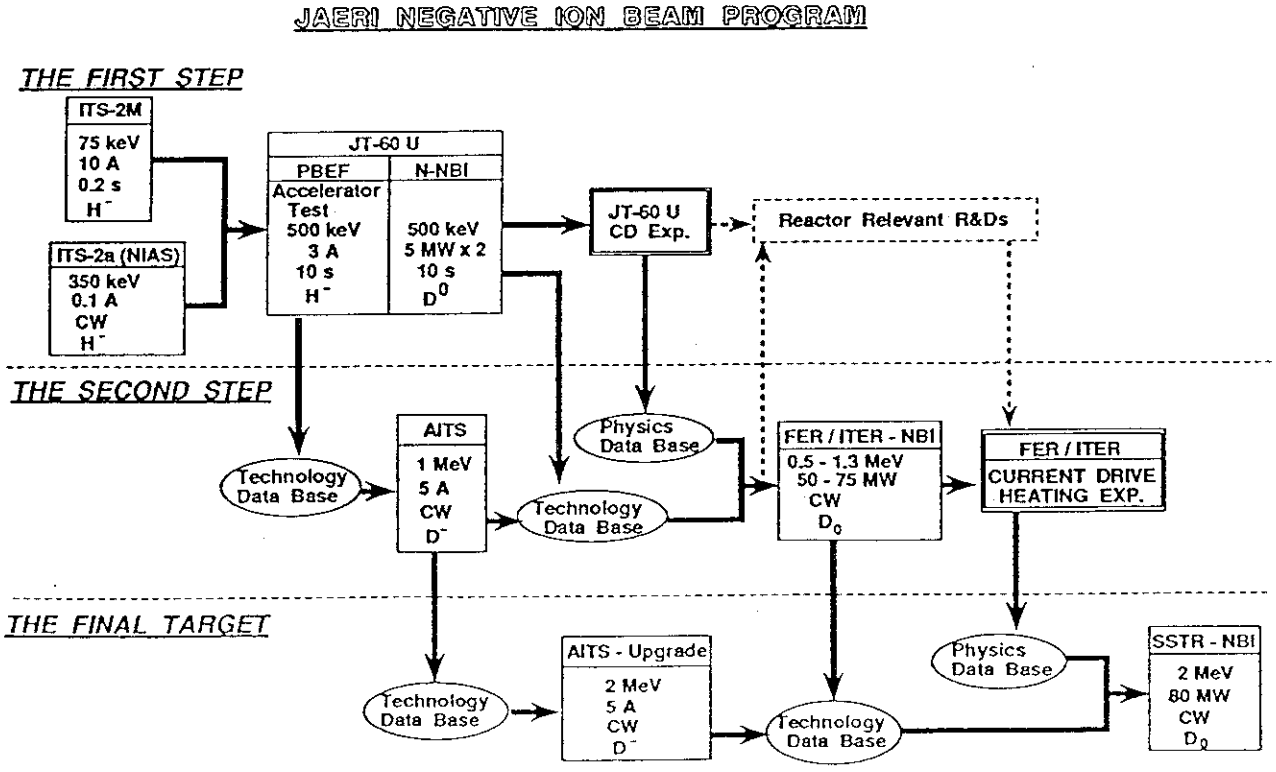

Fig. 2.1-1 A strategy of the development of negative-ion-based NBI systems

2.2 R&D Items and the Goals

There are four major components to be developed for the negative-ion-based NBI system;

1. Ion Source
2. Accelerator
3. High Voltage DC Power Supply
4. Beamline Components

Among these, the most important component is an ion source and accelerator which can produce a multi-ampere convergent negative ion beam at the beam energy of several hundred kiloelectron volts per nucleon. However, we cannot realize a negative-ion-based NBI system even if the ion source and accelerator should be developed. A reliable high voltage power supply and high performance beamline components are indispensable for a reliable NBI system. In order to make clear the R&D items and R&D target values, we have initially proposed a new concept of the negative-ion-based NBI system for the Fusion Experimental Reactor in 1987. Since then, all these conponents are being developed self-consistently in our laboratory. Described below are the R&D items for each major component and the R&D target values required to realize the NBI system.

1. Ion Source
   - a. Negative ion current density at the plasma boundary J^- : $\gtrsim$ 20 mA/cm^2 for D^-, $\gtrsim$ 30 mA/cm^2 for H^-
   - b. Spatial uniformity of the negative ion current density : $\lesssim \pm$ 10 % over ~ 30cm x 100cm
   - c. Source filling pressure : < 0.5 ~ 1 Pa
   - d. Electron extraction J_e : < ~ 10 x J^-
   - e. Total extracted negative ion current : ~ 20 A

2. Accelerator
   - a. Acceleration voltage : 0.5 ~ 2 MeV
   - b. Beam current I_{acc} : > 10 A
   - c. Beam divergence angle (1/2 x 1/e) : < 5 mrad
   - d. Stripping loss : << 10% of I_{acc}
   - e. High voltage insulator : Ceramic or FRP 1.5m ~ 2.5m OD

3. High Voltage DC Power Supply
   a. Voltage : 0.5 ~ 2 MV
   b. Power : 10 ~ 20 MW
   c. Switching Type : AC Switch
   d. Surge Blocker : Amorphous or Ferrite
   e. SF_6 high voltage transmission : Multi-core system

4. Beamline Components
   a. Beam dump element : 1 ~ 2 kW/cm^2
   b. Large metal seal gate valve : 0.5m x 2m Diaghragm Type
   c. Steady state cryo pump system : Alternative regenerating system

   * The long range R&D items include a plasma neutralizer and a energy recovery system. With these agressive R&Ds, the NBI system becomes more efficient and attractive.

Figure 2.2-1 shows a 1.3 MeV, 18 A negative ion source which is one of the most important R&D goals for FER/ITER. In order to develop such high energy and high power negative ion source, a MeV x MW class test facility named AITS is planned at JAERI.

2.3 Outline of the JAERI Test Stands for NBI R&Ds

We have two test stands called ITS-2M and ITS-2a(NIAS) for negative ion beam experiments, and another two test stands called PBEF and JEBIS for high heat flux experiments. The major specifications of each test stand is shown in Table 2.3-1. The side views of both the ITS-2M and ITS-2a(NIAS) are shown in Fig.2.3-1 and Fig.2.3-2, respectively.

Table 2.3-1 JAERI Test Facilities for NBI R&Ds

		NEGATIVE ION BEAM EXPERIMENTS		HIGH HEAT FLUX EXPERIMENTS	
		ITS-2M	ITS-2a (NIAS)	PBEF	JEBIS
OVERALL	SITE	Naka	Tokai	Naka	Naka
	Porarity	Negative and Positive	Negative	Positive	Negative
	Beam Species	H- O- Li- H+	H-	H+ He+ O+ N+ Ar+ etc.	electrons
	Typical Record	50 keV, 10 A, 0.1 s, H-		100 keV, 40 A, 10 s, H+ 75 keV, 80 A, 10 s, H+ > 220 MW/m2	> 2000 MW/m2
POWER SUPPLY	Acceleration	±75 kV 6 A/DC 20 A/1 s 40 A/0.5 s	-350 kV 150 mA/DC 200 mA/5min	+100 kV/80 A/10 s	-100 kV/5 A/1ms-DC
	Pre-Accel.	5 kV/35 A/1 s	10 kV/1 A/DC	10-30 % of Vacc	—
	Electron Suppression	5 kV/12 A/1 s	3 kV/1 A/DC	-3 kV/22 A/10 s	—
	Arc I	150 V/250 A/DC 400 A/1 s 1500 A/0.2 s	100 V/200 A/DC	120 V/2000 A/10 s 180 V/1000 A/10 s	120 V/500 A/DC
	Arc II	200 V/300 A/1 s	100 V/500 A/0.1 s	120 V/2000 A/10 s 180 V/1000 A/10 s	—
	Filament I	15 V/2720 A/10 s	15 V/400 A/DC	12 V/400 A x 8/15 s	15 V/250 A x 4/DC
	Filament II	—	—	12 V/400 A x 8/15 s	—
	Bias I	15 V/200 A/DC	15 V/100 A/DC	—	—
	Bias II	—	15 V/100 A/DC	—	—
	Coil I	15 V/200 A/DC	—	10 V/200 A/10 s	±200 A
	Coil II	—	—	10 V/200 A/10 s	—
	Radio Frequency	2.45 GHz/5 kW/DC	—	—	—
	Recovery	—	—	—	5 kV/5 A/DC
Vacuum System	Chamber	60 cm OD x 540 cm L	50 cm OD x 200 cm L	Two Beamlines	120 cm ID x 219 cm H
		170 cm OD x 180 cm H		1. Vertical Line	
				2. JT-60 Prototype NBI	
	Turbo-Molecular Pump	2,000 l/s x 3	2,000 l/s x 1	2,000 l/s x 3	3000 l/s x 1
	Cryosorption Pump	10,000 l/s x 1			
	Cryocondensation Pump	100,000 l/s x 3		2,400,000 l/s	
Diagnostics	Scannning Calorimeter	1	1	1	1
	Scannning Faraday Cup	1	1	—	—
	Multi-channel Calorimeter	1	1	1	1
	Multi-channel Faraday Cup	1	1	—	—
	Momentum Mass Analyzer	1	—	—	—
	Spectrometer	1	—	—	—
	Infrared Camera	—	—	1	1
	High Speed Video Camera	—	—	1	1
Footnotes	Major Characteristics	10 A Volume-Cesium Negative Ion Source	350 keV negative ion accelerator	90 % Proton Source	Plasma Electron Gun

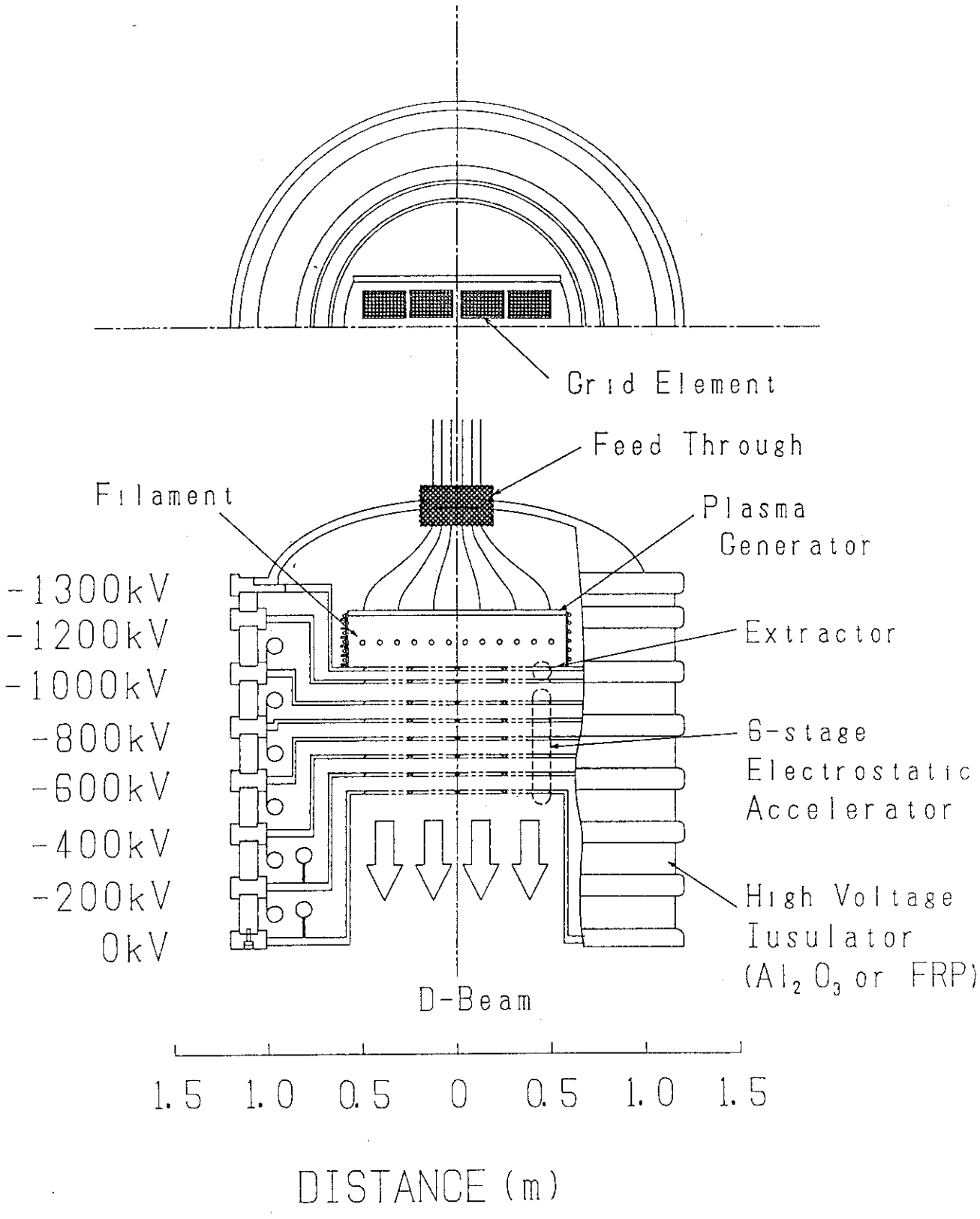

Fig. 2.2-1 A 1.3 MeV, 18 A deuterium negative ion source for FER/ITER.

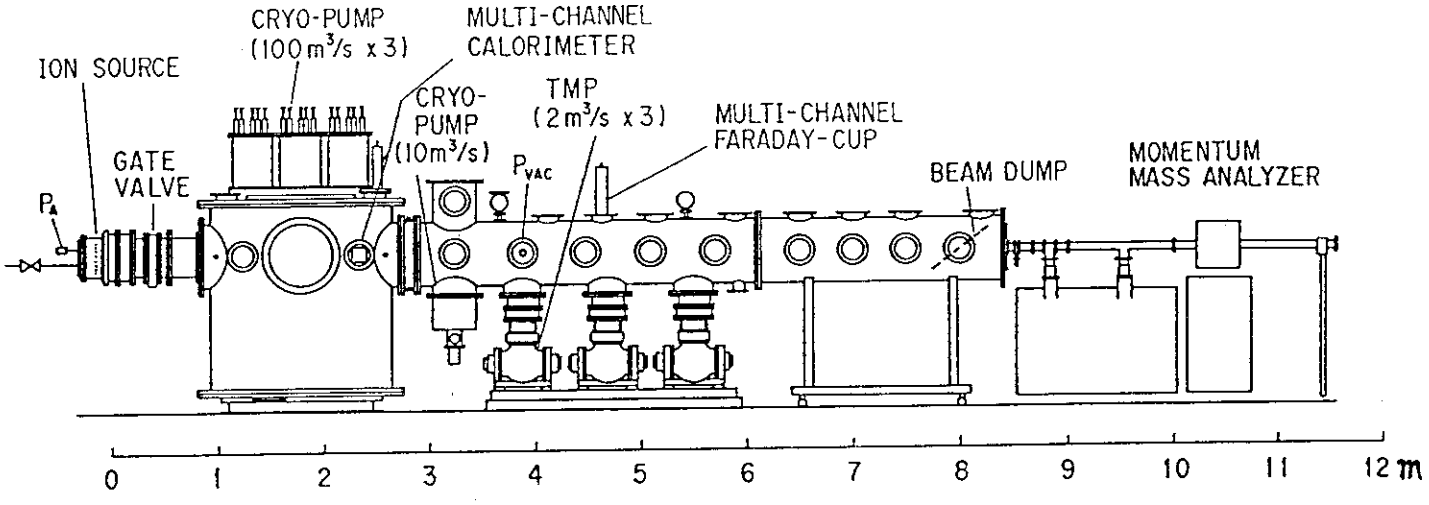

Fig.2.3-1 Beamline of the ITS-2M test stand.

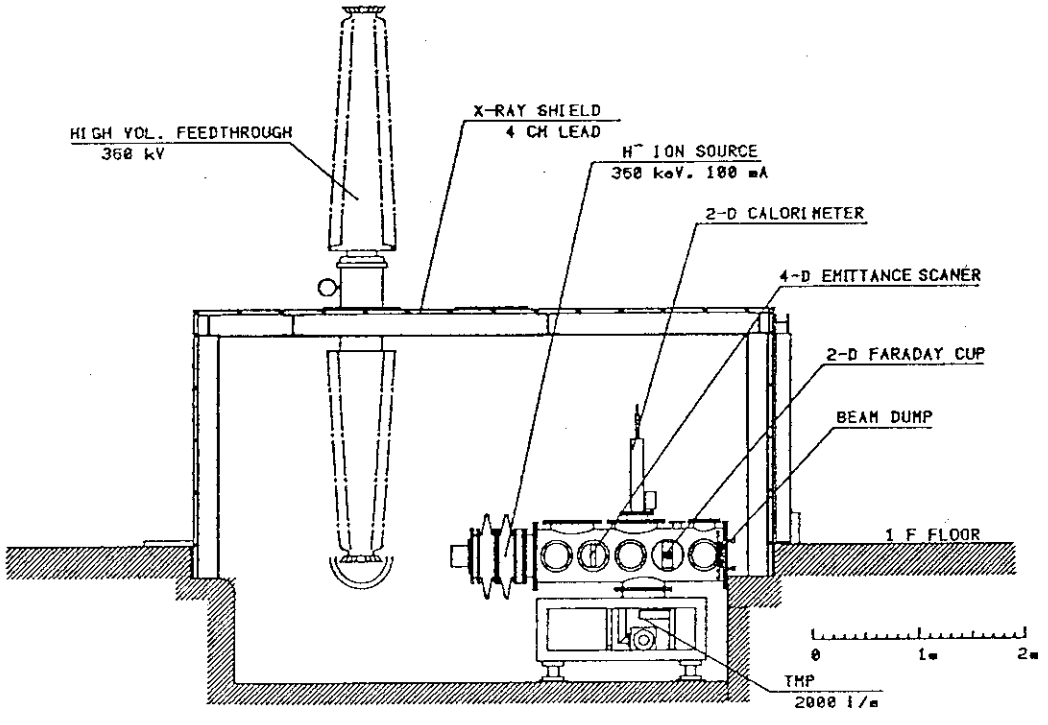

Fig.2.3-2 Layout of the ITS-2a(NIAS) test stand.

3. R&D RESULTS OF NEGATIVE ION SOURCES AND ACCELERATORS

3.1 Negative Ion Production

Development of a high current negative ion source is the most critical issue in realizing the high energy neutral beam system. At JAERI, we started to develop the negative ion source in 1984, and our goal is to construct a high current (> 10 A) D^- ion source that is directly applicable to the neutral beam injectors for future fusion reactors. Out of three major methods to generate the negative ions; i.e. double charge exchange, surface production and volume production, we chose the volume production. Because this method has big advantages over the other two methods;

(1) The structure of the source is simple, and scale-up is easy.
(2) Produced negative ions have low thermal energies. Hence, low beam divergence is expected.
(3) Operation of the source is easy and reliable.

These advantages makes the volume production method the most attractive one for use in neutral beam injectors.

When we started the development, however, the negative ion current obtained in the volume source was of the order of mA, while more than one ampere negative ion current had already been achieved in other two methods.

Therefore, our efforts have been concentrated mainly on increasing the negative ion current and the current density. After some basic studies on the volume production, we constructed large volume sources called 'One-Ampere Negative Ion Source'[1] and 'Multi-Ampere Negative Ion Source'[2]. Optimization of the volume source has been performed by using these two sources.

Figure 3.1-1 and Figure 3.1-2 show the One-Ampere Source and the Multi-Ampere Source, respectively. Both sources have rectangular multicusp plasma generators, where a source plasma is created by arc discharge between the anode and the tungsten filaments. The negative ions produced in the plasma are accelerated by multi-aperture extractor, which consists of four (or five) grids called plasma, extraction, electron suppression, (ion suppression) and acceleration grids. Major specifications of these sources are summarized in Table 3.1-I.

In the volume source, the negative ions are considered to be produced by a two-step process [3]; In the first step, vibrationally excited hydrogen molecules are produced mainly by the collision between hydrogen molecules and energetic electrons. In the second step, the negative ions are produced by the dissociative attachment of electrons to the vibrationally-excited molecules. Since the optimum electron energies for these two steps are distincitively different (60 eV vs. >1 eV), the effective method to enhance the negative ion production is to divide the plasma chamber into two regions and to optimize the electron energy distributions in both regions, respectively. In order to form this "tandem chamber" configuration, all volume sources presently developed utilize a transverse magnetic field called "magnetic filter".

Figure 3.1-3 shows an example of magnetic field configuration and typical orbits of the primary electrons in the One-Ampere Negative Ion Source. In this figure, the magnetic filter field is created by a pair of strong magnets installed outside the source plasma. The energetic electrons emitted from tungsten filaments are confined in the upper region (discharge region) of the chamber, where vibrationally excited hydrogen molecules are produced efficiently. Although the energetic electrons cannot go through the filter field, the cold electrons can diffuse with the ions to the region close to the plasma grid (extraction region). As a result, the electron temperature becomes an order of 1 eV in the extraction region, where the negative ions are produced by the dissociative attachment. In the One-Ampere and the Multi-Ampere Sources, various kinds of magnetic filter have been utilized to optimize the negative ion production.

References

[1] Y. Okumura et al.; Proc. 4th International Symp. on the Production and Neutralization of Negative Ions and Beams, BNL, 1986, p.309.
[2] M. Hanada et al.; Rev. Sci. Instrum. 61 (1990) p.499.
[3] M. Bacal et al.; J. Appl. Phys. 52 (1981) p.1247.

Table 3.1-1 Specifications of the One-Ampere and the Multi-Ampere Sources

	One-Ampere Source	Multi-Ampere Source
PLASMA GENERATOR		
SIZE	21 cm x 36 cm 7-35 cm depth	24 cm x 48 cm 15 cm depth
CATHODE	W-filament x 8	W-filament x 16
MATERIAL	SUS	Copper
MAGNETIC FILTER	Rod Filter External Filter Electro-Magnetic	Rod Filter External Filter PG Filter
EXTRACTOR		
GRID AREA	12 cm x 26 cm	15 cm x 40 cm (14 cm x 36 cm)
APERTURES	9 mm x 209	9 mm x 434 (11.3 mm x 253)
EXTRACTION AREA	133 cm2	276 cm2 (253 cm2)
TRANSPARENCY	43 %	46 % (50%)
GRID	4 Grids	5 Grids
MAX. VOLTAGE	40 kV	75 kV
COMMENTS	1.6 A, 31 keV H- ion beam was obtained in 1987	10.2 A, 50 keV H- ion beam was obtained in 1990

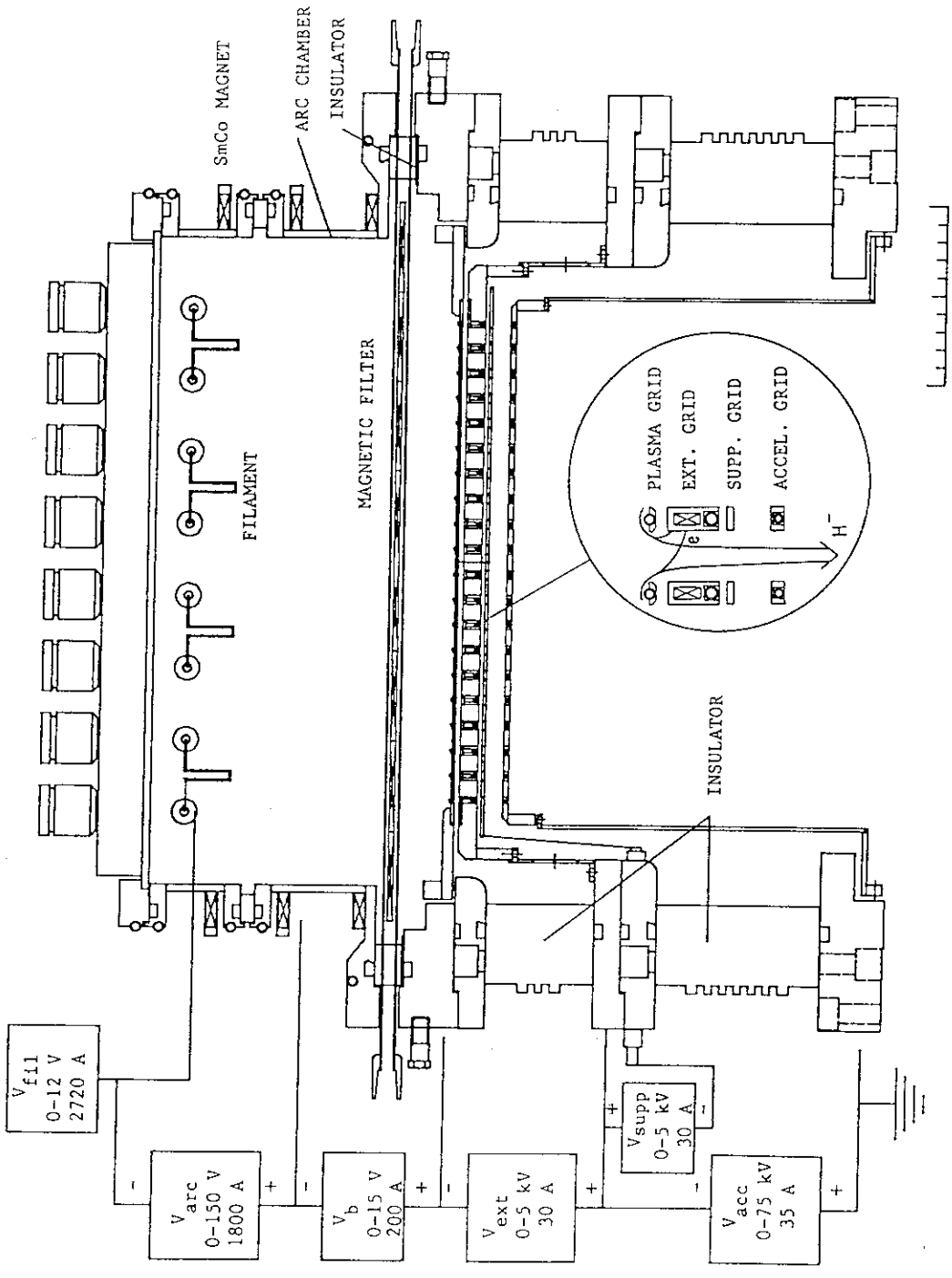

Fig. 3.1-1 Cross section view of the One-Ampere H^- Ion Source and electrical connection of power supplies.

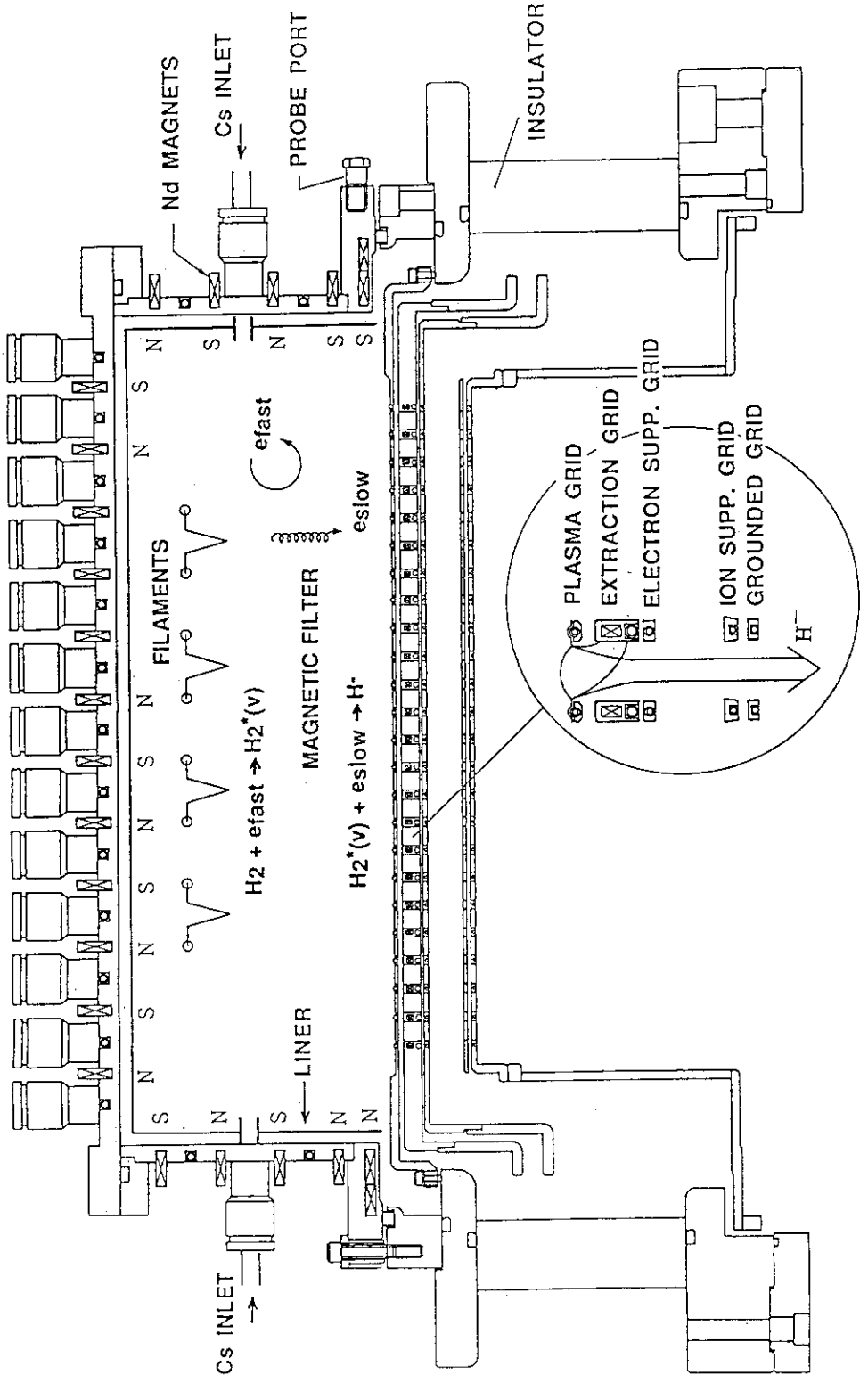

Fig. 3.1-2 A schematic of the Multi-Ampere H^- Ion Source, which produced 10.2 A, 50 keV H^- ion beams for 0.1 s.

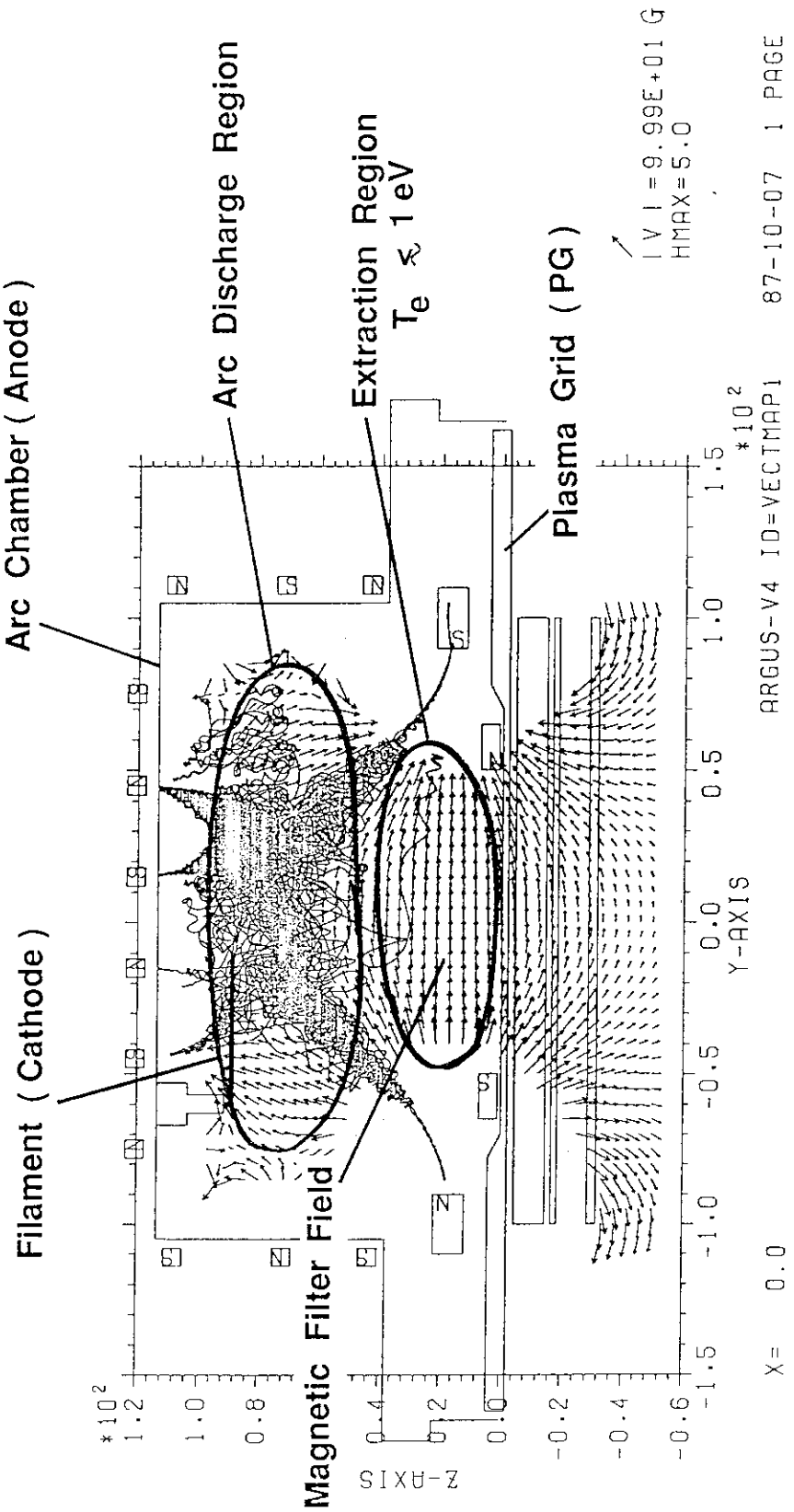

Fig. 3.1-3 Magnetic field configuration and typical orbits of the primary electrons emitted from the filament in the One Ampere Source.

3.1.1 Optimization of Arc Discharge

The negative ion production depends strongly on the arc discharge conditions. We studied the optimum arc discharge conditions for H^- ion beam production using the Multi-Ampere Negative Ion Source coupled with a 14 cm x 36 cm extractor, where the magnetic filter field is produced by the magnets mounted outside the arc chamber ('External Filter').

(1) Arc Current Dependence

The Negative ion current increases with an arc discharge current as shown in Fig. 3.1.1-1, where the filling pressure in the arc chamber P_A, the arc discharge voltage V_{arc} are kept constant. The highest negative ion current of 3.1 A was produced at the arc current of 1.2 kA. This current corresponds to the negative ion beam current density of 12 mA/cm^2, which is defined at the exit of the extractor.

The negative ion current tends to saturate at the higher arc current. This saturation was initially found at JAERI [1]. The reason why the saturation occurs can be explained as follows;

a. At the higher arc current, dissociation of molecular ions is enhanced to produce protons and free atoms which destruct both the excited molecules and the H^- ions.
b. The electron temperature increases with the discharge power and becomes too high for the efficient dissociative attachment of an electron to the vibrationally excited molecules. Additionally, the H^- ion loss by electron impact detachment is enhanced.

(2) Filling Gas Pressure Dependence

Figure 3.1.1-2 shows the pressure dependence of negative ion current for different arc discharge currents [2]. There is an optimum pressure that makes the H^- ion current maximum for each discharge current. The reason why the H^- ion current decreases at higher pressure is mainly attributed to the loss of H^- ions by the collisions with H_2 molecules.

It should be noted that the optimum pressure increases with the discharge current. In other words, the larger H^- current requires the higher source pressure. For a practical use in the neutral beam

injectors, however, the source has to be operated at a pressure as low as 0.5-1.0 Pa. Otherwise the stripping loss of H^- ions in the accelerator column becomes too big, resulting in a low acceleration efficiency and a severe heat dissipation in the accelerator grids. The reduction of the source pressure is, therefore, an important subject for the ion source development.

(3) Arc Voltage Dependence

The dependence of the H^- ion current on the arc discharge voltage is shown in Fig. 3.1.1-3 for two different types of magnetic filter in the One-Ampere Negative Ion Source [3]. The arc current was kept to be 200 A by regulating the filament temperature. Although the optimum arc voltage that gives the highest arc power efficiency is around 70 V for both types of the filter, the efficiency decreases rapidly with the arc voltage in case of 'weak filter'. This may be considered as follows; since the energy of the primary electrons increases with the arc voltage, those energetic electrons are apt to escape from the filter and give undesirable effect on H^- production and also enhance the loss of the H^- ions. The dependence of the power efficiency on the arc voltage is weak in the case of 'strong filter'.

References

[1] Y. Okumura et al.; Japan Atomic Energy Research Institute Report JAERI-M 84-098, 1984.
[2] Y. Okumura; Kakuyugou Kenkyu 60, 1988, p.329.

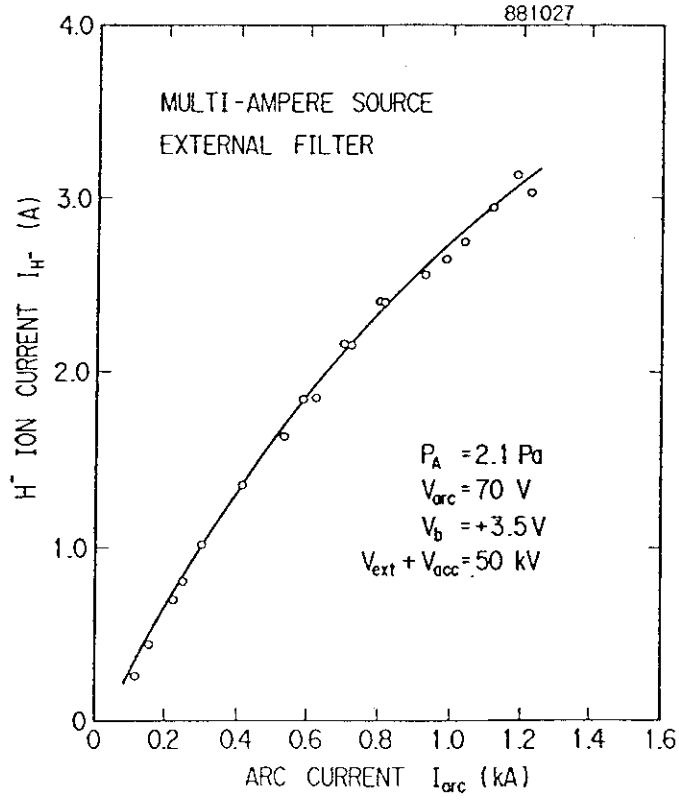

Fig. 3.1.1-1 Dependence of H^- ion current on the arc discharge current. The H^- ion current increases linearly with the arc current but tends to saturate at the higher arc current.

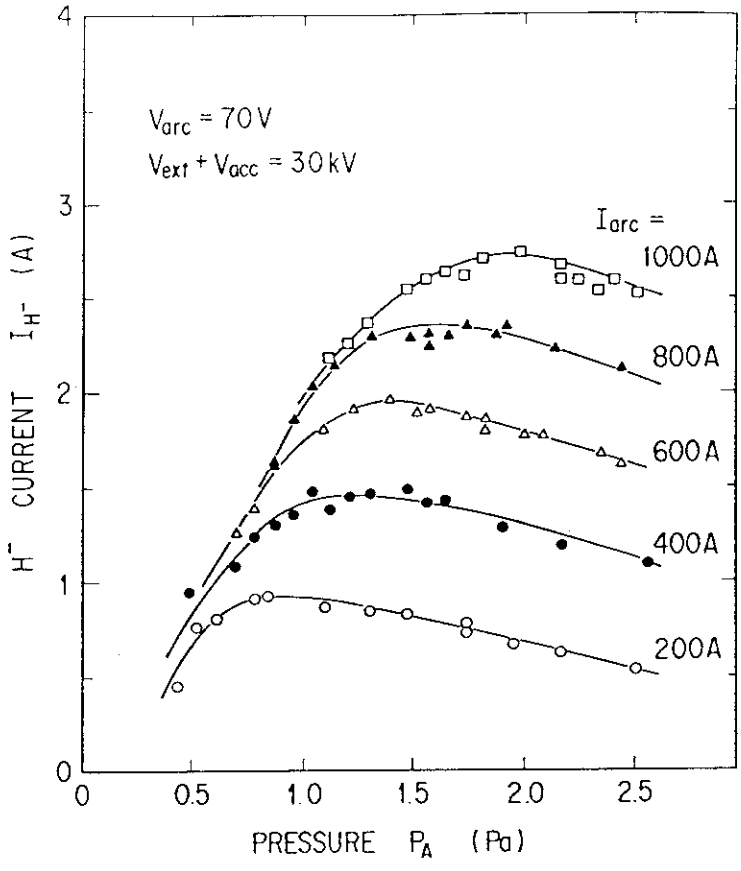

Fig. 3.1.1-2 Dependence of the H^- ion current on the pressure in the plasma generator for different arc discharge current. The optimum pressure that gives highest H^- current increases as the arc discharge current increases.

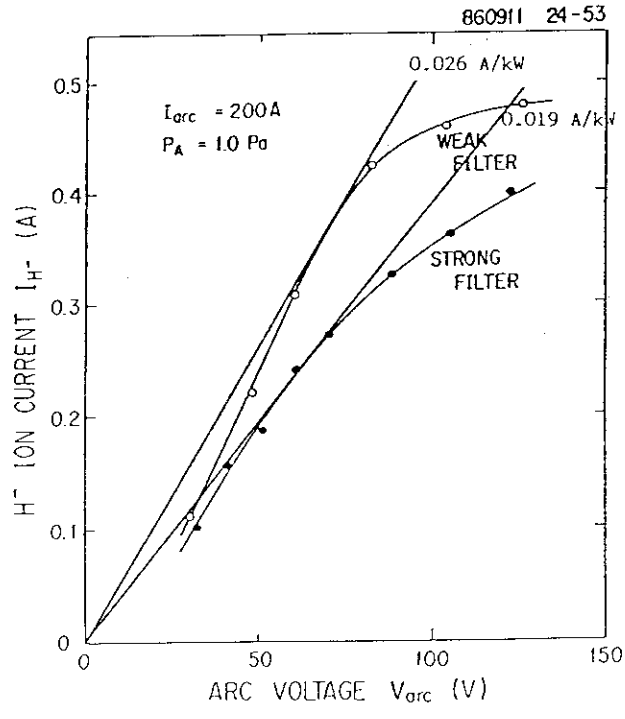

Fig. 3.1.1-3 Dependence of H^- ion current on the arc discharge voltage for two types of magnetic filter. The highest power efficiency is obtained at the arc voltage of around 70 V.

3.1.2 Optimization of Magnetic Filter Configurations [1]

Since negative ion production in the volume source is thought to be two-step process [2], the plasma is divided into two regions, i.e. an arc discharge region and an extraction region, by a transverse magnetic field called "magnetic filter". It was suggested in the early days of the negative ion research that the filter configuration affected the negative ion production considerably[3]. Especially in the negative ion source for NBI, which is required to produce a high current beam, it is necessary to extract the ions at high current density from a wide area.

Although many structures of the magnetic filter have been designed and tested so far [3-5], it had not been attempted to compare their performances on the negative ion production systematically. At JAERI, installing three types of magnetic filters within One Ampere Negative Ion Source, an optimization of the filter configurations was conducted. The filters are illustrated in Fig.3.1.2-1. They are called a "rod filter", an "external filter", and an "electro-magnetic (E-M) filter", respectively.

(1) Filter Strength Dependence

The strength of each magnetic filter was optimized in order to obtain a maximum current from 9 apertures in the centre region of the extraction area. The optimum filter strengthes were 200 G.cm for the rod filter, 300 G.cm for the external filter, and 150 G.cm for the E-M filter. Although theoretical model predicts that the negative ion production depends on the magnetic flux (magnetic field (G) x field thickness (cm) = Bl), the optimum Bl took various value for each filter. From an analysis on the filter field profiles, it seems that the magnetic field strength affects the negative ion production strongly rather than the thickness does, namely, the negative ion production depend on B^2l [5] rather than Bl.

(2) Filter Position Dependence

The dependence of the H^- yield on the filter position was studied using the E-M filter. The result is shown in Fig.3.1.2-2. When the distance between the filter and the plasma grid was changed from 60 mm to 40 mm, the H^- current was improved considerably. However, as the

filter was displaced closer toward the plasma grid, the current saturated gradually, then the improvement became negligible at a distance less than 30 mm. This result indicates that there is a limit to the improvement of H^- current even by installing the filter closer enough to the plasma grid.

(3) Comparison of Maximum Current Density

The comparison of H^- current densities obtained by the three filters are show in Fig.3.1.2-3. The H^- current density of 22 mA/cm^2 was extracted with the external filter. It seems that the H^- current density was enhanced by applying a transverse magnetic field on the extraction surface [6]. On the other hand, the current densities obtained with the rod filter and the E-M filter were lower than that with the external filter. Since these two filters have "obstacle" strcutures immersed in the plasma at the anode potential, the filters themselves become plasma loss areas. Consequently, the plasma density is low for the same arc current compared to that of the external filter. Then the H^- current density is influenced very much by the filter configuration.

(4) Comparison of Spatial Uniformity of the H^- Prtoduction

By changing the location of 9 apertures opended on the extraction area, the uniformity of the H^- current densities was investigated for each filter. An example of the rod filter is shown in Fig. 3.1.2-4. Corresponding to the formation of an uniform magnetic filter field, the deviation of the H^- current densities over the extraction area were suppressed below 15 % in the rod filter, and 7 % in the E-M filter. In the external filter, on the contrary, the deviation was as high as 30%. Since the magnetic field formed by the external filter expands widely into the source region and the field strength varies over the extraction area, the Bl value varies appreciably along the radial direction, eventually the H^- uniformity becomes worse in the external filter.

(5) Extraction of 1 A negative ion beam

The H^- current extracted through 209 apertures for the external filter is shown in Fig.3.1.2-5 as a function of the arc discharge current. The maximum H^- beam current of 1.6 A was obtained, where the

average H^- current density was 12 mA/cm^2, and the current density in the center region was 22 mA/cm^2. This is due to the poor uniformity over the extraction area.

In order to realize a high current negative ion source for NBI, two critical specifications have to be satisfied, i.e. high current density and good apatial uniformity. From the experiments mentioned above, the characteristics of the three filters are summarized in Table 3.1.2-1. Although the highest current density was obtained with the external filter, the uniformity was relatively worse. In the rod and the E-M filters, on the other hand, the current densities were limited to moderate values in spite of their good spatial uniformity. A further study is necessary to realize both the high current density and the good uniformity over the wide extraction area.

References

[1] T. Inoue et. al., Nucl. Instrum. and Meth. B37/38 (1989) 111-115
[2] M. Bacal, A. M. Bruneteau, H. J. Doucet, W. G. Graham and G. W. Hamilton, Proc. 2nd Int. Symp. on the Production and Neutralization of Negative Hydrogen Ions and Beams, BNL 51304 (1980) 95
[3] K. W. Ehlers and K. N. Leung, Rev. Sci. Instrum. 53/9 (1982)
[4] A. J. T. Holmes, T. S. Green and A. F. Newman, Rev. Sci. Instrum. 58/8 (1987) 1369
[5] A. J. T. Holmes, Rev. Sci. Instrum. 53/10 (1982)
[6] M. Bacal, J. Bruneteau, P. Devynck, and F. Hamillion, Proc. 4th Int. Symp. Production and Neutralization of Negative Hydrogen Ions and Beams, BNL, AIP Conf. Proc. No. 158 (1986) 246

Table 3.1.2-1 Summary of the results obtained with the three types of magnetic filters.

Filter	Uniformity (deviation)	Current Density @ centre	Total H^- Current
Rod	○ (15 %)	12 mA/cm^2	1.26 A
External	X (30 %)	22 mA/cm^2	1.60 A
Electro-magnetic	○ (7 %)*	9 mA/cm^2 *	0.90 A *

* at 400 A discharge

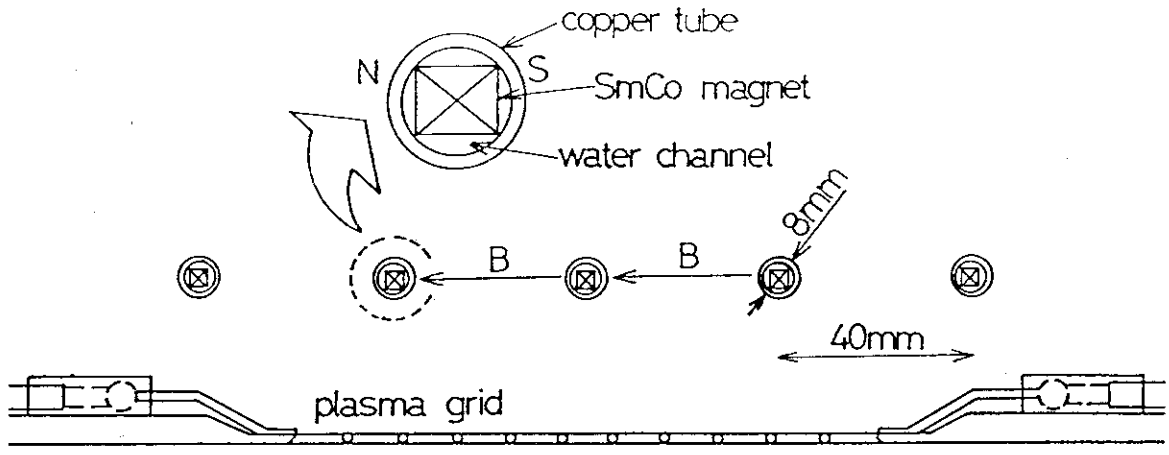

(a) rod filter

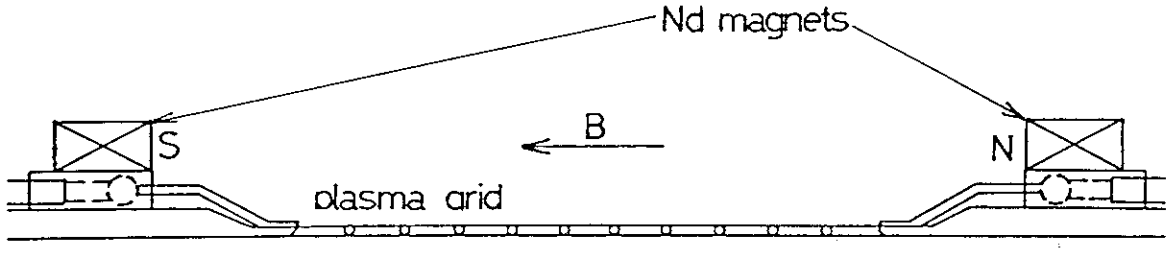

(b) external filter

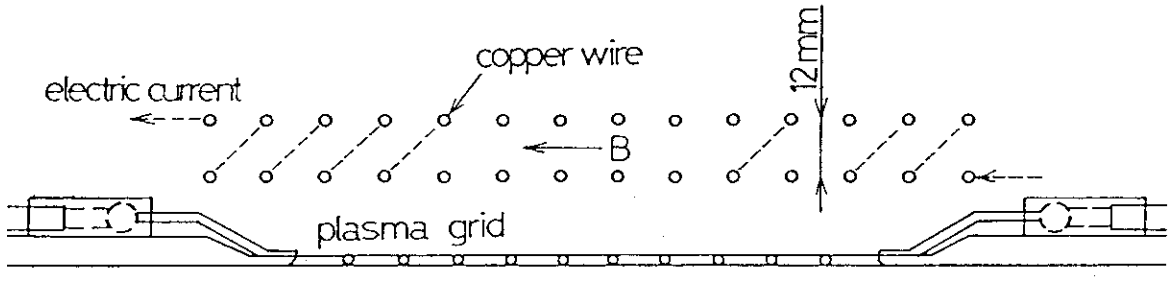

(c) electro-magnetic filter

Fig. 3.1.2-1 Cross-sectional views of three types of magnetic filters. (a) rod filter : an array of five water cooled copper tubes, in which samarium-cobalt magnets are installed. (b) external filter : a pair of neodymium magnets placed on the plasma grid outside the extraction area. (c) E-M filter : two rows of copper wires which are connected to each other to form a rectiangular solenoid coil.

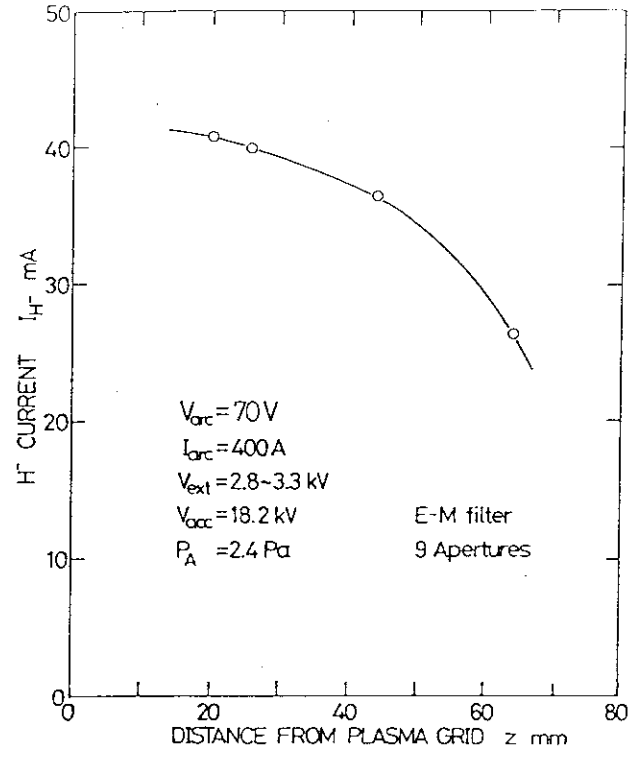

Fig. 3.1.2-2 Dependence of the H^- current density on the position of the E-M filter.

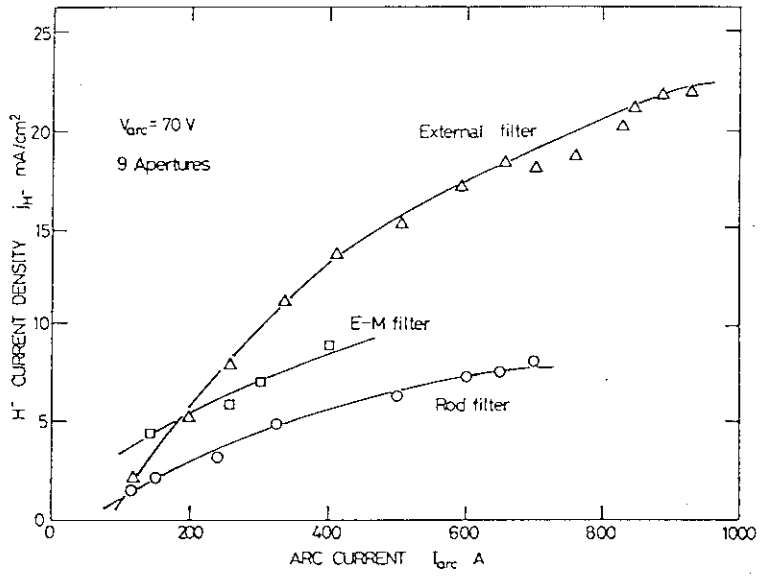

Fig. 3.1.2-3 H^- current densities as a function of arc discharge current. The ion beam was extracted through 9 apertures in the centre.

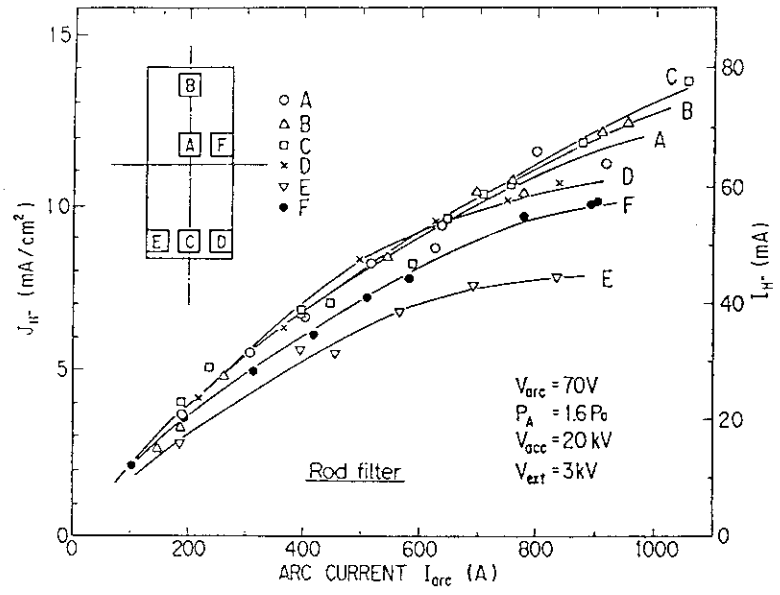

Fig. 3.1.2-4 Dependence of H^- current densities extracted from various location of extraction area in the rod filter configuration. The location of the 9 apertures used for each curve is shown in the left side of the figure.

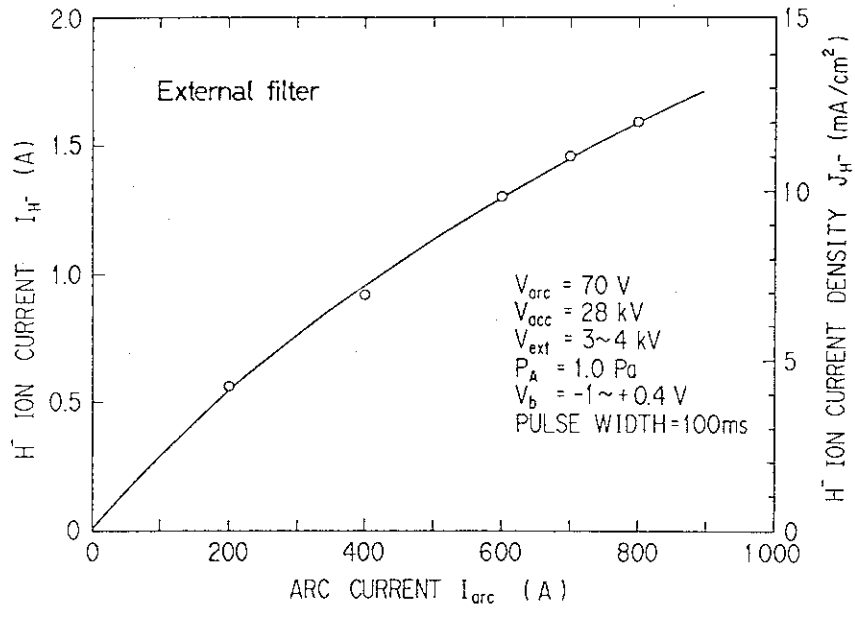

Fig. 3.1.2-5 Total H^- current as a function of the arc discharge current in the external filter.

3.1.3 PG ElectroMagnetic Filter [1]

From the results of three filter configurations mentioned in the preceding sub-section 3.1.2, the conditions for an ideal filter configuration can be listed below;

(1) the filter field is uniform spatially over the wide extraction area,
(2) the filter strength can be controlled easily depending on the arc discharge conditions,
(3) there is no large plasma loss area such as the rods inside the plasma,
(4) the filter field can be produced close to the plasma grid.

To satisfy the above four conditions, we devised a new magnetic filter called a PG electromagnetic filter. The concept of the PG filter is shown in Fig. 3.1.1-1. The PG filter produces an uniform filter field over a large extraction area by flowing a high current through the plasma grid itself. The inverse filter field produced on the side of the extraction region works also as an electron suppression or deflection. In order to confirm the performances of this magnetic filter configuration, this filter was installed in the Multi-Ampere Negative Ion Source and tested.

Figure 3.1.3-2 shows the dependence of the H^- ion current on the arc discharge current. This figure also shows the H^- ion currents in the rod filter and the external filter. The maximum H^- ion current in the PG filter was 3.4 A (13 mA/cm2) at the arc discharge current of 1.3 kA, the arc voltage of 70 V and the source filling pressure of 2.1 Pa, where the optimum net filter strength was 430 Gauss.cm at a plasma grid current of 700 A. The H^- ion current in the PG filter is larger than that in the external filter. This will be due to the good uniformity of negative ion production, which can be confirmed by the trapezoid beam profile. Although the difference of the H^- ion currents between the PG filter and the external filter is small in the present experiment, the PG filter will be superior in enlarging the grid width and in obtaining good beam optics.

Reference

[1] M.Hanada et al. : Rev.Sci.Instrum. 61, 499 (1990).

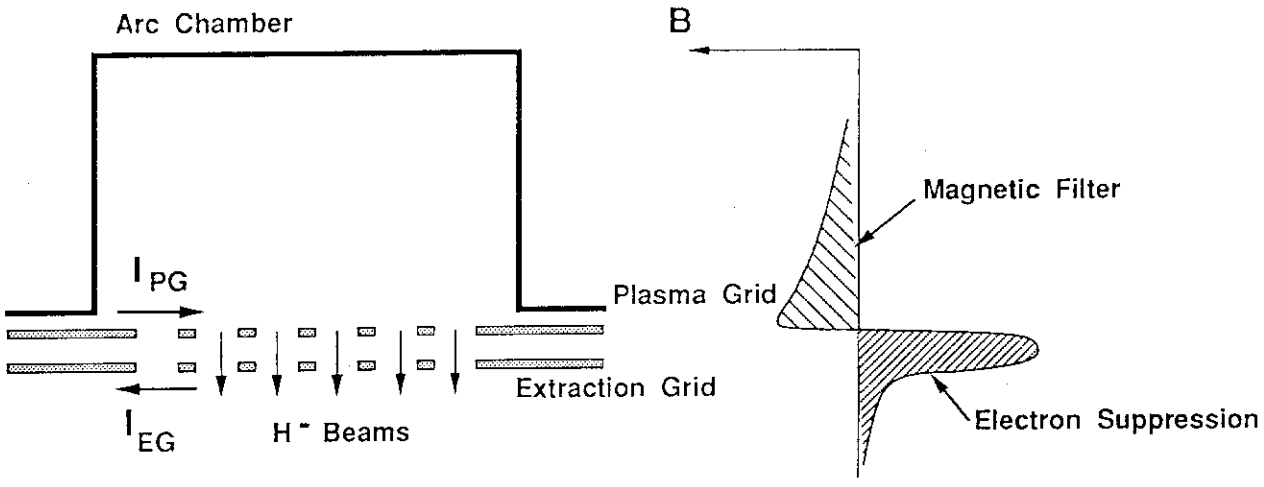

Fig. 3.1.3-1 Concept of the PG filter

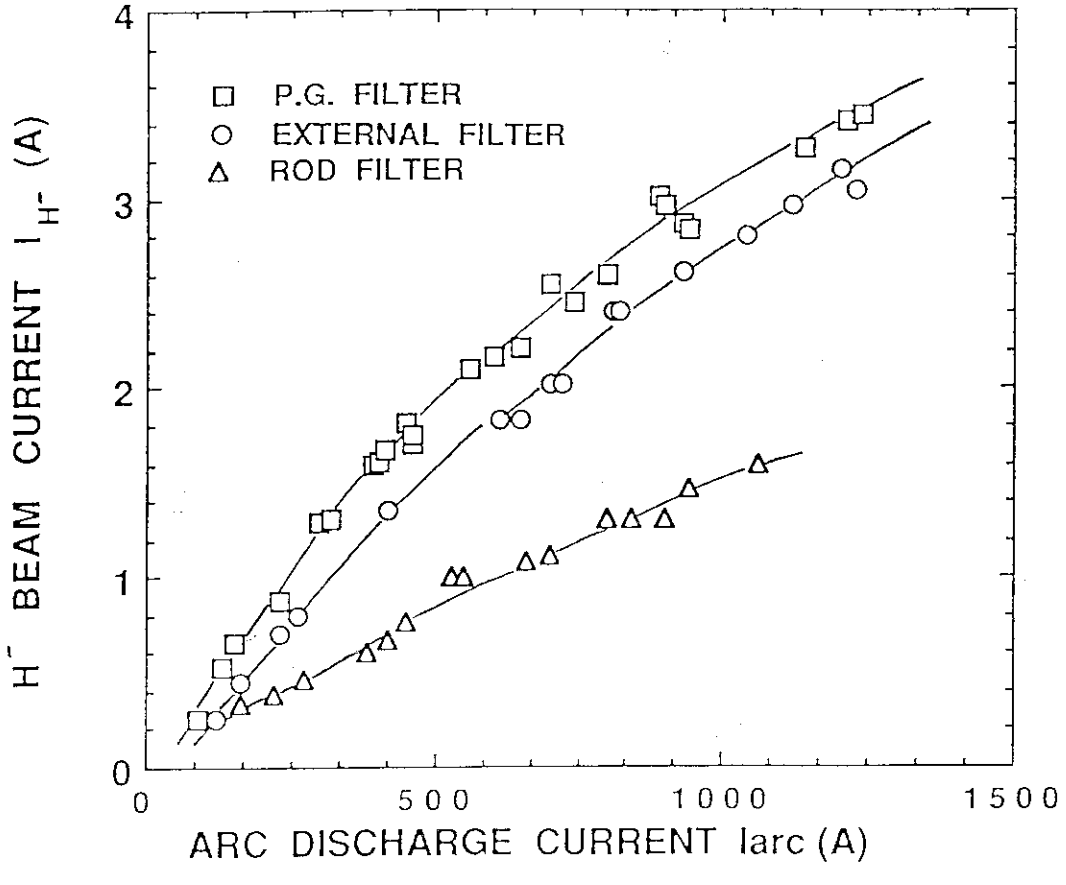

Fig.3.1.3-2 The dependence of H^- ion current on the arc current

3.1.4 Cesium Vapor Injection [1,2,3]

It is reported that the H^- ion production efficiency in a volume source is remarkably improved by mixing cesium vapor in the discharge [4,5,6]. To investigate whether or not the same effect is observed in a large multicusp volume source, we injected a small amount of cesium vapor into the Multi-Ampere Negative Ion Source. In this experiment, the plasma grid is made of molybdenum plate, which is insulated thermally by ceramic spacers in order to control its temperature. The inner surface of the plasma generator is covered with a stainless-steel liner, which is also heated by the arc discharge to prevent the cesium condensation.

(1) Enhancement of Negative Ion Current

The dependence of H^- ion current on the arc discharge current is shown in Fig. 3.1.4-1 for different source pressures. The negative ion current obtained before the cesium injection is also shown. Without cesium, the H^- ion current achieved at the optimum pressure was 1.7 A, which was about 30 % lower than the value obtained in the original Multi-Ampere Source because of the existence of the liner. However, once the cesium was injected, the H^- ion current was enhanced remarkably. At the pressure of more than 0.7 Pa, the H^- ion current increased with arc discharge current almost linearly. The highest H^- ion current of 10.2 A was obtained at the arc current of about 800 A. The H^- ion current density reached to 36 mA/cm^2. This remarkable enhancement is considered to be due to the surface production by the atomic hydrogen incident on the plasma grid [3].

The consumption rate of the cesium is extremely small. Once the cesium vapor of about a hundred miligrams was injected to the source, the cesium effect lasted more than a week without additional cesium. Typically, the source was operated for 0.1 second every 50 seconds. Thus, the consumption rate was about 0.1 g/3000 shots for 0.1 s beam pulse (or 0.2 second Arc/ 5 second Filament pulse).

(2) Optimum Filling Pressure

Figure 3.1.4-2 shows the H^- ion current as a function of the pressure in the plasma generator for various arc currents. Without

cesium, the optimum filling pressure increased with the arc current [7]. However, in the cesium-seeded ion source, the optimum pressure dose not depend on the arc current. Moreover this optimum value decreased to less than 1 Pa.

(3) Other Effects

Extracted electron current became almost zero when the plasma grid was biased positively with respect to the anode. Impurity contents (O^- and OH^-) in the negative ion beam was less than 1 %, and no metal impurity was observed.

References

[1] Y. Okumura et al.; Proc. 5th International Symp. on the Production and Neutralization of Negative Ions and Beams, BNL, 1989.
[2] H. Kojima et al.; Proc. 13th Symp. on Ion Sources and Ion-Assisted Technology, Tokyo, 1990, p.145.
[3] Y. Okumura et al.; Proc. 13th Symp. on Ion Sources and Ion-Assisted Technology, Tokyo, 1990, p.149.
[4] S.P. Antipov, L.I. Elizarov, M.I. Martynov, and V.M. Chsnokov: Pribori I Texnika Eksperimenta 4, 42 (1984).
[5] S.R. Walther, K.N. Leung, and W.B. Kunkel: J. Appl. Phys. 64, 3424 (1988).
[6] K.N. Leung, C.A. Hauck, W.B. Kunkel, and S.R. Walther: Rev. Sci. Instrum. 60, 531. (1989).
[7] Y. Okumura: Kakuyugo kenkyu 60, 329 (1988) in Japanese.

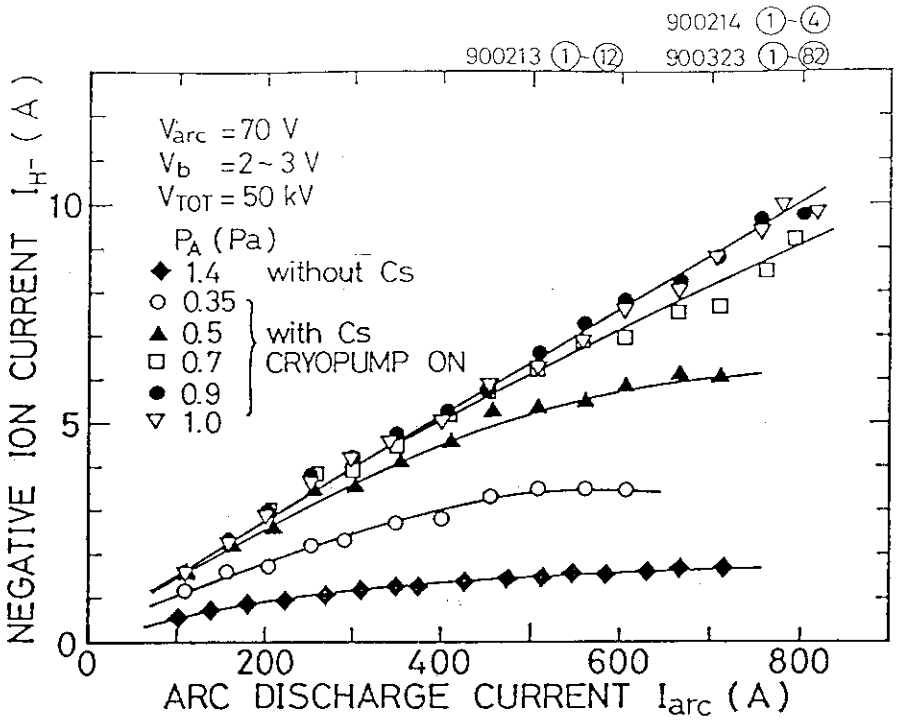

Fig. 3.1.4-1 H^- ion current obtained in Cs-seeded Multi-Ampere Negative Ion Source. The H^- current without cesium is also shown.

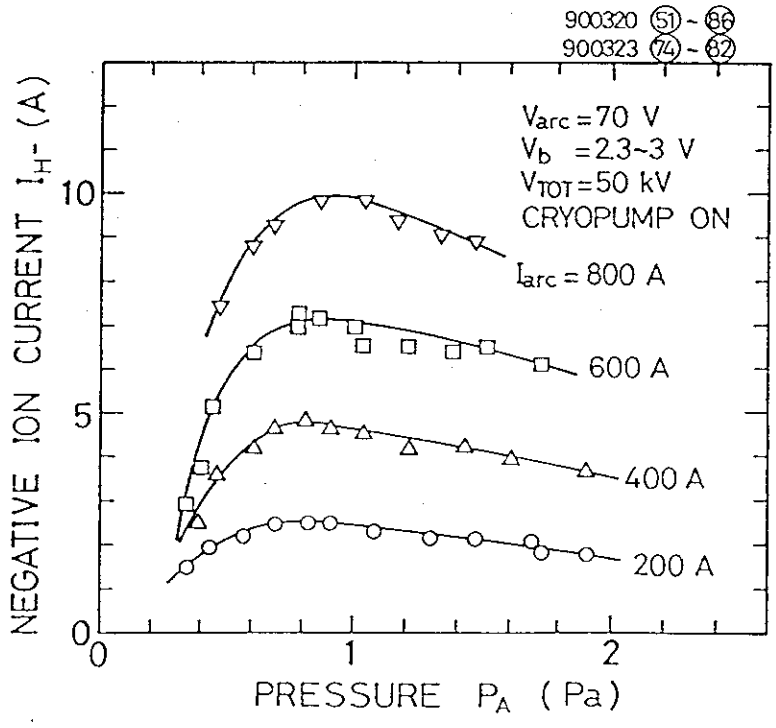

Fig. 3.1.4-2 Dependence of the H^- ion current on the pressure in the plasma generator for different arc discharge current. The optimum pressure that gives highest current does not depend on the arc discharge current. This figure should be compared with Fig. 3.1.1-2, which was obtained in the original source.

3.1.5 Comparison of H^- and D^- Production [1]

Although deuterium beams are used in the actual NBI for fusion reactors, most of the experiments on the negative ion production have been performed with hydrogen. Therefore, it is important, from both a physics and a NBI design points of view, to make clear the mass dependence of the negative ion production.

Preliminary tests of D^- production were performed at LBL [2] and Culham lab.[3]. They reported that (i) D^- current is about a half of H^-, and (ii) electron current accompanied with D^- is considerably higher than that of hydrogen operation. Both of them affects severely the design of negative-ion-based NBI. However, these results were obtained by small sources which were optimized only for hydrogen. The mass effect was not clear in an ampere class large ion source, which can operate at higher plasma density in the optimum source conditions for each gas species.

As part of the U.S.-Japan Fusion Cooperation Program, we tested the JAERI One Ampere Negative Ion Source at LBL with both hydrogen and deuterium , where cesium was not utilized. By varying the filter strength from 450 G.cm to 930 G.cm, we compared the differences of production, transport, and extraction of the negative ions.

(1) Mass Effect of Negative Ion Production

By changing the strength of the filter magnets, the ion source was operated at various arc conditions. Fig.3.1.5-1 shows the negative ion currents as functions of the magnetic filter strength. The data were taken at the optimized conditions for each gas species. The optimum filter strength for D^- production is stronger than that for H^-. The maximum current densities, which were obtained at the corresponding optimum filter strength for each gas species, were 10.4 mA/cm^2 for H^- and 8.4 mA/cm^2 for D^- at the arc discharge power of 40 kW. The ratio of the ion current densities (J_{D^-}/J_{H^-}) is about 0.8, which is higher than $1/\sqrt{2}$.

(2) Mass Effect of Extracted Electron Current

Electron currents as functions of the bias voltage are shown in Fig. 3.1.5-2 for both gas species. The electron current in deuterium operation was more than twice of that in hydrogen at the zero bias voltage. As the bias voltage increased, the electron currents dropped exponentially. The curve of the electron current in deuterium operation appeared as if that of hydrogen were shifted by 2 V to the higher bias voltage. The variation of the ion beam current is shown in Fig. 3.1.5-3. The shift was also observed in the ion currents. The H^- current decreased monotonously with increasing bias voltage starting from V_b = 0 V (i.e. anode potential), while the D^- current kept constant up to 3 V.

Because of the heavier mass of the deuterium ions, it is expected that the ion loss rate is smaller in the deuterium plasma than in the hydrogen one. Hence the deuterium plasma potential may be 2 V higher than that of the hydrogen. By applying the plasma grid bias 2 V higher in the deuterium plasma, the same extraction condition as the hydrogen operation can be achieved. This explains the shift of the extracted currents. Thus, the D^- production is not different from that of H^- basically by optimizing the filter strength and the bias voltage.

References

[1] T. Inoue et al., Rev. Sci. Instrum. 61/1 (1990) 496
[2] K. N. Leung, Proc. US-Japan negative ion neutral beam and diagnostic development workshop, Dec. 15-17 (1986) Nagoya
[3] L. M. Lea, A. J. T. Holmes, G. O. R. Naylor and D. C. Clark, Proc. IAEA technical committee meeting on negative ion beam heating, Jul. 15-17 (1987) Culham

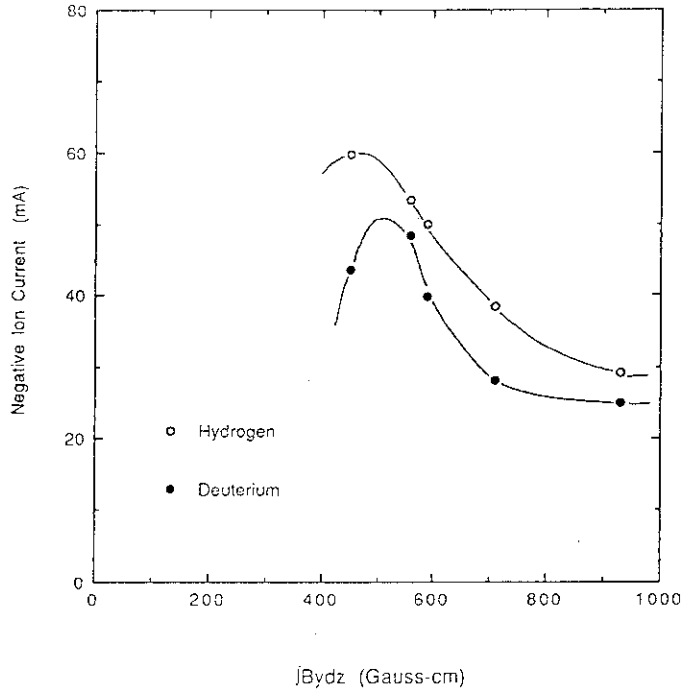

Fig. 3.1.5-1 Dependences of the hydrogen and deuterium negative ion current on the magnetic filter strength.

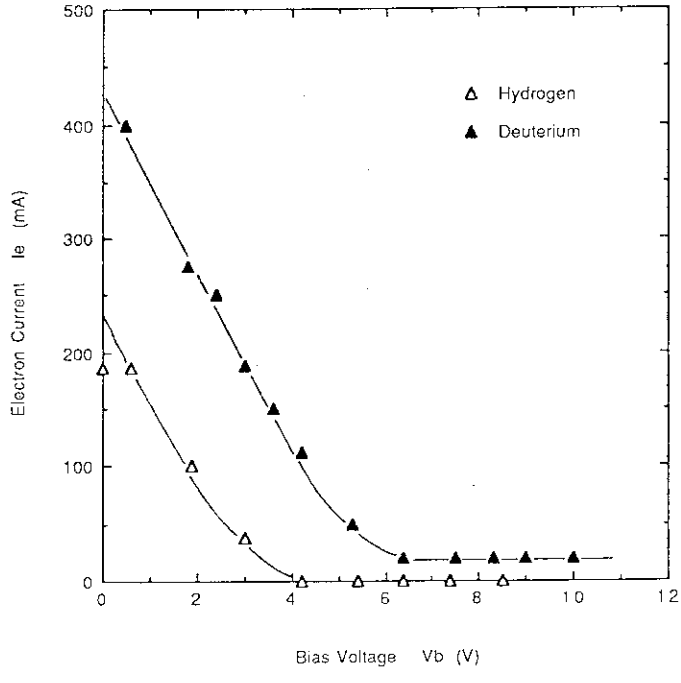

Fig. 3.1.5-2 Electron currents as a function of plasma grid bias voltage.

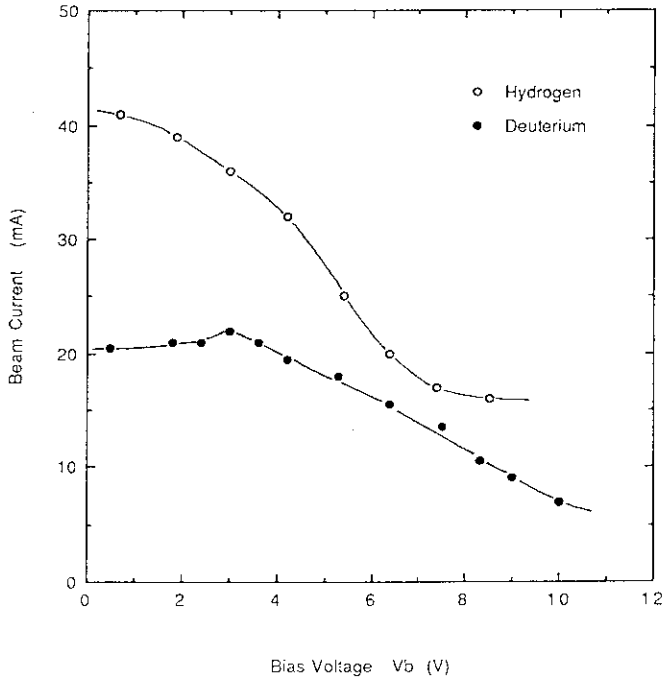

Fig. 3.1.5-3 Ion currents as a function of plasma grid bias voltage.

3.1.6 Other Optimizations

Many challenges, some of them were successful and some were not, have been performed in order to enhance the H^- current density.

(1) Chamber depth optimization [1]

The One Ampere Negative Ion Source was designed so that the arc chamber depth can be changed by installing or removing the side wall units. The H^- productions for three different chamber depths of 7cm, 11cm, and 17cm were examined.

The motivation to optimize the thickness of the source plasma is to investigate the location of the H^- production region in the arc chamber. The thin plasma will reduce the collisional loss of the vibrationally-excited molecules. Additionally, it can be expected that H^0 particles, which cause the loss of H^- by electron detachment process, will be decreased. These are considered to be reasons why a sheet plasma was successful as reported by J.Uramoto [2].

From a Langmuir probe measurement, it was confirmed that the plasma density increased with decreasing the chamber depth for a constant arc power. Thus the plasma density seemed to be proportional to the power density. The plasma thickness produced in "7 cm chamber" was only 3 cm with the peak density of $5.6 \times 10^{12}/cm^3$, which was three times higher than that of "17 cm chamber".

The H^- current densities for the three cases are shown in Fig. 3.1.6-1. In spite of a big difference of the plasma density profile, the H^- current densities were not affected very much by the plasma properties. The highest current densities achieved were about 22 mA/cm^2 for each case.

(2) Pre-dissociation of hydrogen molecules

Whether or not is the atomic hydrogen a "poison" for H^- production? It was discussed at IAEA workshop at Culham in 1987 [3]. The One Ampere Source seemed convenient for the pre-dissociation experiment; the discharge chamber was divided into two regions by a copper thin plate with cusp magnets. Several apertures were drilled on the dividing plate. By turning on the intense arc discharge in the upper chamber, atomic hydrogens are formed by the dissociation of H_2 molecules, and are

supplied through the apertures into the lower discharge chamber. Checking the difference between H^- current obtained with and without discharge in the upper chamber, the answer is given quite easily.

The result shows that the H^- current increases with the arc discharge power supplied in the upper chamber. It seemed that the increase was due to supplemental power input from the plasma leaking through the dividing plate. We could not have a conclusion about the influence of the atomic hydrogen on the negative ion production.

(3) Gas mixing experiment [4]

The gas mixing into the arc discharge plasma was performed from an interest how the H^- production was affected by the electron density in the extraction region. A significant increase of H^- yield was reported by argon or xenon mixing at LBL [5]. However the data could not be reproduced by Ar mixing at JAERI. The result obtained by the One Ampere Source is shown in Fig.3.1.6-2. Actually, the extraction current increased more than a factor of two by Ar mixing. This indicates that the electron density in front of the plasma grid was increased. On the other hand, H^- current kept constant for the pressure region concerned.

In addition, it was tested to mix the air into the chamber as a check of air leak effect on the H^- production. Once the air introduced into the source during the discharge, H^- current was reduced by several tens of percent. In order to recover the H^- current, it was necessary to clean up the chamber wall surface.

(4) Mistery of filament on H^- production

One of the important R&D issues on the high current negative ion source is the cathode. Although the experiments described in this section have been performed with tungsten filaments, it seems hard to use it in the NBI for fusion reactor from the view point of filament life.

An R&D on a long life cathode is mentioned in sub-section 3.6.1. However, the other crucial problem is the compatibility with the negative ion production. From this aspect, several trials have been performed for investigating the effect of the filament diameter, the filament current, and the filament number.

Concerning the filament current, we observed that H^- current increased after the filaments turned off. Since the magnetic field

formed by the heater current interferes in the source cusp field, the plasma, which is not suitable for the H^- production, will be produced. The thinner the filament diameter is, the smaller is the heater current required for maintaining the discharge. Therefore, this interference can be reduced by a thinner filament. It was also found that the increase of the filament number installed in the source decreased H^- current. This is due to increase of the cathode area immersed in the plasma, i.e. the ion loss area, then the reduced plasma density lead to a decrease of the H^- yield.

Hall et al.[6] reported that the population of vibrationary excited molucules are strongly affected by a filament materials. We also tested tungsten and tantalum filaments, and observed about 50 % of increase in H^- current at maximum[7]. It seemed that the filament material deposited on the chamber wall has some effects on H^- production.

(5) Effect of Chamber wall material [8]

Ehlers et al.[9] and Fukumasa et. al.[10] reported the wall effect on H^- production in low density plasmas. In order to clarify the effect even at a high density plasma condition, and also from the study mentioned above (4), the chamber surface materials were changed by depositing some metals on the chamber wall surface. The dependence of H^- current density on the gas pressure in the chamber is shown in Fig. 3.1.6-3. Three cases of the wall conditions (W, Al and Cu) were plotted in the figure. It was apparently different by the chamber wall conditions. It was confirmed that the surface affects the volume produced H^- yield even at the high plasma density conditions. Aluminum surface gives about 20 % higher H^- ion yield than copper (main material of the ion sources) or tungsten (usually the wall is covered with the filament material).

Reference

[1] K. Watanabe et al., Proc. 12th Symp. on Fusion Eng., Oct. 12-16, (1987) Monteray

[2] J. Uramoto, Institute of Plasma Phys. report, IPPJ-852, (1987), Nagoya

[3] For example, A. M. Bruneteau et. al., Proc. IAEA Tech. Committee Meeting on Negative Ion Beam Heating, 15-17 July, (1987), Culham

[4] Y. Okumura, ibid.
[5] K. N. Leung, K. W. Ehlers, and R. V. Pyle, Rev. Sci. Instrum. 56 (1985) 2097
[6] R. I. Hall et. al., Phys. Rev. Lett., 60/4 (1988) 337
[7] M. Bacal, "Investigation of volume H^- ion sources", Report on the visit to the NB group at JAERI NAKA, (1988)
[8] T. Inoue, Presented at "3rd Kakuyugo Rengoh Kohenkai", (1988), Tokyo
[9] K. W. Ehlers et. al., Proc. 4th Symp. on Production and neutralization of negative ions and beams, BNL, Upton, (1986) 282
[10] O. Fukumasa et. al., J. Phys. D : Appl. Phys. 20 (1987) 237

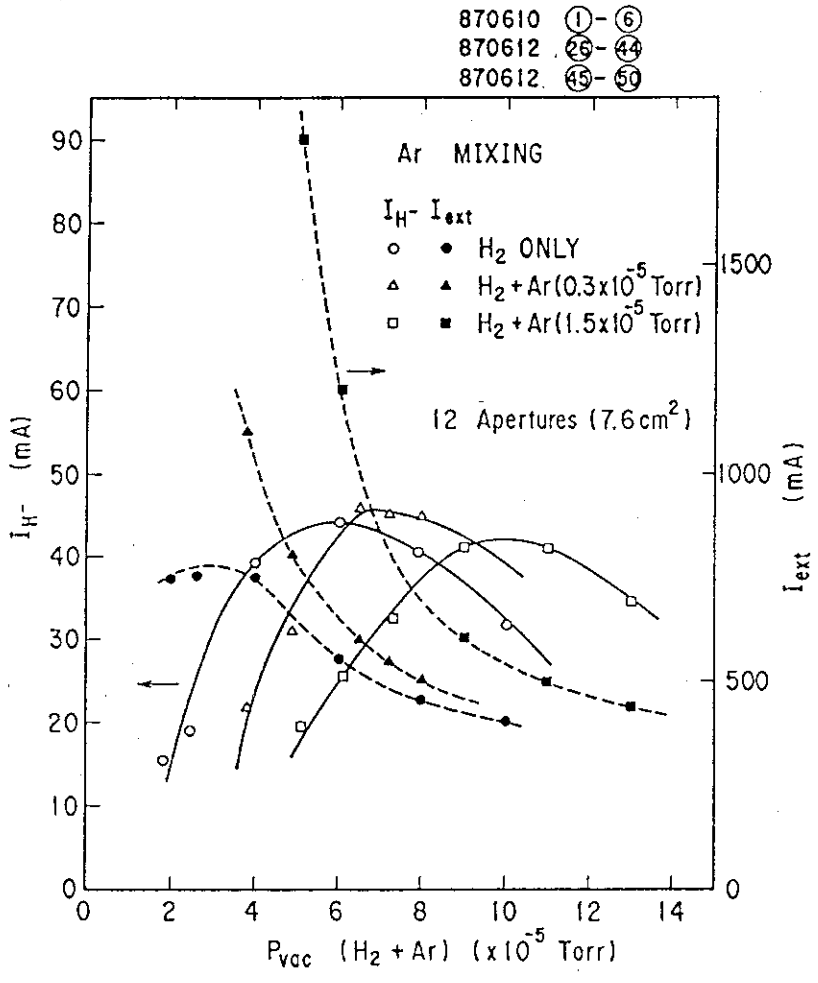

Fig. 3.1.6-1 H^- current densities as functions of the arc discharge current. The chamber depth was changed for three cases.

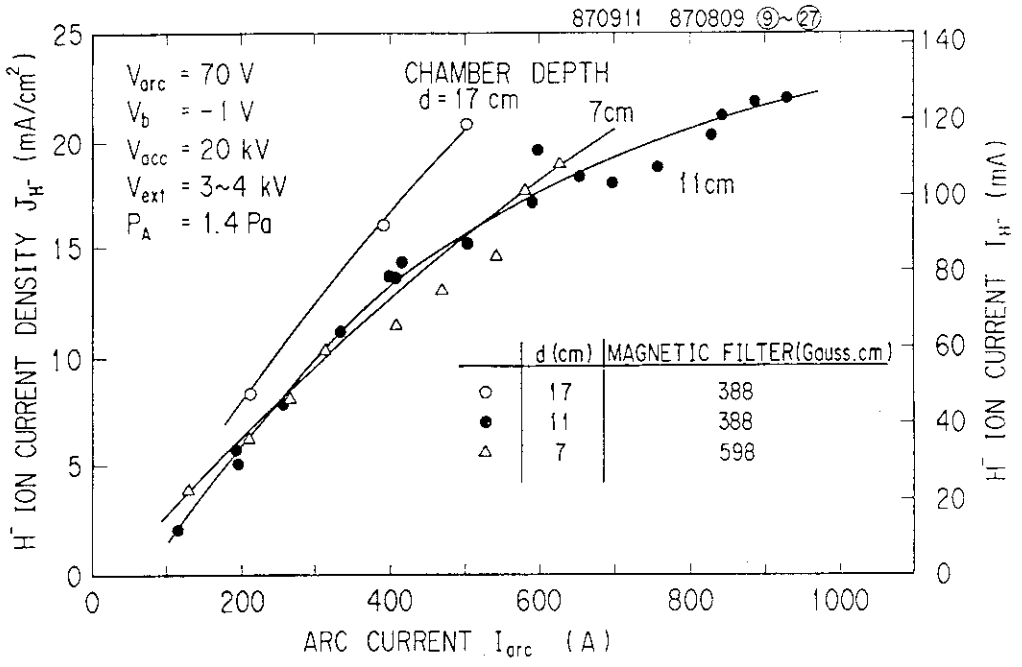

Fig. 3.1.6-2 Effect of argon mixing into the arc discharge. The extraction current (Iext), or electron current, increased significantly by argon mixing, while H^- current was almost constant.

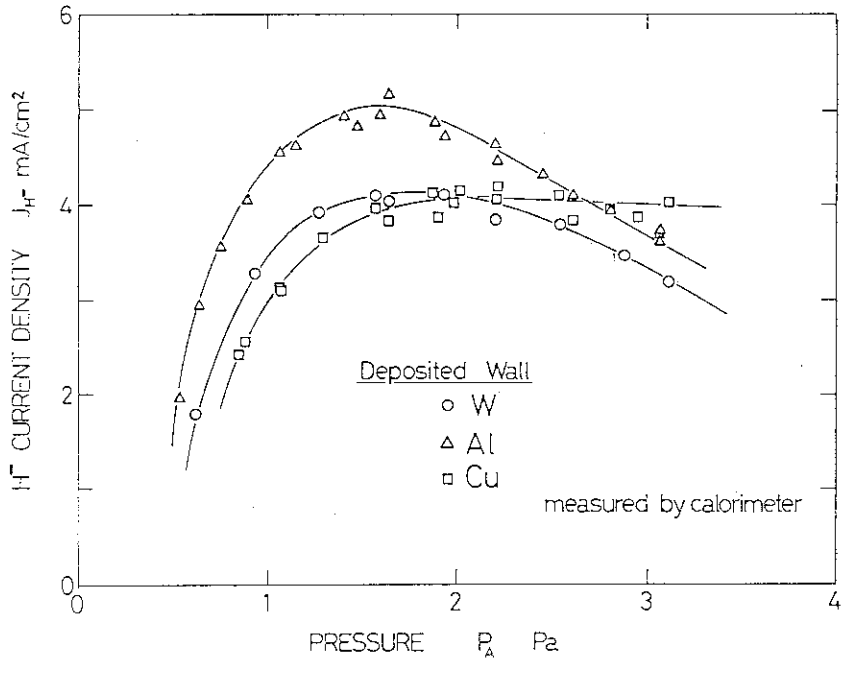

Fig. 3.1.6-3 The dependence of H^- current density on the gas pressure in the chamber. Three cases of the wall conditions (W, Al and Cu) were plotted in the figure.

3.1.7 Impurities in the H^- Ion Beam [1]

The impurity concentration in the H^- ion beam was measured by a momentum mass analyzer. Figure 3.1.7-1 shows an example of the mass spectrum, which was obtained in the Multi-Ampere H^- Ion Source at the H^- ion current of 4.8 A and the beam energy of 50 keV. In the spectrum, there are some impurity peaks of O^- and OH^-. The peak at M=15.1 corresponds to the O^- ions dissociated from OH^-. We have scanned the mass number up to M=200, but no metal impurity was observed.

Since the line density of the residual hydrogen gas from the ion source to the mass analyzer is as high as 5×10^{15} molecules/cm^2, some of the negative ions are converted to positive ions. Taking into account the conversion efficiency, the O^- impurity in the original ion beam was estimated to be 0.8 %. The concentration is typically a few percent at the beginning of the experiment, but it decreases to less than one percent by discharge cleaning of the source.

The impurity level was confirmed by Doppler-shifted spectroscopy of the beam. Figure 3.1.7-2 shows a spectrum of Doppler-shifted Balmer-alpha light. Besides the peaks of full and extraction energy particles, we can see a small peak at energy of E/17, which corresponds to H atoms dissociated from OH^- ions. Taking into account the excitation cross section, we estimated the OH^- impurity level to be around 1 %, which was consistent to the momentum mass analysis.

Reference

[1] Y.Okumura, H.Oohara, M.Hanada, Y.Matsuda, and H.Kojima; Japan Atomic Energy Institute Report JAERI-M 89-090 (1989)

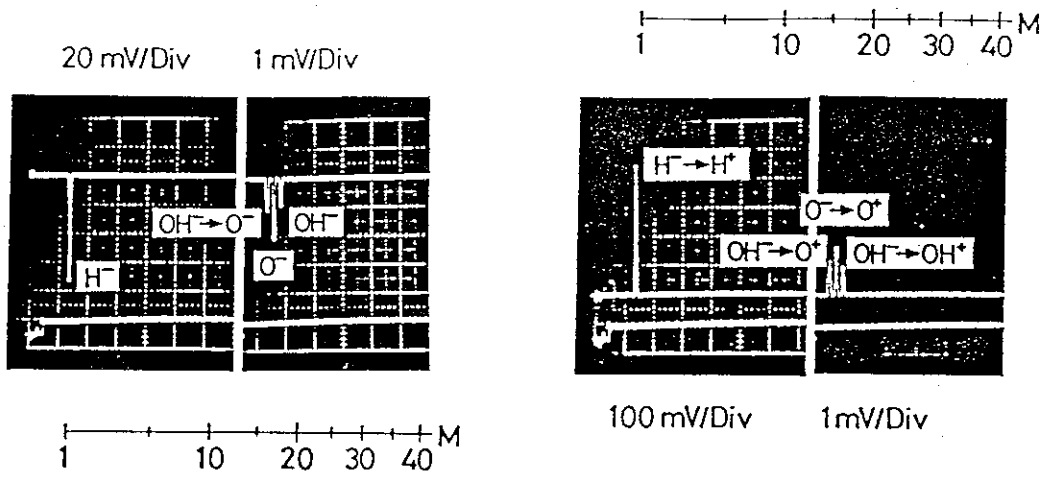

Fig. 3.1.7-1 An example of the mass spectrum measured in the Multi-Ampere H^- Ion Source at 4.5 A, 50 keV.

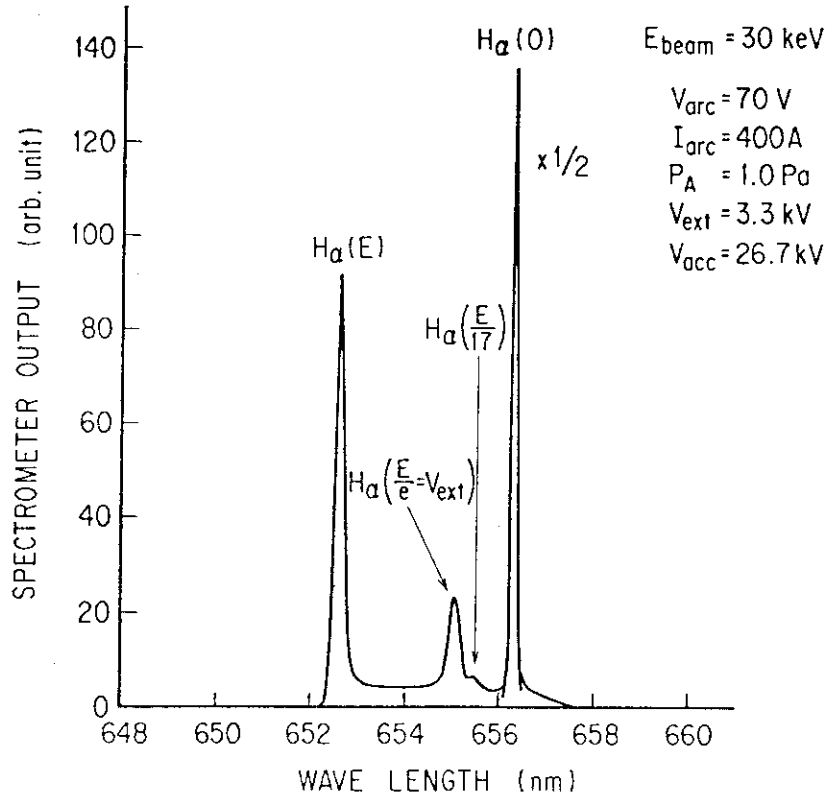

Fig. 3.1.7-2 Doppler-shifted spectrum of Balmer-alpha light of the negative ion beam. The very small peak at $E=E_{beam}/17$ corresponds to the signal from the hydrogen particles dissociated from OH^-.

3.2 Electron Suppression

Since the negative ions are produced in a plasma and have no more than thermal energies (< 1 eV), a large amount of electrons are extracted together with the negative ions in the volume source. Those electrons not only reduce the acceleration efficiency but also cause a severe heat dissipation in the extractor and the accelerator grids. Therefore, electron suppression is one of the key subjects which should be studied.

3.2.1 Effect of Bias Voltage

Biasing the plasma grid electrically in positive with respect to the anode is very effective to suppress the electron extraction[1]. Figure 3.2.1-1 shows the typical dependence of the extracted electron and negative ion current on the bias voltage. This data was taken in the Multi-Ampere Source [2] in Cs-free operation. The extracted electron current, which is nearly equal to the extraction current (I_{ext}), decreases significantly when the grid is biased positively, while the H^- ion current is almost constant for negative bias voltage and decreases slightly at high positive bias voltage. The Multi-Ampere Source is operated typically at V_b= +2 V, where the electron current is about five times larger than the negative ion current. However, if we permit the reduction of the negative ion current by about 30 %, the electron current can be suppressed to nearly the same value with the negative ion current by biasing the grid above +5 V.

3.2.2 Electron Suppression in the Extractor [3]

Even if the bias voltage is optimized, a substantial amount of electrons are extracted with the negative ions. In order to prevent those electrons from escaping to the acceleration region, the One-Ampere and the Multi-Ampere Sources employ an extraction/acceleration grid system. In this system, a large amount of electrons are extracted together with the negative ions by applying a potential up to a few kV as a first step. Then those electrons are deflected by a transverse magnetic field, which is formed by a pair of small magnets inserted in the extraction grid, and strike the grid wall. Only the negative ions pass through the extraction region and enter the acceleration region to be accelerated further. A cross section view of the grid system is

shown in Fig. 3.1-1 together with the electrical connection of power supplies. The unique feature of our grid system is that there is an additional grid called electron suppression grid. This grid is introduced to make an electrostatic barrier against the secondary and the reflected electrons emitted from the extraction grid.

Figure 3.2.2-1 shows an experimental result on electron suppression which was obtained in the same grid geometry as the One-Ampere Source. The electron suppression factor, that is defined by the ratio of the escape electrons to the extracted electrons ($=(I_{acc}- I_{H}-)/(I_{ext}- I_{H}-)$), was measured as a function of extraction voltage for various strength of the deflection magnets. It was found that, without the suppression grid, the electron suppression is very difficult due to the escape of secondary electrons (see the solid lines in the figure). However, by introducing suppression grid and applying a negative potential to the grid with respect to the extraction grid, the factor decreases considerably as shown by the broken line.

In summary, the electron current in the accelerator region could be suppressed to almost zero by biasing the plasma grid and employing the three grid (plasma, extraction and electron suppression grids) system.

References

[1] K. N. Leung et al.; Rev. Sci. Instrum. 54 (1983) p.56.

[2] M. Hanada et al.; Rev. Sci. Instrum. 61 (1990) p.499.

[3] Y. Okumura et al.; Proc. 11th Symp. on Fusion Engineering, Austin, Texas, (1985) p.113.

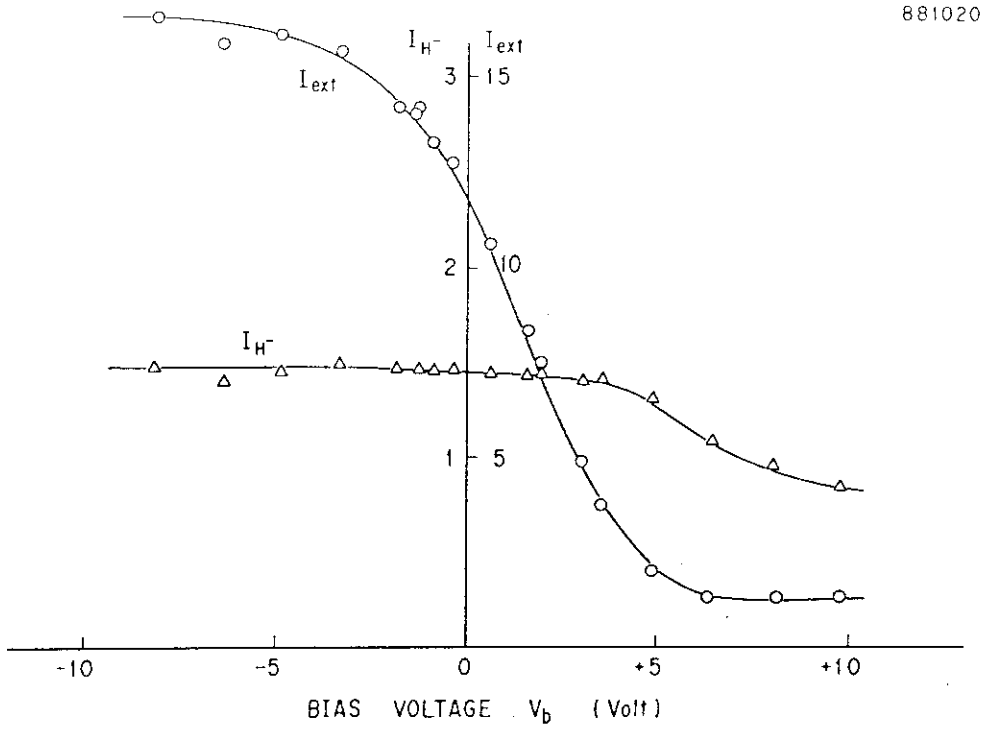

Fig. 3.2.1-1 Dependence of extraction current (I_{ext}) and the H^- ion beam current (I_{H^-}) on the bias voltage of plasma grid. The extraction current is a sum of extracted electron and the H^- ion currents ($I_{ext} = I_e + I_{H^-}$). The electron current decreases significantly as the grid was biased positively.

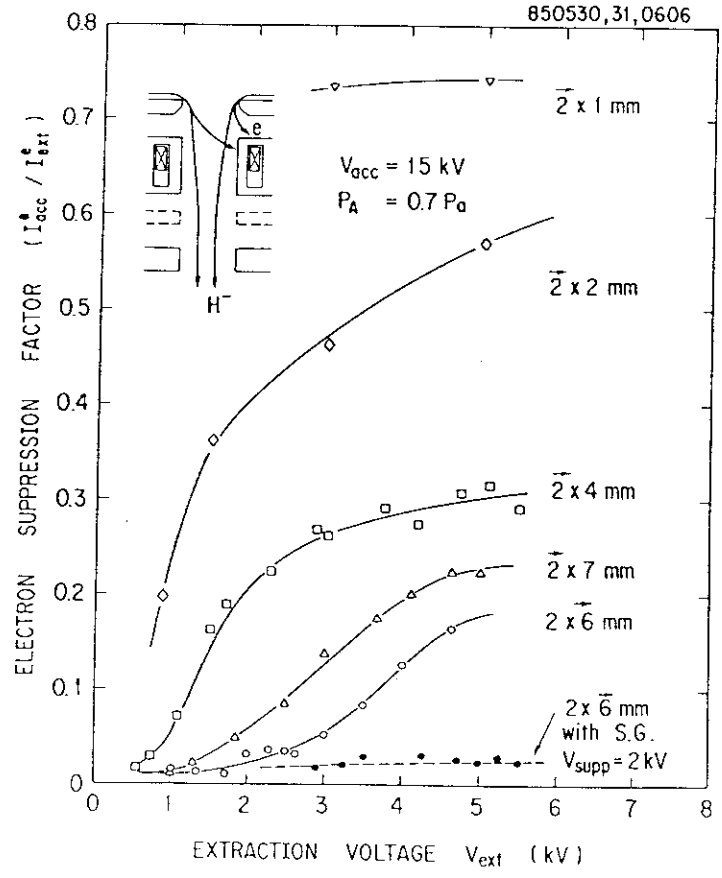

Fig.3.2.2-1 Dependence of electron suppression factor on extraction voltage for various magnetic configurations. Effect of the electron suppression grid is shown by a broken line.

3.3 BEAM EXTRACTION

3.3.1 Negative Ion Extraction Characteristic

The H^- extraction seemed considerably different from that of positive ions, since the H^- extraction is accompanied with high current of electron. Additionally, transverse magnetic field which may also affect the H^- extraction is formed by a pair of magnets installed in the second grid to suppress the electron current.

We usually plot the negative ion current as a function of extraction voltage applied between the plasma (first) grid and the extraction (second) grid. An example of H^- and D^- (and also electron) extractions is shown in Fig. 3.3.1-1. A problem is how to account the electron current into the characteristics. In the figure, D^- and electron currents are normalized to produce the same space charge equivalence as H^-, i.e. D^- current is multiplied by 2 and electron one is divided by 1800 [2].

When the extraction voltage is low, the H^- equivalent current increases steeply as the voltage, that is proportional to $V^{3/2}$ [2,3,4] like positive ion extraction. This indicates that the negative ion extraction including electrons in this region is dominated by the Child-Langmuir law.

For extraction voltage above a threshold, there is a gentle rise in H^- and D^- currents. This change for weaker dependence (or limit) is interpreted as emission limit [3] or "depletion [5]" of negative ions. Then the gentle rise is supposed to be a "fringing effect" of the plasma boundary [6].

References

[1] T. Inoue et al., Rev. Sci. Instrum. 61/1 (1990) 496
[2] J. W. Kwan, private communication
[3] R. McAdams et al., 4th Int. Symp. on Production and Neutralization of Negative Ions and Beams, Brookheaven, NY. (1986) : AIP Conf. Proc. 158, 298, Ed. by J. G. Alessi
[4] J. H. Whealton et al., Proc. 3rd European Workshop on Production and Application of Light Negative Ions, Amsterdam, 3 (1988)

[5] M. Bacal, J. Bruneteau, P. Devynck, 4th Int. Symp. on Production and Neutralization of Negative Ions and Beams, Brookheaven, NY. (1986) : AIP Conf. Proc. 158, Ed. by J. G. Alessi

[6] Y. Okumura, private communication

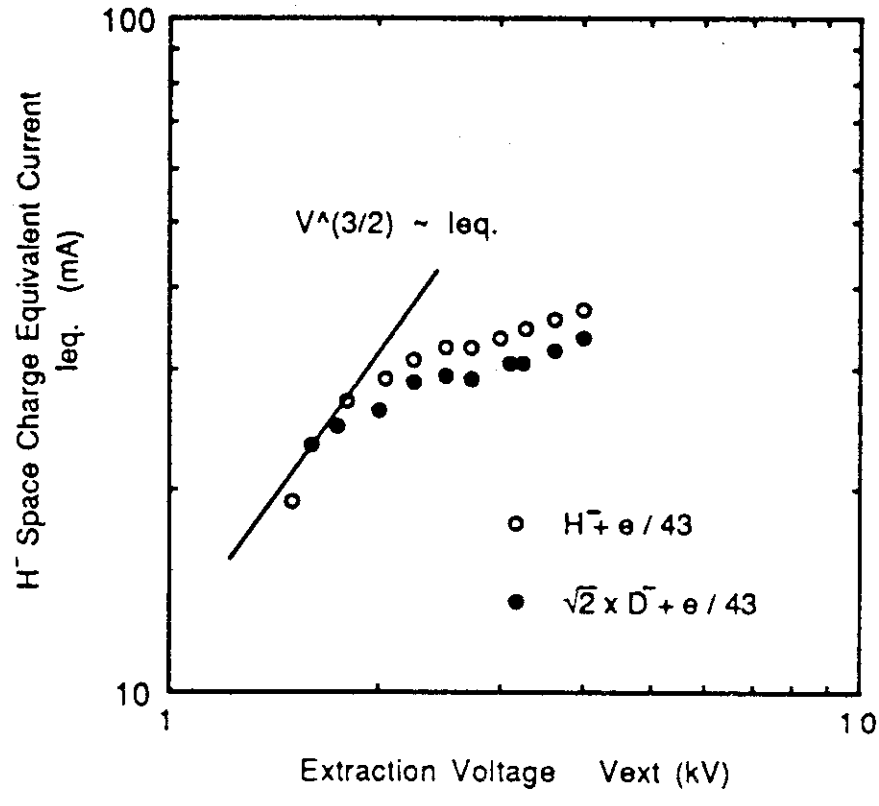

Fig. 3.3.1-1 The extraction characteristic of negatively charged particles from an arc discharge plasma. The currents are normalized as to produce the same space charge equivalence as H^-.

3.3.2 Optimization of Negative Ion Extractor

Prior to the high energy beam experiment, we are testing a beam optics of an extractor combined with a pre-accelerator as an initial test of a pure volume source at ITS-2a. Fig. 3.3.2-1 illustrates the configuration. The beam is produced through a single aperture with an energy of 40 keV or more. In this test, we have measured a very small divergence of H^- beam by Faraday cup. The beam divergence angle defined by the e-folding half-width was estimated to be 2.4 mrad.

The measurement is available to H^- temperature estimation, because, if we neglect beam aberration in electrostatic lens, the beam divergence is simply defined by H^- temperature. Although the profile measured has a two dimensional structure, the minimum value is taken for the estimation, which seems to contain smaller aberration component. Assuming that the ion temperature distribution function in the source is Maxwellian, the temperature limited divergence is given by the following equation:

$$\omega_T = \frac{\sqrt{\pi}}{2}\sqrt{\frac{T_{H^-}}{E}}$$

Where E and T_{H^-} are the beam energy and the ion temperature respectively. Substituting $_T$ = 2.4 mrad, and E = 40 keV, the H^- temperature is estimated to be T_{H^-} = 0.3 eV, which is considerably low compared to that of the positive ion beams.

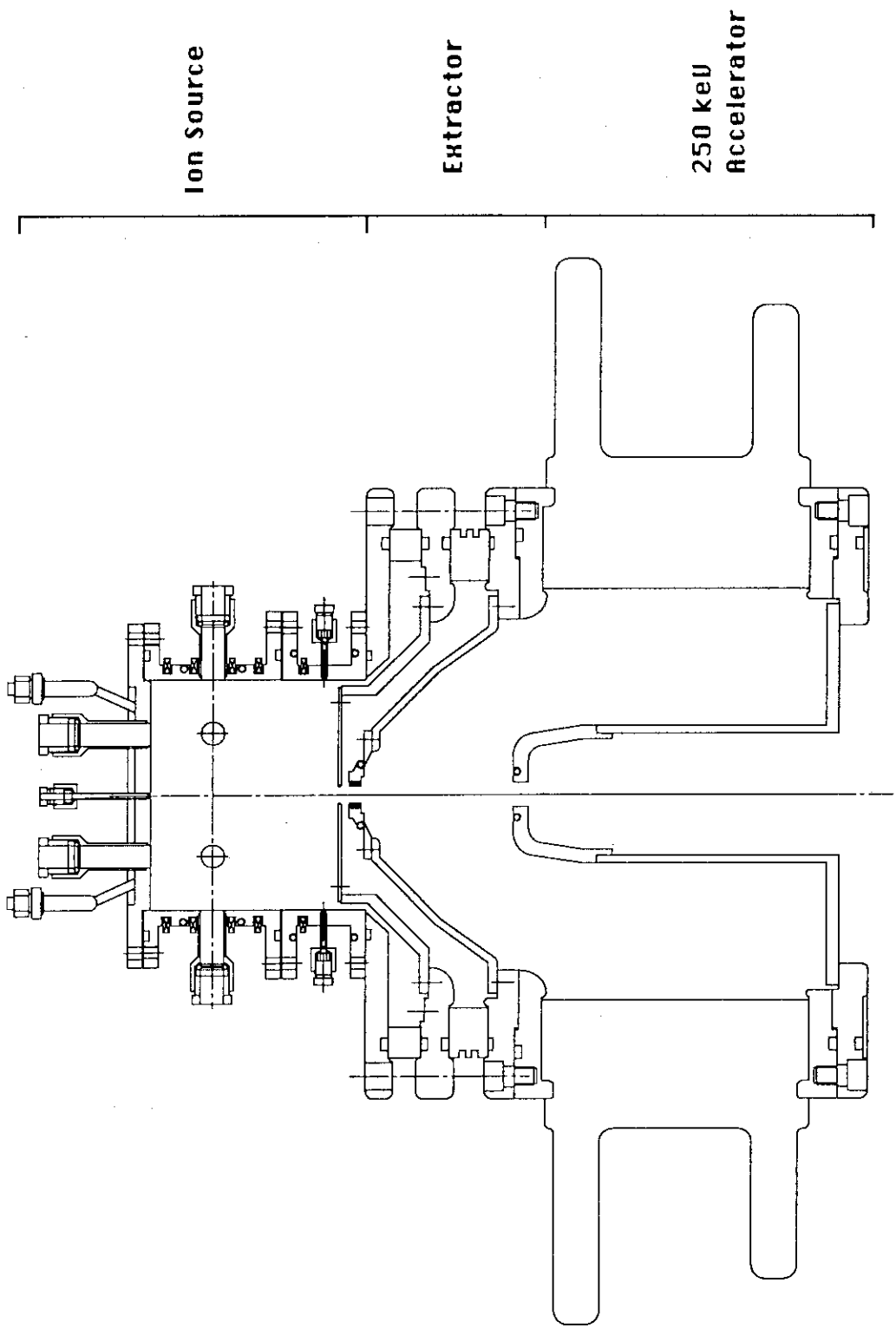

Fig. 3.3.2-1 A schematic diagram of ITS-2a extractor and pre-accelerator.

3.3.3 Beam Optics of the Multi-Ampere Source

An accelerator of a high energy ion source is composed of a pre-accelerator and a main-accelerator. Optimization of the beam optics in the pre-accelerator which accelerate the negative ions up to about 50 keV is important to obtain a small beam divergence less than 5 mrad (0.29 degrees, e-folding half-width) for the next NBI system. The accelerator of the multi-ampere ion source which produced 10 A negative ion beams [1] corresponds to the pre-accelerator of the high energy ion source. Therefore, we investigated and optimized the beam divergence by utilizing the multi-ampere ion source. The result of the simulation using the two-dimensional code [2] for the positive ion beam was compared with the experimental results and the applicability of the 2D code to the negative ion beam simulation was investigated [3,4].

Figure 3.3.3-1 shows a schematic of the accelerator of the multi-ampere negative ion source. The negative ion beams were extracted from the multi-aperture extractor which has 434 apertures within the area of 15 cm X 40 cm. The beam divergence was measured at the position of 1.85 m from the ion source. The beam divergence was evaluated assuming that the ion beam is produced from a point source. Figure 3.3.3-2 shows the beam divergence as a function of the extraction voltage. Optimum extraction voltages are varied with the acceleration voltage. The minimum beam divergence obtained under the point source assumption is limited to 2.4 degrees, because the beam divergence was measured near the source, namely, 1.85 meters from the accelerator. The broken line shows the beamlet divergence by the 2D computer simulation. since the tendencies of the beam divergence variation agreed well with the experimental results, the 2D simulation code for the positive ion beam can be applied to the negative ion beam simulation. A typical example of the simulation is shown in Fig. 3.3.3-3.

More precise simulation including electrons can be done by the modified three-dimensional computer code [5] which was originally developed by K.Ota [6]. Figure 3.3.3-4(a) shows an example of 3D beam orbits of negative ions and electrons. The current densities of the negative ions and electrons are 10 mA/cm^2 and 50 mA/cm^2, respectively. The acceleration voltage is 23 kV. Figure 3.3.3-4(b) shows a cross sectional view of the accelerator. The electrons are reflected by the

magnetic field which is produced by the permanent magnets in the extraction grid. The H^- ion trajectories are scarcely affected by the magnetic field.

References

[1] H. Kojima et al., Proc. 13th Symp. on Ion Source and Ion-Assisted Technology, Tokyo, 1990, p.145.
[2] Y. Ohara : Japan Atomic Energy Research Institute Report JAERI-M 6757 (1976).
[3] K. Watanabe et al., Proc. 13th Symp. on Ion Source and Ion-Assisted Technology, Tokyo, 1990, p.153.
[4] K. Watanabe et al., Proc. 2nd Int. Symp. on Advanced Nuclear Energy Research, Mito, 1990, p.447.
[5] Y. Ohara : Electron space charge and 3D magnetic field are taken into consideration.
[6] K.Ota et al., Kakuyugo Kenkyu, 52 (1984)(in Japanese).

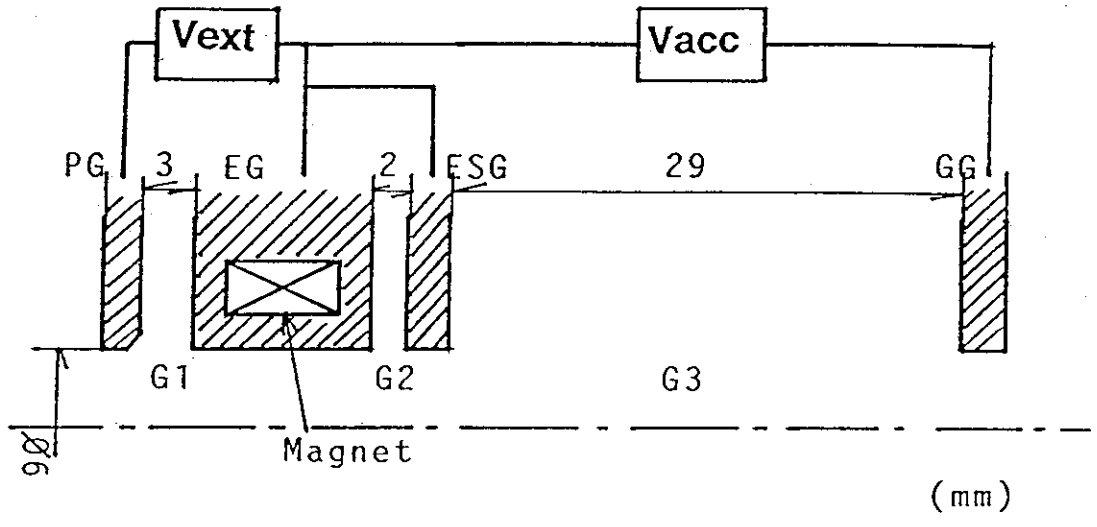

Fig. 3.3.3-1 A cross-sectional view of the 50 keV accelerator of the multi-ampere negative ion source.

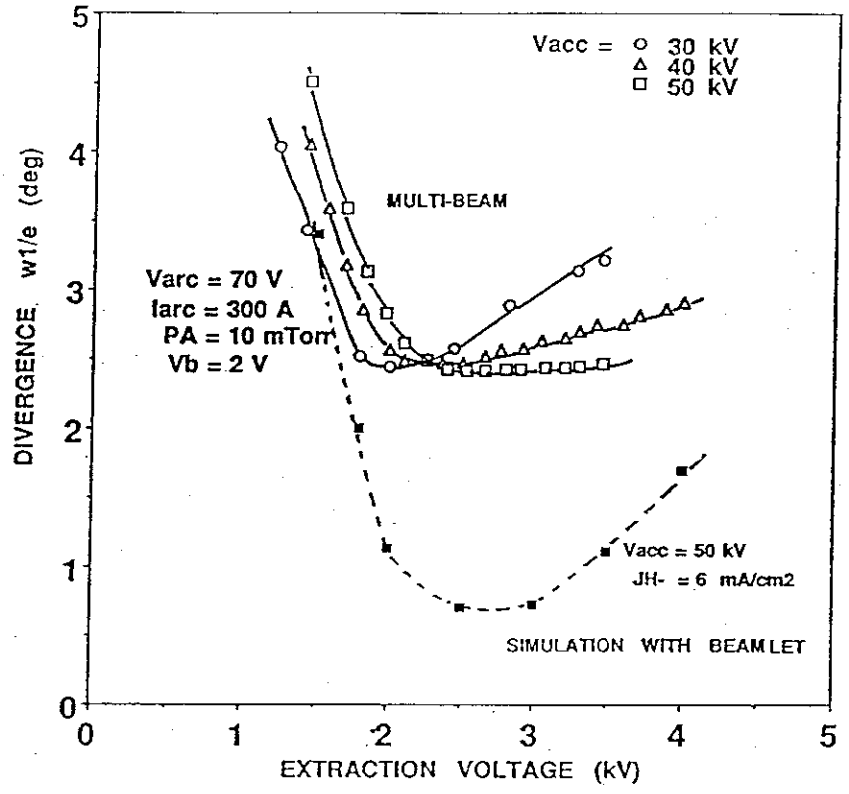

Fig. 3.3.3-2 Beam divergence as a function of the extraction voltage.

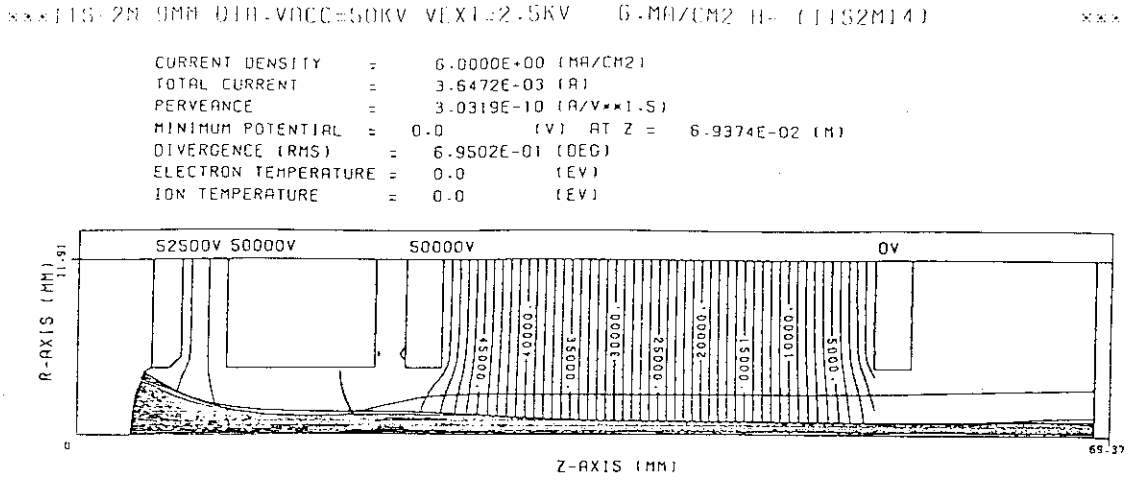

Fig. 3.3.3-3 An example of the beam orbit simulation.

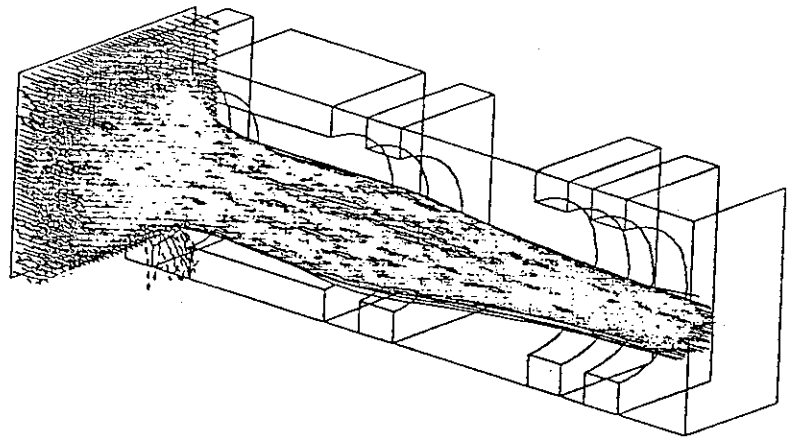

VPL=-23.10(KV)
V1 =-23.00(KV)
V2 =-20.00(KV)
V3 =-20.00(KV)
V4 = 0.0 (KV)
V5 = 0.0 (KV)
TE = 1.00(EV)
TI = 1.00(EV)

	J (MA/CM**2)	R	Z	THETAX (DEG)	THETAY (DEG)	OMEGAX (DEG)	OMEGAY (DEG)
———	1.00E+01	1.00E+00	-1.00E+00	0.0	1.03E+00	2.71E+00	2.98E+0(
------	5.00E+01	5.44E-04	-1.00E+00	0.0	0.0	0.0	0.0

(a) Beam orbit simulation with the 3D code.

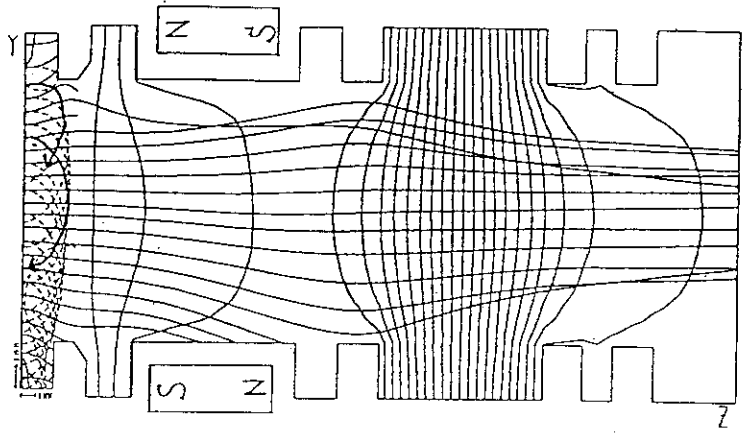

VPL=-23.10(KV)
V1 =-23.00(KV)
V2 =-20.00(KV)
V3 =-20.00(KV)
V4 = 0.0 (KV)
V5 = 0.0 (KV)
TE = 1.00(EV)
TI = 1.00(EV)

	J (MA/CM**2)	R	Z	THETAX (DEG)	THETAY (DEG)	OMEGAX (DEG)	OMEGAY (DEG)
———	2.00E+01	1.00E+00	-1.00E+00	0.0	-2.69E-01	3.43E+00	3.71E+00
------	1.00E+02	5.44E-04	-1.00E+00	0.0	0.0	0.0	0.0

(b) A cross sectional view of the accelerator.

Fig.3.3.3-4 3D simulation of the trajectories of negative ion beams and electrons in the extraction region.

3.4 Beam Acceleration and Transport

3.4.1 Multi-single Type Acceleration [1]

One of the most important points in developing a high energy and multi-ampere negative ion accelerator is to suppress the stripping loss of beam ions in the accelerator due to the collisions with the background gas molecules. In the conventional multi-aperture type accelerator as shown in Fig. 3.4.1-1(a), where each beamlet from the pre-accelerator is accelerated through an individual channel of the main accelerator(multi-multi type), it is difficult to lower the gas conductance. Hence, we proposed an accelerator with high gas conductance, where multiple beamlets from the pre-accelerator are merged into a single large beam in the main-accelerator(multi-single type). This acceleration system makes it possible to reduce the stripping loss approximately by half compared with that in the multi-multi type accelerator.

A multi-single type accelerator which can deliver a 500keV D^- sheet beam has been designed using a two-dimensional ion beam simulation code [2]. Figure 3.4.1-1(b) shows one of the optimum system, where three sheet beamlets from the pre-accelerator are merged in the main accelerator. Electrons accompanied by the negative ion beams are deflected by the transverse magnetic field produced by the magnets installed in the second electrode and are dumped on it. In order to obtain a good beam optics with this system, optimization of the beam emittance at the exit of the pre-accelerator is essential. Namely, the convergence angle and the steering angle of each beamlet must be optimized. The convergence angle are determined so as to compensate the space-charge-expansion in the main-accelerator, since the focusing effect can not be expected in the main-accelerator. The peripheral two beamlets are steered so as to be merged into the central beamlet and to be a large single beam with good beam optics. In this design, the steering is performed by the axial displacement of the central two rods in the fourth electrode.

Figure 3.4.1-2 shows a design of 500keV main-accelerator where 5 beamlets are merged. With increasing number of beamlets to be merged, the required electric field strength in the main-accelerator becomes

high. Therefore, the maximum number of the beamlets will be limited by the voltage holding characteristics of the accelerator.

References

1. Y. Ohara, Y. Matsuda, Y. Okumura, and K. Watanabe ; Proceedings of the 12th Symp. on Ion Sources and Ion-Assisted Technology, pp.143-146, Tokyo (1989).

2. Y. Ohara : BEAMXY code simulating a non-axisymmetric sheet beam (X-Y)in a transverse magnetic field (Z).

(a) Multi-Multi Type Accelerator

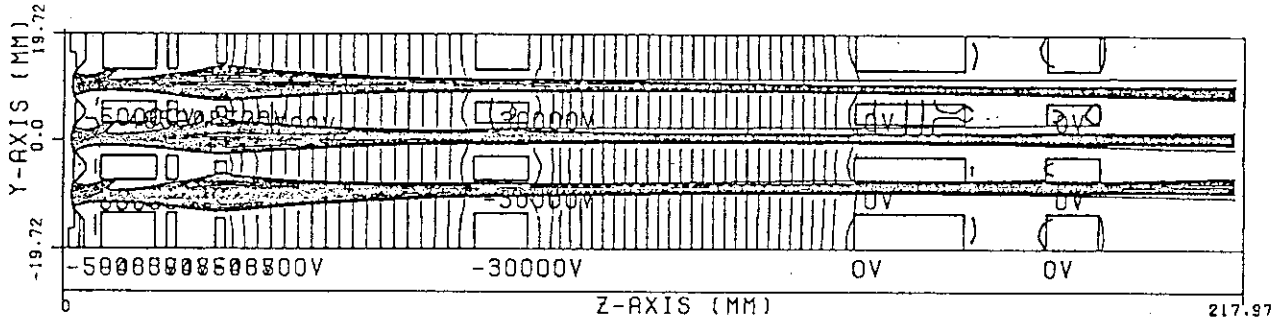

(b) Multi-Single Type Accelerator

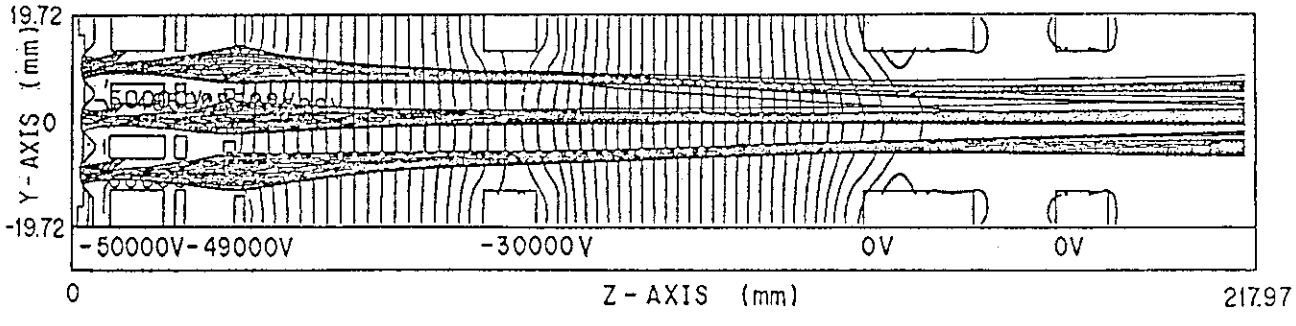

Fig. 3.4.1-1 A 2D sheet beam simulation in a 500keV negative ion accelerator. The D^- ion current density and the electron current density at the emitter are assumed to be 50mA/cm^2 and 1000mA/cm^2, respectively.

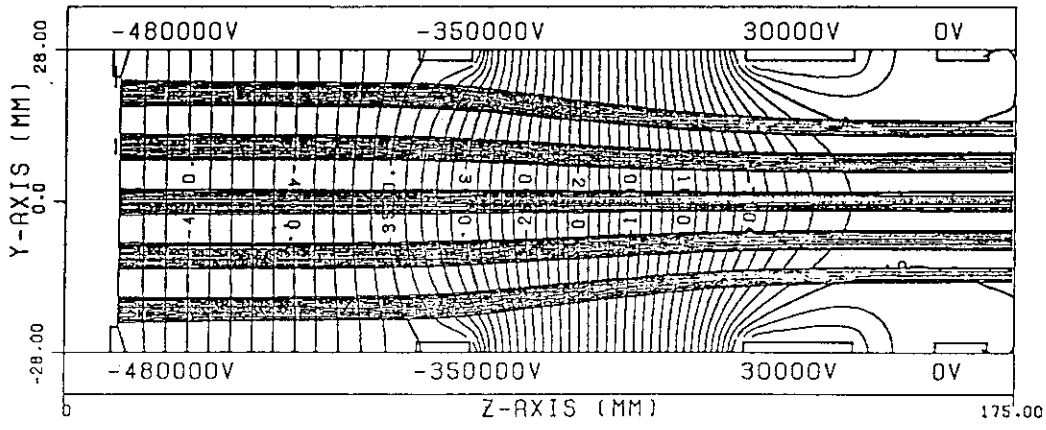

Fig. 3.4.1-2 Five convergent sheet beamlets from the extractor are merged in a 500keV main accelerator. Each beamlet with the D^- current density of 50mA/cm^2 is injected in the main accelerator at an initial energy of 20keV.

3.4.2 Experiment Simulating 500 keV Acceleration

The design of the multi-single type 500 keV accelerator as described in the precedent sub-section, has been tested experimentally [1]. This accelerator consists of a pre-accelerator and a main-accelerator. Each electrode in the pre-accelerator has three slots whose dimensions are 5 mm X 50 mm, and the electrode in the main-accelerator has a slot of 26 mm X 70 mm with high gas conductance. In order to demonstrate the possibility of the merged beam acceleration with small divergence, we measured the beam divergence at the beam energy of 50 keV keeping the same perveance of 500 keV acceleration. Figure 3.4.2-1 shows the configuration of the accelerator and the beam orbits. Figure 3.4.2-2 shows the beam divergence as a function of extraction voltage. There is an optimum extraction voltage for a fixed acceleration voltage. Furthermore, the beam divergence became small with increasing acceleration voltage. The range of optimum extraction voltage became wider with high acceleration voltage. These experimental result shows that the three beamlets can be merged successfully to a single beam.

References

[1] Y.Ohara. : Proc. 12th Symp. on Ion Sources and Ion-Assisted Technology, Tokyo, 1989, p.143.

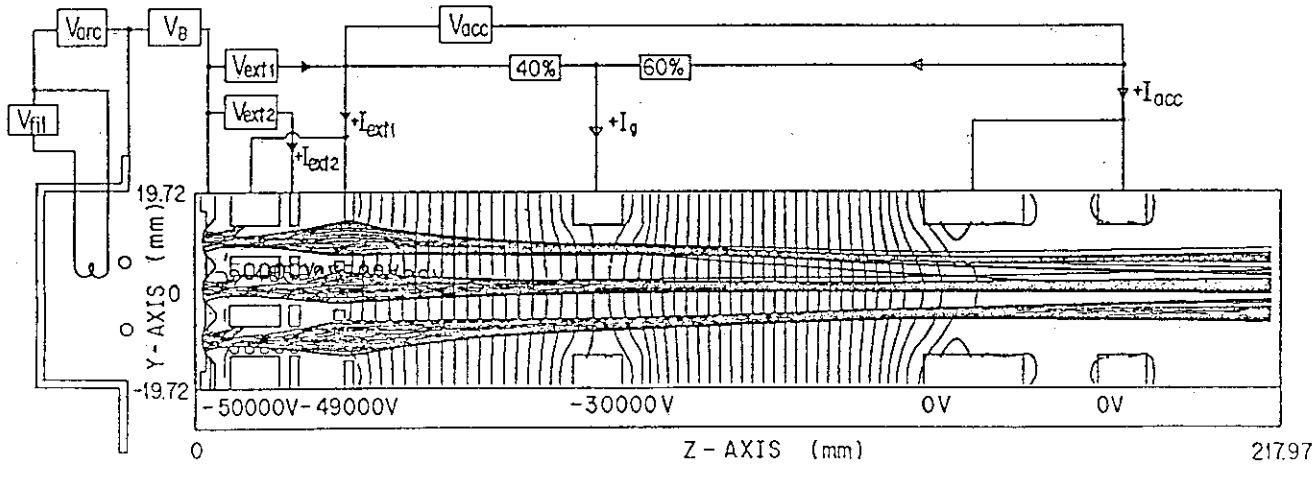

Fig. 3.4.2-1 H^- beam trajectory.

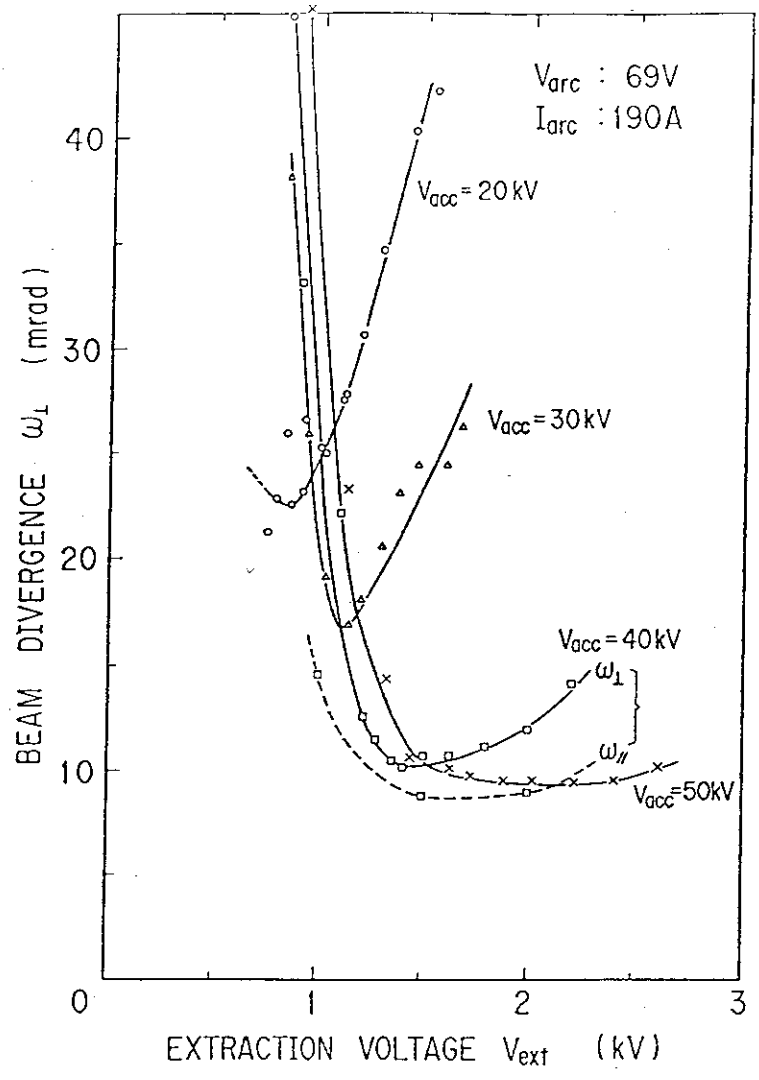

Fig. 3.4.2-2 H^- beam divergence as a function of the extraction voltage as a parameter of the acceleration voltage V_{acc}.

3.4.3 ElectroStatic Magnetic Quadrupole Acceleration (ESMQ)

Electrons are produced in the accelerator due to the electron stripping of the negative ions by collisions with background gas molecules. It is important to prevent the electrons from being accelerated to high energy, because high energy electrons generate X-ray that may decrease the voltage holding of the accelerator and give high heat load on the acceleration grids. For this purpose, Electrostatic Magnetic Quadrupole Acceleration system has been proposed [1]. In this system, magnets are buried in the acceleration grids to produce a quadrupole magnetic field inside the aperture (Fig.3.4.3-1).

A preliminary investigation using a beam envelop code has been carried out. Results are as follows:

1. Electrons are diverged or converged largely in the aperture and most of the electrons cannot go through the downstream aperture.
2. Divergence of negative ions is not disturbed by the magnetic field. Higher current ion beam can be accelerated through each channel with this quadrupole magnetic field.
3. The leakage of the magnetic field from the grid plate is very small. Hence, the negative ion production and the voltage holding characteristics are not influenced.

References

[1] M. Mizuno and Y. Ohara : To be submitted for publication.

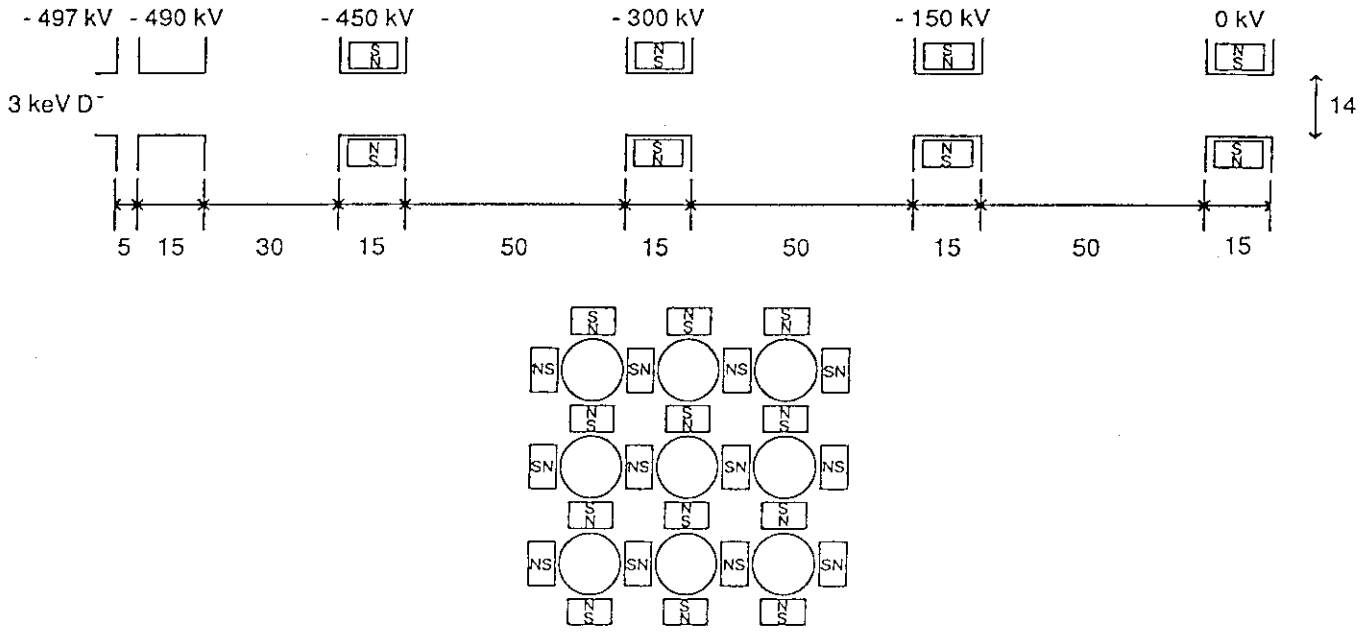

Fig.3.4.3-1 ElectroStatic Magnetic Quadrupole acceletator

3.4.4 4D Emittance Scanner

A four dimensional emittance scanner using a micro channel plate (MCP)[1] has been devised and its performance has been confirmed experimentally.[2] This scanner is composed of a pin hole, a deflection electrode, a two-stage micro channel plate with a fluorescent screen, an ocular lens and a CCD camera, as shown in Fig.3.4.4-1. The pin hole with inner diameter of 5μm is made in the stainless steel foil of 12.5μm in thickness. Beam particles through the pin hole are separated electrostatically by the parallel plate deflection electrodes into negative ions, positive ions and neutrals. Each particle collides with the surface of MCP, causing an electron avalanche in each micro channel. The amplified electron beam is accelerated further to the surface of the fluorescent screen and makes an image of beam particles on the screen. The image on the screen is focused by the ocular lens on the CCD camera sensor. The above components are installed in a box, which is scanned two-dimensionally across the beam crosssection. The image on the screen at each scanning point are stored in a digital video memory, and utilized to obtain a 4D emittance diagram, namely a super emittance diagram.[3] The intensity of the image at each point on the screen is expressed by 8 bit data, namely 64 intensity levels.

The performance of this system was confirmed using a small ion source with a single aperture extraction system which can deliver a 14 keV negative hydrogen ion beam. A typical image stored in the digital video memory is shown in Fig.3.4.4-2. The relationship of the incident particle flux and the total counts of the image is shown in Fig.3.4.4-3. The total counts increased linearly with the particle flux so long as the particle flux is less than $4 \times 10^{12}/cm^2 \cdot s$, where the MCP voltage and the screen voltage are 0.95kV and 1.3kV, respectively. A typical 4D super emittance diagram is shown in Fig.3.4.4-4. From this figure, conventional 2D emittance diagrams can also be obtained.

With this system, it is also possible to estimate the gas cell line density by the ratio of the total counts of each beam components. Additionally, it is possible to observe a beamlet steering angle and to obtain a focal point of the multiple beams.

References

1. S. Matsuura, S. Umebayashi, C. Okuyama, K. Oba : IEEE Transactions on Nuclear Science, NS-31, No.1, pp.399-403 (1984).
2. Y. Ohara, T. Inoue, Y. Matsuda, and Y. Okumura : to be submitted for publication.
3. Claude Lejeune and Jean Aubert : Adv. in Electronics and Electron Physics, Supplement 13A, Academic Press 129 (1980).

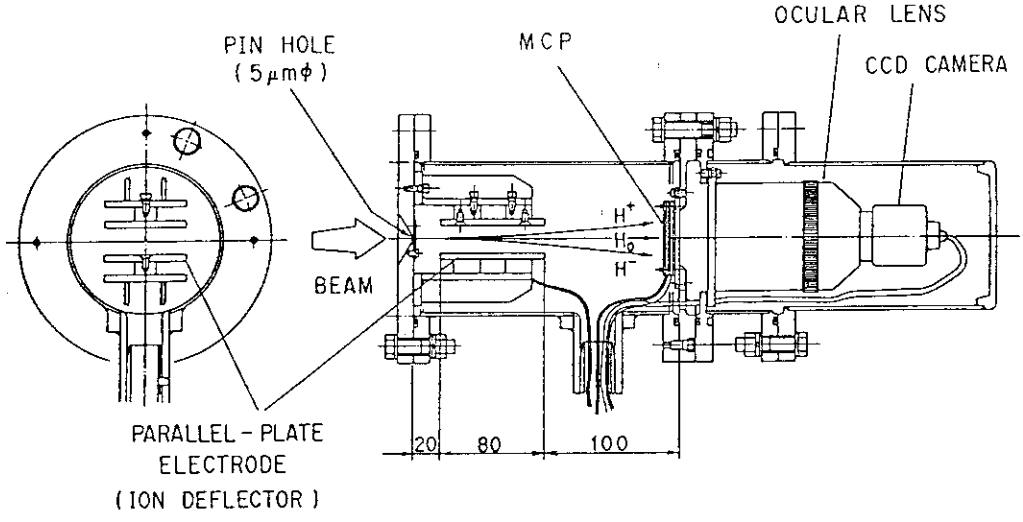

Fig. 3.4.4-1 Crosssection of the 4D emittance scanner.

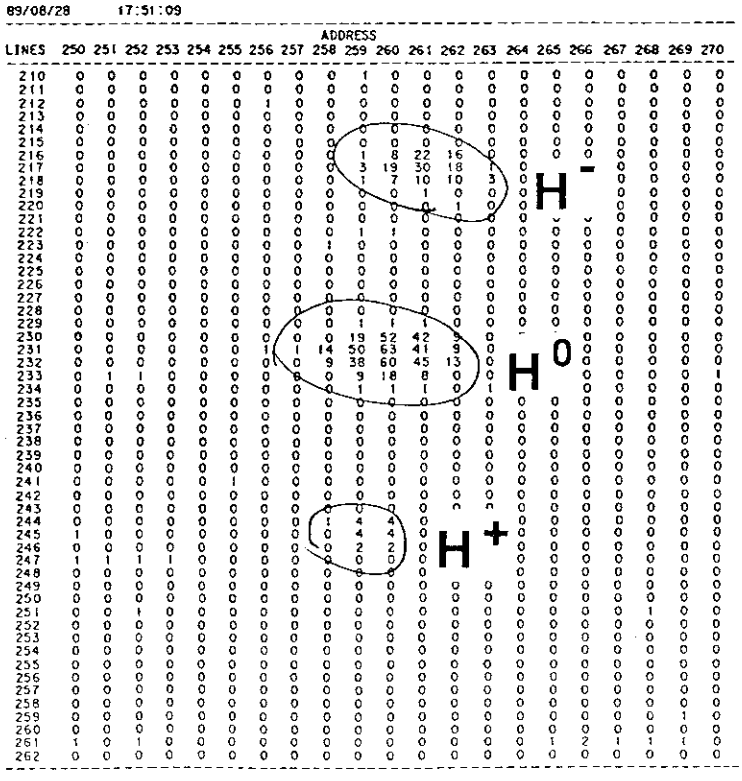

Fig. 3.4.4-2 A typical image stored in the digital video memory.

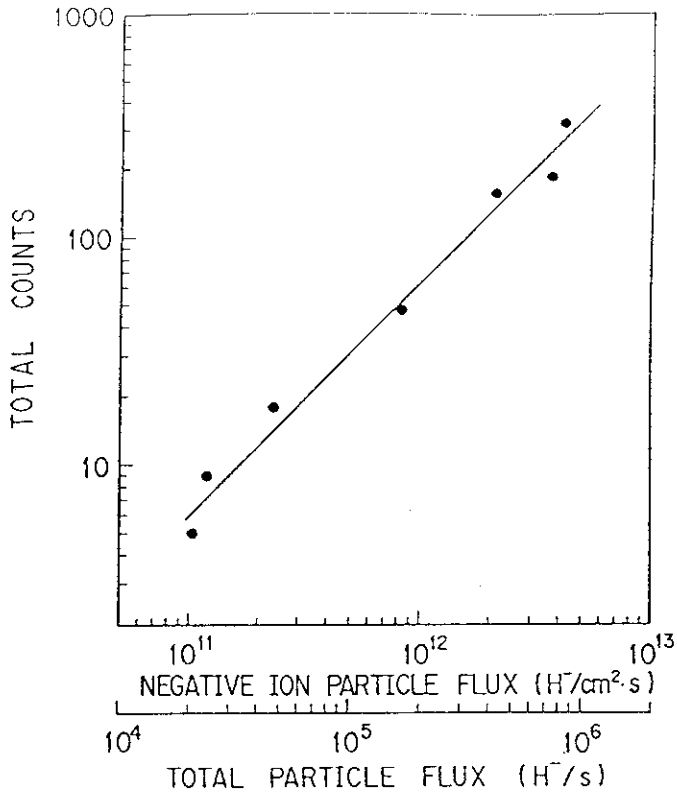

Fig. 3.4.4-3 Relationship of the negative ion particle flux and the total counts of the H^- image.

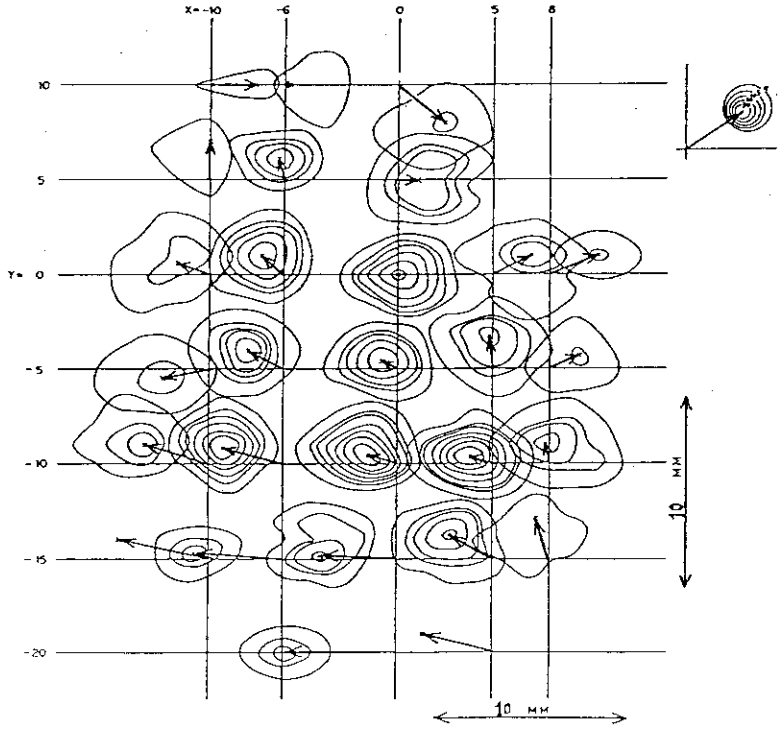

Fig. 3.4.4-4 A typical super emittance diagram of the 14keV negative hydrogen ion beam.

3.4.5 Space Charge Expansion of Negative Ion Beams [1]

The purpose of this study is to confirm that the beam can be transported from the accelerator to the neutralizer and also in a long neutralizer without space charge blown-up even at a low pressure. The negative ion beams with various diameter were fired from the One Ampere Negative Ion Source. The beam divergence were measured at various gas pressure ranging from 10^{-3} to 1 Pa. From this experiment, following results were obtained.

(1) Figure 3.4.5-1 shows a comparison of space charge expansion for H^-, H^+, and He^+ beams. Although the beam divergence is almost constant for a wide range of the pressure in the beamline, the beam divergence becomes larger below a critical pressure for each ion beam due to the space charge expansion. As shown in the figure, the critical pressure of H^- beams is lower by one order of magnitude compared to that of positive ion beams.

(2) The dependence of space charge expansion of the negative ion beam on the background gas species was measured. The result is shown in Fig. 3.4.5-2 for argon and xenon. The critical pressure decreases considerably with the mass number of the gas species. For the heavier positive ions produced by the collisions with the H^- beam ions, the longer drift time will be required to escape from the beam column. Then the negative space charge of the beam will be easily compensated.

(3) A beam with larger diameter indicated more intense space charge neutralization. This is because the drift time of the positive ions to escape from the beam column increases with the beam radius.

(4) The H^- current was varied by regulating the arc discharge current. The beam divergences for three cases of the H^- current density are shown in Fig. 3.4.5-3 as a function of the pressure in the beam drift region. The critical pressure is independent of the H^- current density. Since the beam plasma, which neutralize the beam space charge, is produced by the beam itself, the density of the beam plasma depends on the intensity of the beam. Therefore the beam blow up due to the space charge is independent of the beam current density.

From these experiment, it was indicated that the space charge expansion is strongly dependent on the beam plasma characteristics. Then normalized generation rate[2], which corresponds to the ratio of the positive ion density to the beam particle density, was introduced from a particle balance equation of the positive ions in the beam plasma. An example of the experimental data summarized by the normalized density is shown in Fig. 3.4.5-4. The results indicate that the beam divergence becomes large at the normalized generation rate of less than about 1.

Reference

[1] T. Inoue, Presented at U.S.-Japan workshop on negative ion beam, Nov. 15 (1988)

[2] E. B. Hooper, Jr., O. A. Anderson, and P. A. Willmann, Phys. Fluids 22/12 (1979) 2334

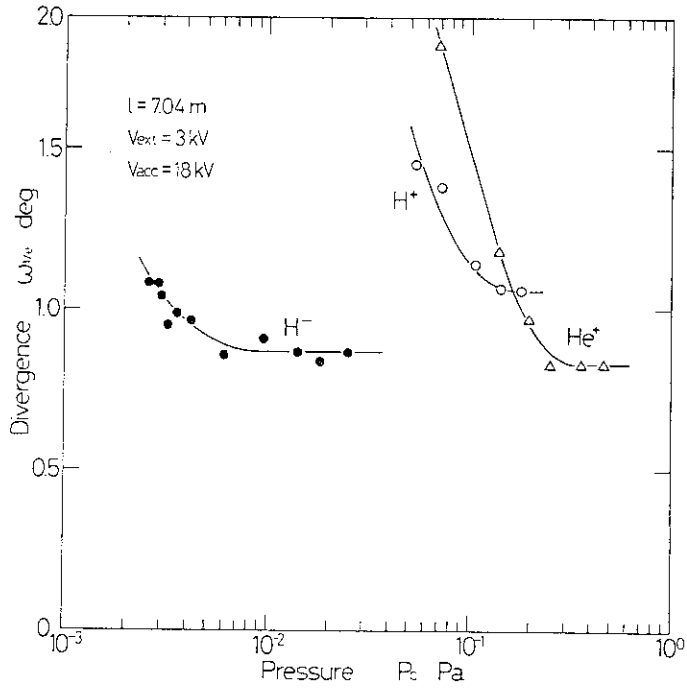

Fig. 3.4.5-1 The divergence of the various ion beams as functions of the pressure in the beanline.

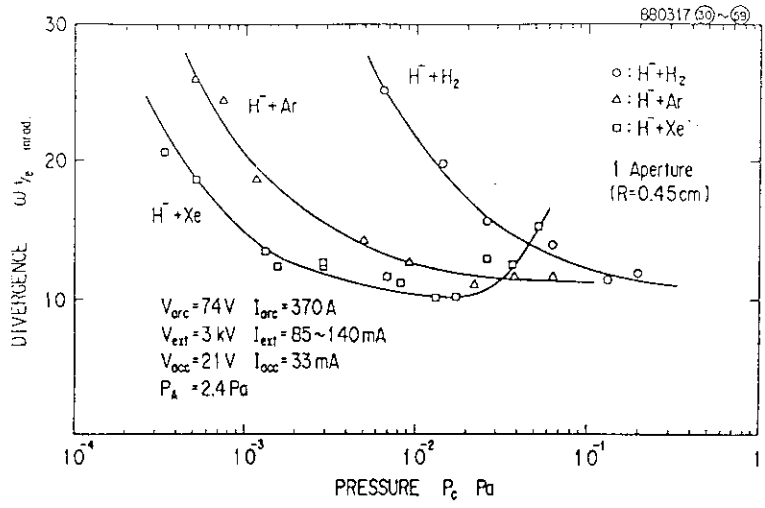

Fig. 3.4.5-2 Space charge expansion of the negative ion beam for three different gas species in the beam drift region.

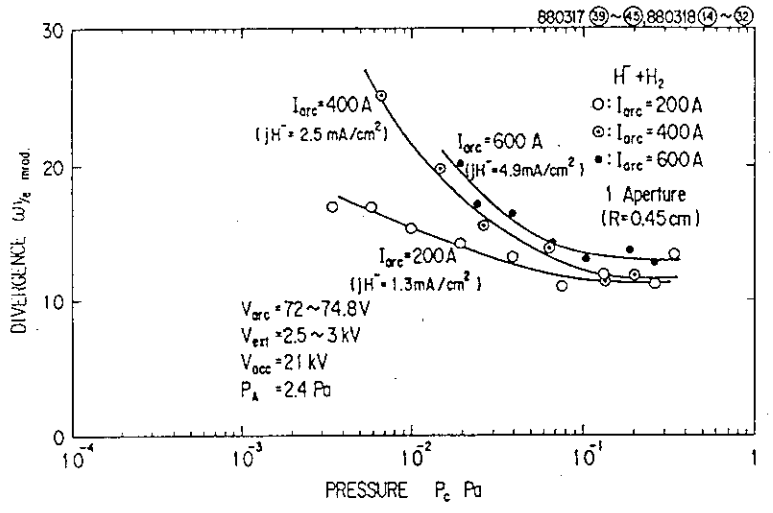

Fig. 3.4.5-3 Space charge expansion of the negative ion beam as a parameter of the negative ion current density.

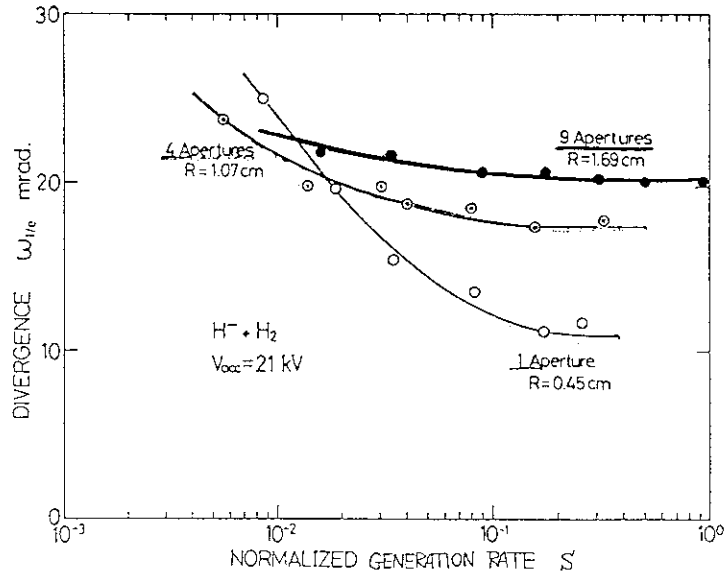

Fig. 3.4.5-4 Dependence of the beam divergence on the normalized generation rate; an example for various radius of the negative ion beam.

3.5 Stripping Loss of Negative Ions in the Accelerator

3.5.1 Measurement of Stripping Loss by a Spectroscopic Method

Since the negative ion has a big cross section for neutralization, some of the extracted negative ions collide with residual gas particles and neutralized in the extractor and accelerator column. This stripping loss is a serious problem in a volume source, because the operating pressure of a volume source is generally very high. Not only the negative ion current decreases but also a large amount of electrons are produced and accelerated, resulting in a low acceleration efficiency and a high heat dissipation in the accelerator grids.

Estimation of the stripping loss is not easy, because we have not enough information about the residual gas temperature which might be very high due to the heating by arc discharge. Therefore, we measured the stripping loss directly by a spectroscopic method. In this method, the energy distribution of the H^- ion beams was measured by Doppler-shifted spectroscopy of Balmer-alpha light. The beam contains fractional energy neutrals which are stripped in the accelerator column before fully accelerated. From the amount of the fractional energy neutrals, we can estimate the stripping loss.

Figure 3.5.1-1 shows an example of the spectrum. Besides the unshifted and full-energy peaks which correspond to the beam plasma and fully accelerated particles, respectively, we can see a lot of signals between the two peaks. The third peak denoted $H_\alpha(E=V_{ext})$ corresponds to the fractional energy particles which are neutralized in the extraction grid where the negative ions propagate for some distance at the same energy of extraction voltage.

The stripping loss ratio ($n\sigma l$) measured by this method is shown in Fig. 3.5.1-2 by circles as a function of the pressure in the plasma generator. The stripping loss increases with gas flow rate into the ion source. The stripping loss ratio was also estimated from the gas flow calculation using the Monte-Carlo computer code which assumed a constant gas temperature. The calculated value is also shown in Fig. 3.5.1-2 by solid and broken lines. The measured values agree well with the calculation if we assume the gas temperature to be 400 K (broken line).

The stripping ratio of negative ions is estimated to be 45 % for the One-Ampere H^- Ion Source at a typical operating condition of I_{H^-}=1.6 A and P_A= 1.5 Pa, where I_{H^-} is fully accelerated negative ion current and P_A is the pressure in the plasma generator.

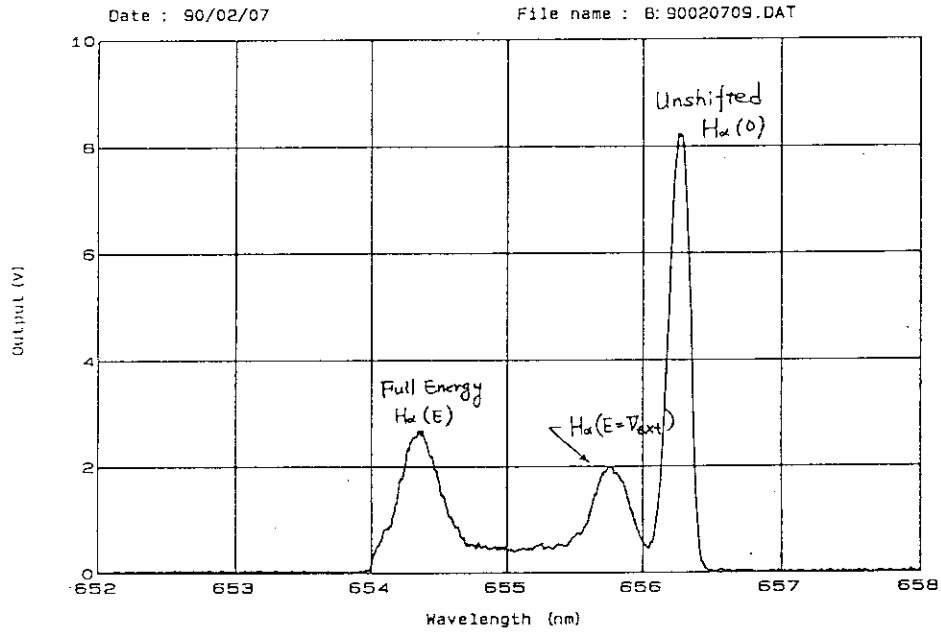

Fig. 3.5.1-1 An example of Doppler-shifted spectrum of Balmer-alpha light (656.3 nm). The negative ion beam contains a lot of fractional energy neutrals which are produced in the accelerator column by neutralization of negative ions.

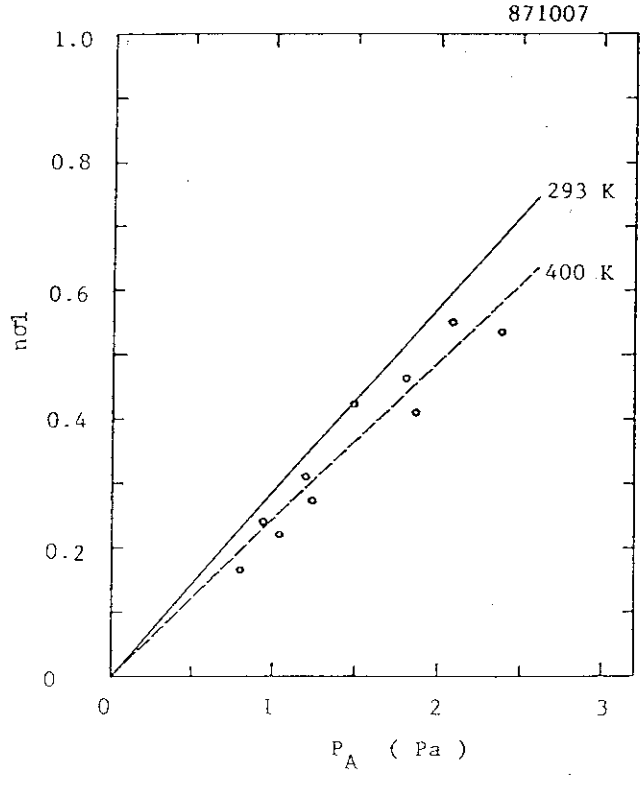

Fig. 3.5.1-2 Stripping loss ratio (1-exp(-nσl)) of negative ions as a function of the pressure in the plasma generator.

3.5.2 3D Monte-Carlo Gas Flow Code Development

To estimate the stripping loss of the negative ions in an accelerator, a 3D Monte Carlo gas flow code has been developed. This code calculates both the temperature and density distributions of the molecular gas flow along the beam axis. Since the gas flow rate through the accelerator is constant, the density distribution is calculated by the following equation:

$$\frac{n_i}{n_0} = \frac{\bar{v}_0 N_i S_0}{\bar{v}_i N_0 S_i} = \frac{\sqrt{T_0} N_i^2 S_0}{\sqrt{T_i} N_o^2 S_i}, \qquad (1)$$

where $\bar{v}$, N, S, and T denote the mean velocity of the molecules, the molecular number, the cross section area of the accelerator channel and the temperature of the molecular gas, respectively. The subscripts 0 and 1 indicate the starting position and the arbitrary position along the axis of the accelerator, respectively. The velocity distribution at the staring position (in the arc chamber) is assumed to be Maxwellian.

In order to take into consideration the energy transfer between the surface of the accelerator electrode and the gas molecules, an accomodation coefficient α is applied in this code. The temperature of the gas molecules after the collision with the electrode T_r is expressed as follows:

$$T_r = T_i + \alpha (T_{wn} - T_i), \qquad (2)$$

where, T_{wn} and T_i are the temperatures of the electrode and the gas molecules before the collision, respectively.

To confirm the validity of this code, the stripping loss of the Multi-Ampere Negative Ion Source was calculated under the assumptions described below;

Numbers of projection molecules	: 5000
Accomodation coefficient	: 0.3
Gas temperature at the strarting position (in the arc chamber)	: 500 K
Temperature of the electrode	: 300 K
Molecule reflection law on the electrode	: cosine law
Molecule reflection law at the boundary between the electrode	: mirror

An example of the molecule trajectories is shown in Fig 3.5.2-1. The molecules frequently collide with the plasma grid and the extraction grid. Consequently, the temperature of the gas molecules rapidly decreases in the extraction region as shown in Fig.3.5.2-2. When the gas pressure is 1.5 Pa and the gas temperature in the arc chamber is 500 K, the total stripping loss both in the extraction and acceleration region is about 45 %, where the average temperature in the extraction region is around 400 K. This value approximately agrees with the experimental value described in section 3.5.1. From this result, this code turned out to be useful for calculating the stripping loss in the accelerator.

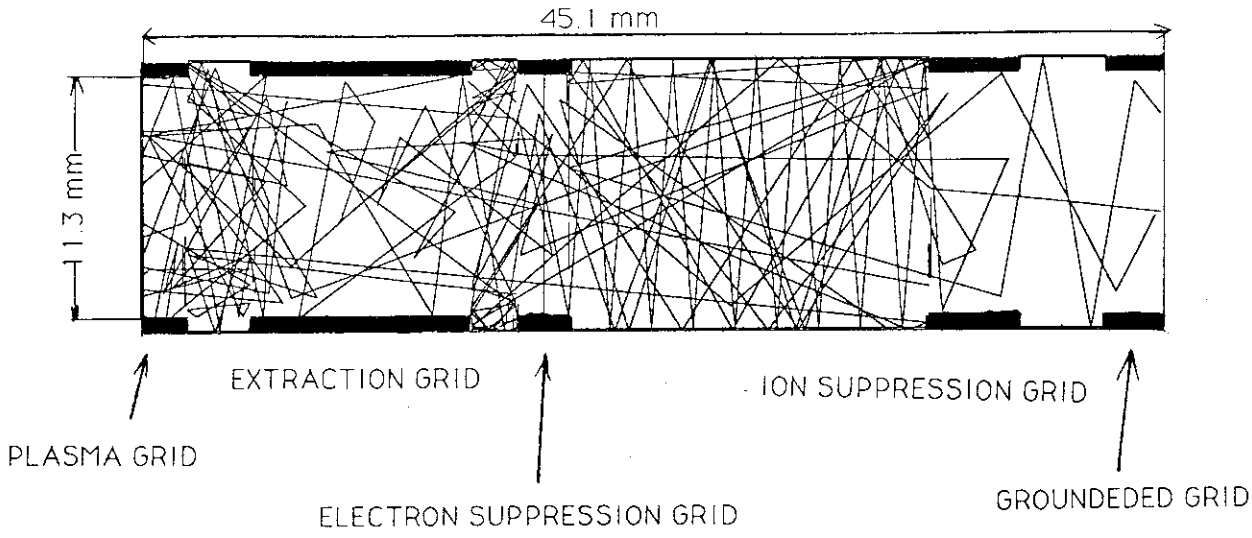

Fig. 3.5.2-1 Typical trajectories of the H_2 molecules in the Multi-Ampere Negative Ion Source

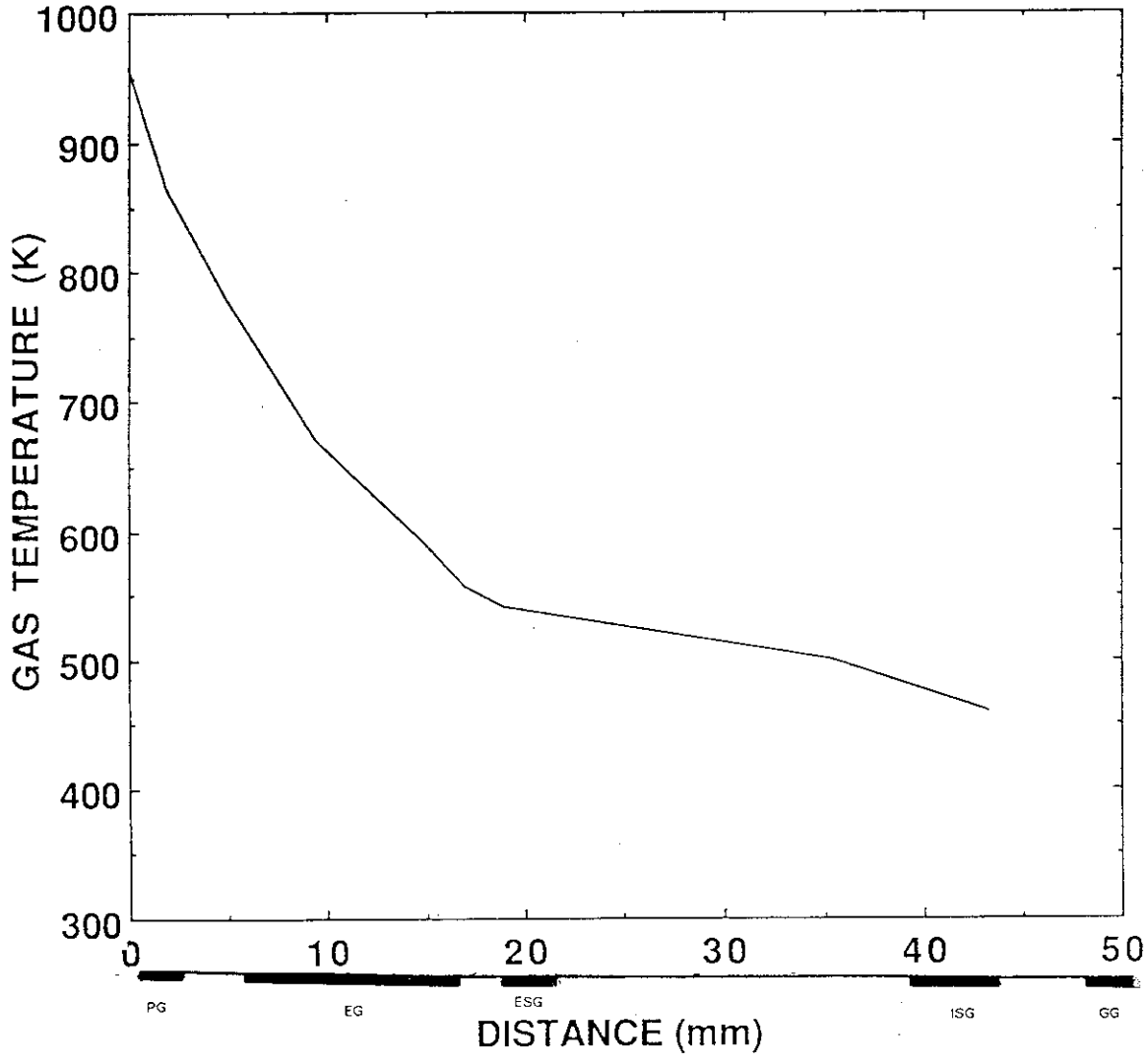

Fig. 3.5.2-2 Temperature distribution along the accelerator axis

3.6 Long Pulse Operation

3.6.1 Long Life Cathode

Target performances of the cathode of ion sources for the next neutral beam injectors would be as follows;

Pulse length	: Steady State
Life time	: more than 1 year
Electron emission density	: 5 to 10 A/cm2

To start the development of the cathode that satisfy the above requirements, we devised, as a first step, a new cathode as shown in Fig.3.6.1-1. The specification of the cathode is given below;

Electron emitter	: barium oxide impregnated porous tungsten cylinder
Inner/outer diameter	: 1.0 cm/ 1.4 cm
Heater	: tungsten rod of 2.5 mm in inner diameter at the center
Heater power	: 140 A x 2.2 V (Once discharge starts, the heater power can be switched off).

Non-stop 10 hour durability test of this cathode was carried out using a magnetic multipole line cusp plasma generator of 20 cm in inner diameter and 27.5 cm in length, under the discharge conditions;

Operating gas	: hydrogen
Gas presuure	: 0.76 Pa
Discharge current	: 50 to 60 A (2 to 2.4 A/cm2 at the cathode surface)
Discharge voltage	: 39 to 45 V.

The discharge was continued for 10 hours without any interruption, and stopped by switching off the discharge power supply.

Thus, this cathode has shown the potentialities for a pulse length longer than 10 hours. This result gives a good perspective to the future development of the long life cathode.

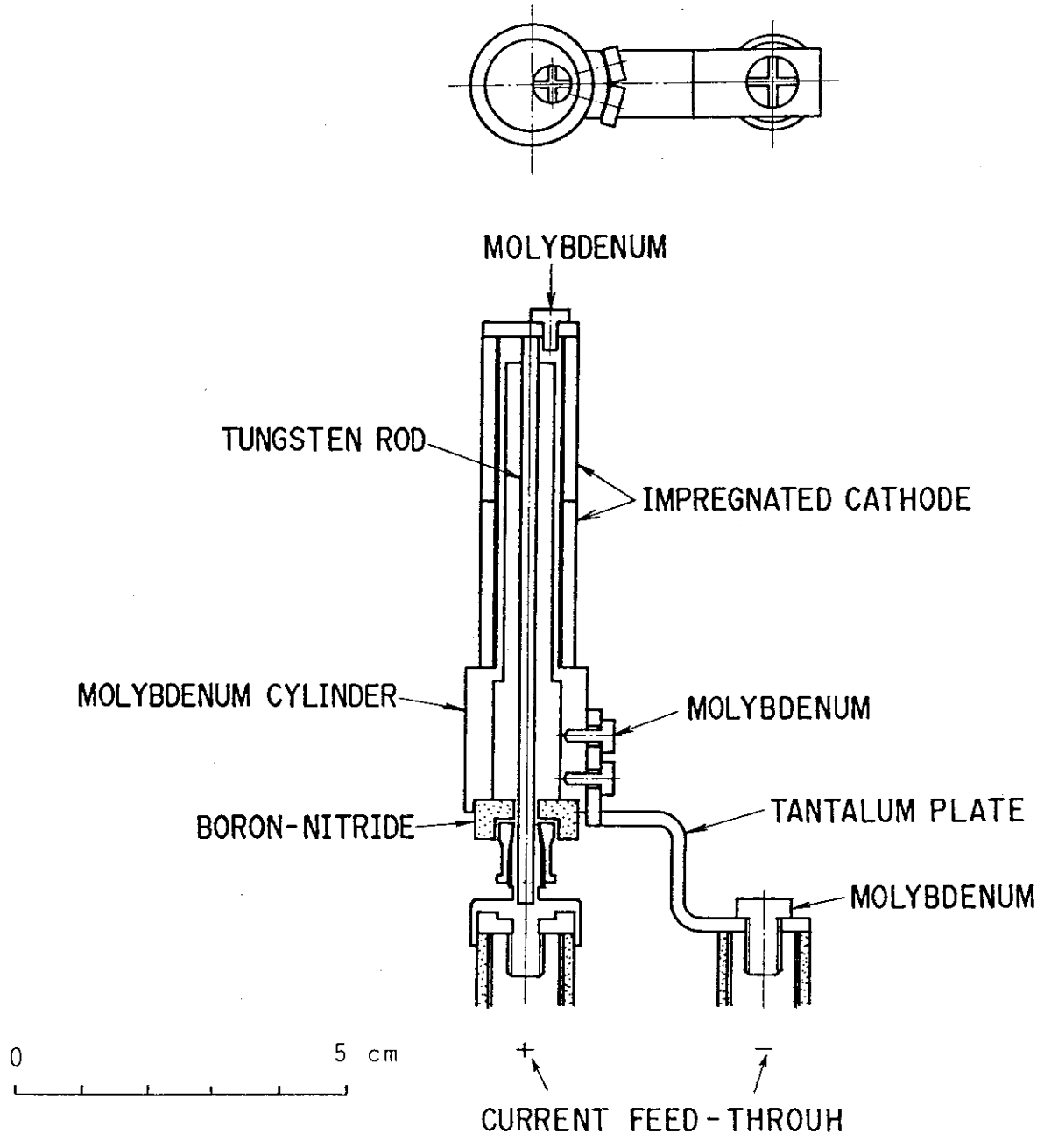

Fig.3.6.1-1 The newly devised impregnated cathode for steady state discharge

3.6.2 Plasma Production by Microwave

A RF ion source has many features. One of them is that it can be operated without hot cathode which limit the operation time. From the view points of application to a negative ion source and a plasma neutralizer, we are developing RF ion sources. The ion source is shown in Fig. 3.6.2-1. The ion source consists of a pair of magnetic coils and a cylindrical vacuum chamber. A waveguide is connected to one side of the chamber. The microwave of 2.45 GHz, 5 kW generated by a magnetron is introduced through a quartz window to the chamber.

Hydrogen plasma and xenon plasma were generated by 5 kW RF power. The plasma density of higher than 10^{12} cm^{-3} was obtained. In the case of Xe plasma, it was confirmed that the ionization rate was higher than 30 %[1].

After optimization of the magnetic field strength, gas pressure, etc., we could obtain similar plasma conditions as that of the volume negative ion source. The hydrogen negative ion current was measured using a negative ion probe. The results show that the negative ion current of 7 mA/cm^2 was obtained when the microwave power was 1 kW.

Reference

[1] Y.Matsuda et al., Proc. 12th Symp. on Ion Sources and Ion Assisted Technology, Tokyo, 1989, p.107.

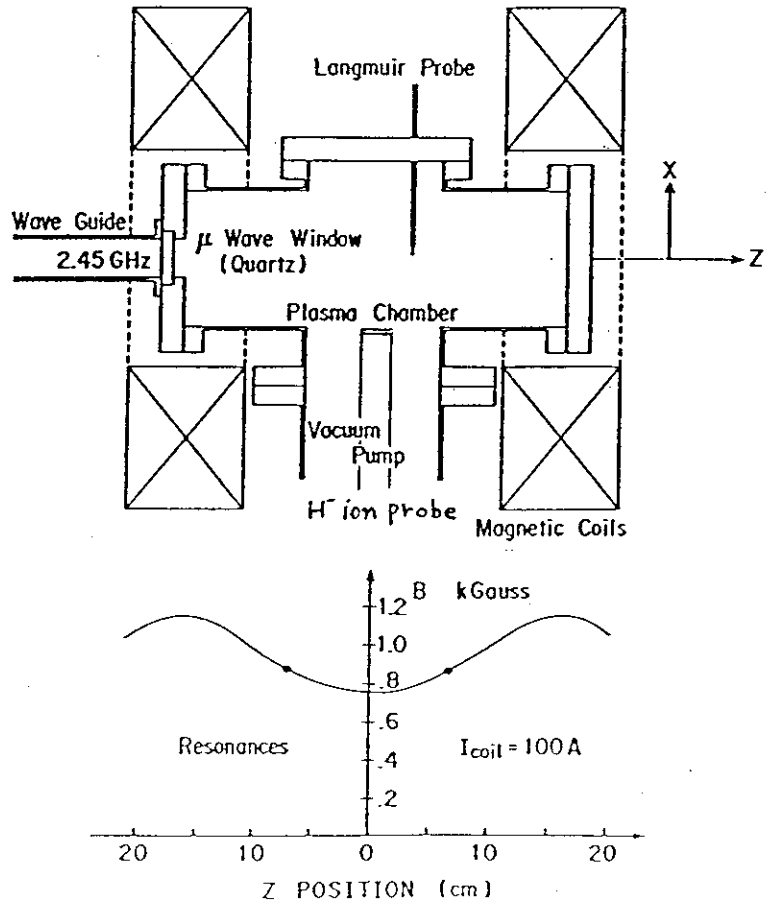

Fig. 3.6.2-1 Schematic diagram of the high density ECR plasma generator.

3.6.3 Long Pulse H^- Ion Source

To demonstrate the long pulse operation of the negative ion source, we have designed and fabricated a new source called Long Pulse H^- Ion Source. The objective of this source is to produce more than one ampere H^- ion beams quasi-continuously at the energy level of 50-75 keV.

Figure 3.6.3-1 shows the cross section of this ion source. The basic design of the source is same as the Multi-Ampere H^- Ion Source, but has some features for the long pulse operation; i.e.

(1) All the elements of the source are efficiently water cooled.
(2) All the elements of the source including SmCo magnets and O^- rings can be heated up to 300 C.(Special magnets and O-ring are used.)
(3) Extraction grids have expansion mechanism (bellow structure) in the peripheral region for thermal expansion.
(4) Many thermocouples are installed to monitor the temperature distribution.
(5) Exchange of cathode is easy.

The source can be operated not only in the pure volume mode but also in the cesium-seeded mode. When a large amount of cesium is condensed in the accelerator column, the source will be baked up to 300 C and the voltage holding will be recovered.

Basic design parameters are listed below;

(Plasma generator)

Size: 22cm x 15 cm depth
Type: magnetically filtered Cs-seeded multicusp source
Cathode: W filament x 4

(Extractor)

Extraction Area: 10 cm x 9 cm
Apertures : 11.3 mm x 44
Grid : 4 grids
Insulator : alumina ceramic

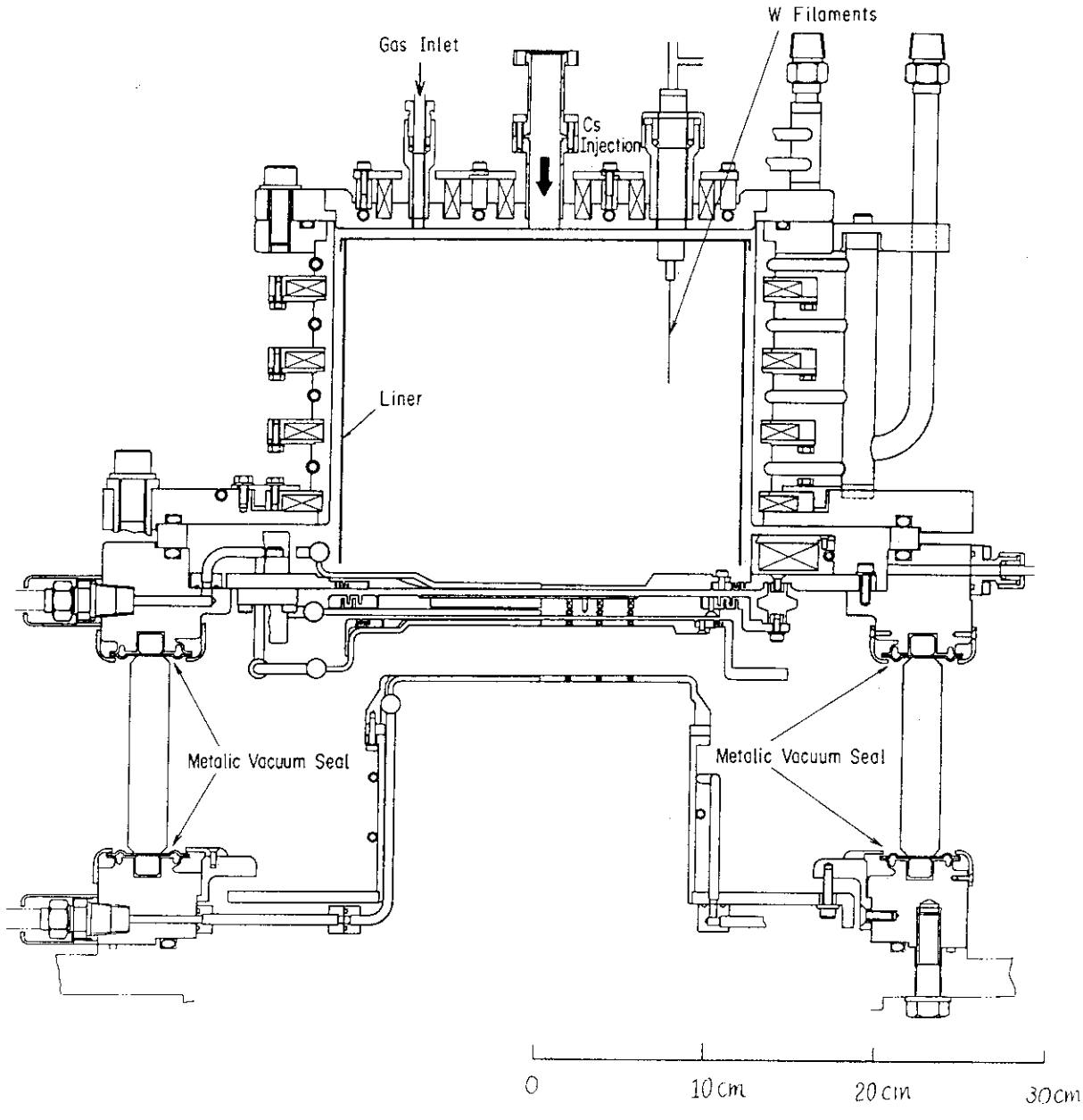

Fig. 3.6.3-1 A crosssection view of the long puse H^- ion source.

3.7 Related Technologies

3.7.1 High Voltage Insulator

A high power negative ion accelerator requires a large high voltage insulator compared to that of the positive ion accelerator, because the acceleration voltage is higher by about one order of magnitude and the ion beam current density is smaller by about one order of magnitude. The major specifications required for the insulator are listed below;

a. Diameter	: 1.5m ~ 2.5m
b. Voltage holding along the inner surface in vacuum	: > 10 kV/cm
c. Outgas	: ~ 10^{-4} Pa.m^3/s << Ion source gas flow rate
d. Vacuum leakage in 5 atm SF_6 gas	: < 10^{-6}Pa·m^3/s
e. Carbonization	: small enough to keep voltage holding characteristics
f. Strength	: enough to support the total weight of the ion source
g. Baking temperature	: 150°C ~ 200°C if Cesium is used
h. Neutron damage	: > 10^{16} n/cm^2

There are several candidates for the materials which have a possibility to satisfy the above specifications, namely, FRP(Fiber Reinforced Plastic), Epoxy, Porcelain, and Alumina Ceramics. As a step to develope such a large insulator of these specifications, we manufactured and tested two types of insulator as shown below.

Type A	Material	: Voidless FRP
	Dimensions	: 2.4m OD x 5.5cm thick x 24cm long
	Temperature(max)	: 40°C
Type B	Material	: Aluminum ceramic
	Dimensions	: 42cm OD x 2cm thick x 10cm long
	Vacuum seal	: Metalized silber brazing
	Baking Temperature	: 200°C

Figure 3.7.1-1 shows the structure and dimensions of the Type A insulator. The voltage holding characteristic at the nominal applied voltage of 150kV is shown in Fig.3.7.1-2. The insulator with vacuum flanges on both sides was placed in a dry nitrogen gas atmosphere. The pressure inside the insulator was kept to be 5×10^{-2} Pa by introducing hydrogen gas. This insulator was able to hold a nominal voltage of 150kV stably. This result shows that the large FRP insulator can be utilized for a accelerator insulating column, so long as the baking of the accelerator should not be required. Concerning the Type B insulator, it is utilized for the long pulse source described in subsection 3.6.3 without any problem. We are now planning to manufacture an alumina ceramic insulator with a diameter of 1.5m. This is a maximum size of an aluminum insulator which can be made at present in Japan.

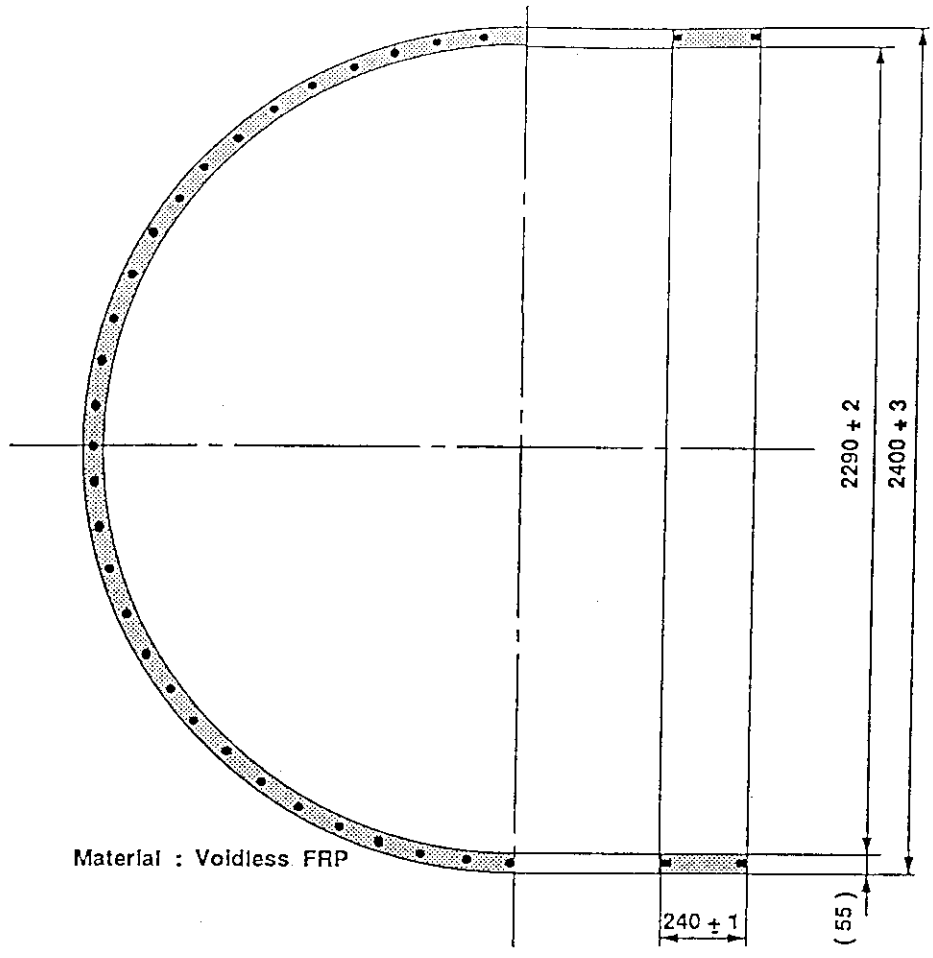

Fig. 3.7.1-1 A large high voltage insulator made of FRP.

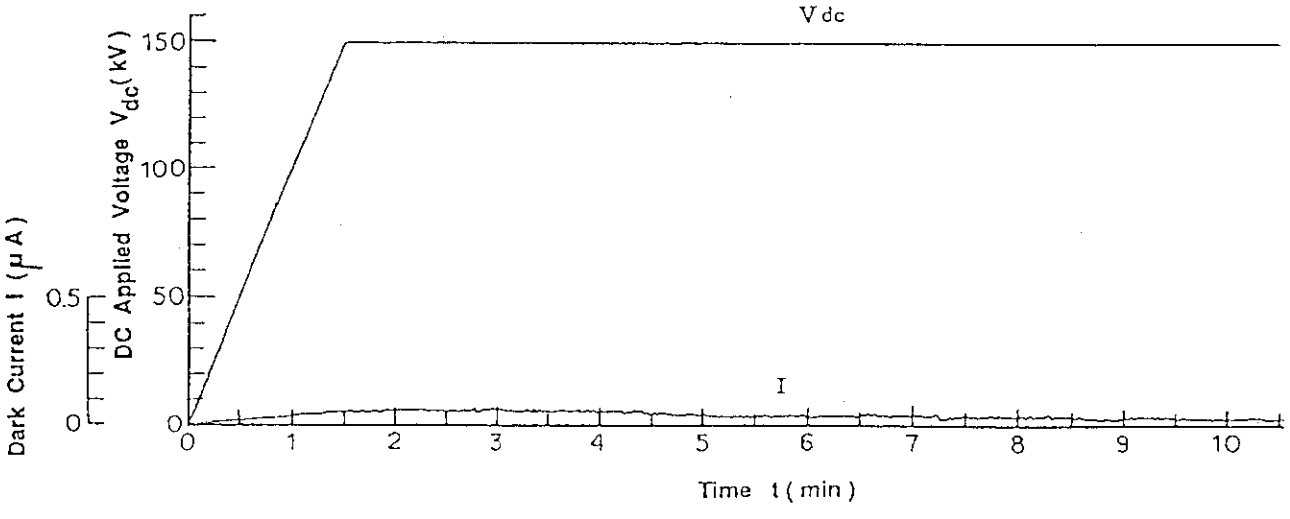

Fig. 3.7.1-2 A time variation of the dark current at the nominal applied voltage of 150kV.

3.7.2 Voltage Holding Experiment

High voltage of 150 - 200 kV must be sustained in each stage of a high energy acceleration system, whose gap length is 5-6 cm. We investigated the DC voltage holding characteristics in the similar condition of the accelerator. Figure 3.7.2-1 shows the experimental set-up. High voltage was fed by a 1 MV, 10 mA DC power supply. A vacuum chamber was made by cylindrical FRP insulator of 625 mm in diameter and 1000 mm in height. A couple of Rogowskii electrode of 160 mm in diameter was mounted in the chamber. The voltage and the currents of both the electrode and the insulator were measured. High voltage was supplied with a rising speed of 100 kV per minute.

Figure 3.7.2-2 shows the flashover voltage as a function of gap length. We confirmed that the breakdown mechanism obeys the Clump theory [1] at least up to the gap length of 50 mm, because the flash over voltage increases as $g^{0.5-0.6}$.

In order to confine the secondary electrons in each stage, it will be necessary to mount permanent magnets in the accelerator electrodes. Therefore, it is necessary to investigate the effect of magnetic field to the flash over voltage. Figure 3.7.2-3 shows the flashover voltage as a function of pressure of both cases of with magnetic filed and without magnetic field. The effects of the magnetic field appear at the higher pressure of 10^{-3} Torr. The flashover voltage became lower when the magnetic filed was supplied. This reason is considered to be the enhanced confinement of the electrons by magnetic field. At the lower pressure of 10^{-3} Torr, we confirmed that the flashover voltages do not depend upon the gas pressure.

In recent years it was confirmed that cesium is very effective to increase the negative ion current [2]. However, if cesium is deposited to the accelerator, the voltage holding characteristics will be degraded. Therefore, the effect of cesium on the voltage holding characteristics has been investigated. Figure 3.7.2-4 shows the result when cesium was deposited on the electrode. The quantity of cesium is considered to be about 0.07 mg/cm^2 and one order higher than that of the actual ion source. When cesium was deposited, a glow discharge ocurred initially followed by a spark breakdown at a higher voltage. The

breakdown voltage is about 70 % of the case without Cs. These results are summarized as follows;

1) Breakdown mechanism obeys the Clump theory at least up to the gap length of 50 mm.
2) The breakdown voltage became lower when the magnetic field was supplied at the higher pressure of 10^{-3} Torr.
3) Breakdown voltage did not depend upon gas pressure at the lower pressure of 10^{-3} Torr.
4) Breakdown voltage is decreased by cesium. However, about 70 % of the voltage in the cesium-free case can be held.

References

[1] L. Cranberg : J. Appl. Phys. 23, 518 (1952).
[2] Y.Okumura et al., Proc. 13th Symp. on Ion Source and Ion-Assisted Technology, Tokyo, 1990, p.149.

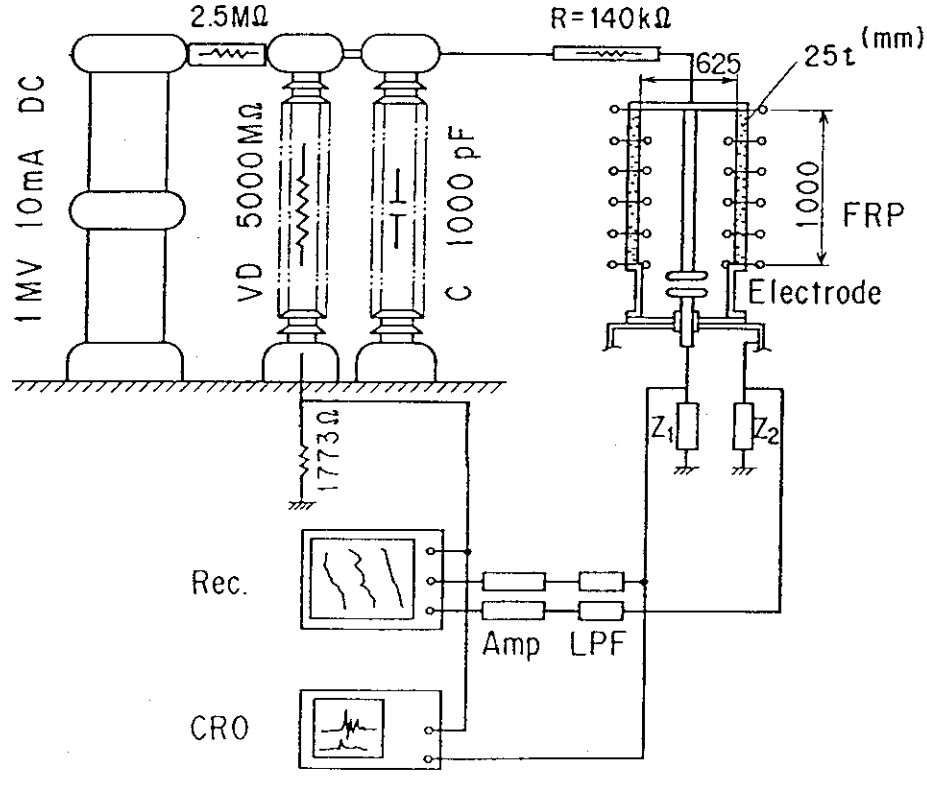

Fig. 3.7.2-1 Experimental set-up.

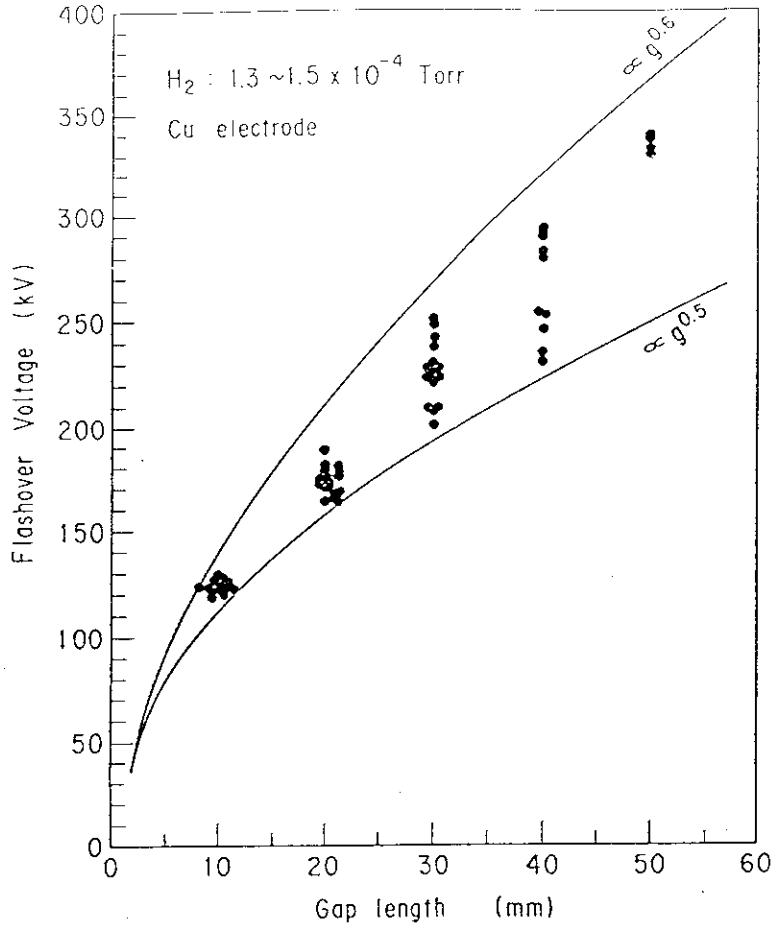

Fig. 3.7.2-2 Flashover voltage as a function of gap length.

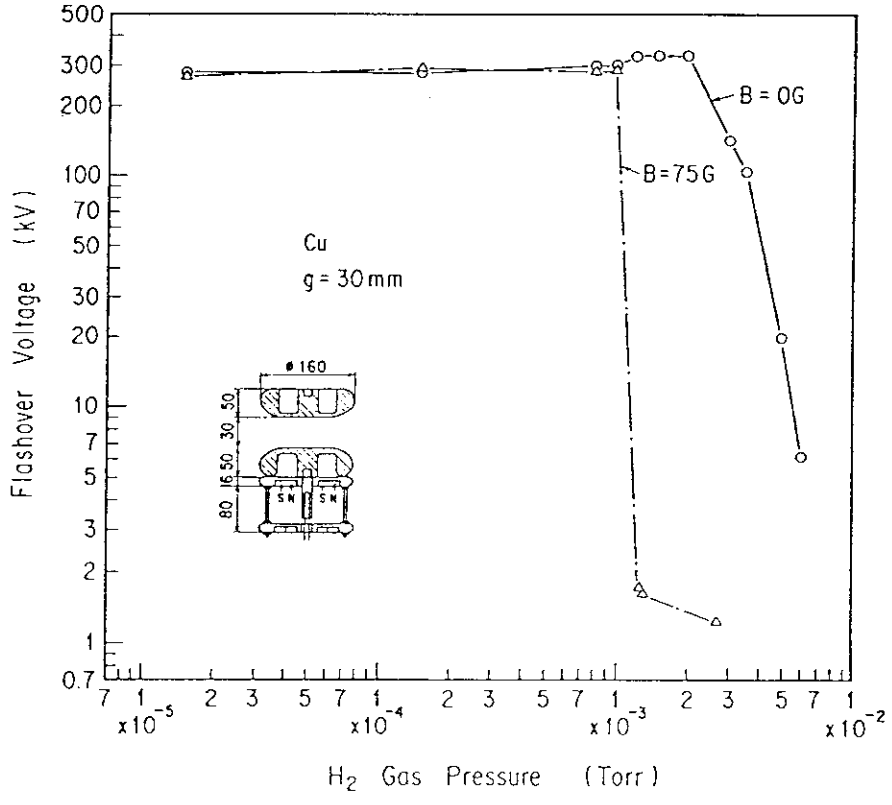

Fig. 3.7.2-3 Flashover voltage as a function of pressure.

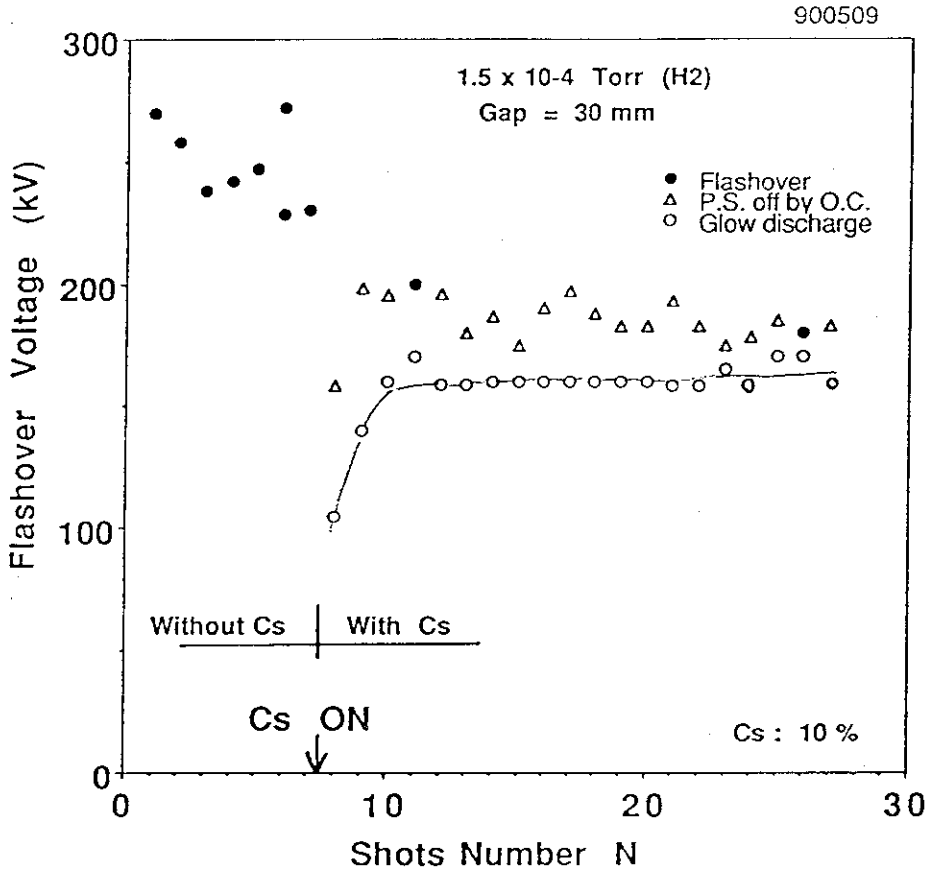

Fig.3.7.2-4 Breakdown voltage when cesium was deposited on the electrode.

3.8 MISCELLANEOUS R&D

3.8.1 Lithium Negative Ion Source for Plasma Diagnostics [1]

From the plasma diagnostic point of view, a high energy Li^- ion beam is promising to measure the plasma ion temperature and the plasma current profile. Hence, we have started a basic research on the Li^- ion source.

A schematic of the Lithium negative ion source is shown in Fig. 3.8.1-1. This has the same configuration basically as a pure volume production type negative hydrogen source. Li vapor was supplied from molybdenum boat installing Li metal, which is heated by radiation of filament and the arc discharge. To prevent Li condensation on the inner wall of the source, entire wall was covered with liner made of molybdenum and tungsten. The Li arc discharge was observed from viewing port mounted on the back plate. The following results were obtained during the initial experiment on a volume production type small Li^- ion source.

(1) The Li^- beam current increased linearly with the liner temperature. Since the temperature rise cause the increase of lithium vapor pressure, the Li^- current increase with the Li vapor pressure. We could not observe saturation of the Li^- current even at a higher pressure than 200 mTorr.

(2) The ratio of extracted electron to Li^- was remarkably high, such as an order of 10^6.

(3) A dependence of Li^- current on arc voltage shows an interesting characteristics as shown in Fig. 3.8.1-2. With decreasing the arc discharge voltage from 15 V, the negative ion current increased and reached an asymptotic limit at the voltage of less than 10 V. This is due to physical property of lithium; i.e. the dissociation energy is 1.06 eV, and the energy for production of vibrationally excited diatomic molecule is 1.8 - 2.5 eV. Since the energy which is important for the Li^- production is very low, it is recommendable not to increase the arc voltage higher than 10 V for high current Li^- production.

(4) The maximum Li^- current density of 1.1 $\mu A/cm^2$ was obtained at the optimized operation.

Reference

[1] T. Inoue, presented at IAEA three large tokamak NBI workshop, Oct. 24 (1989), Naka

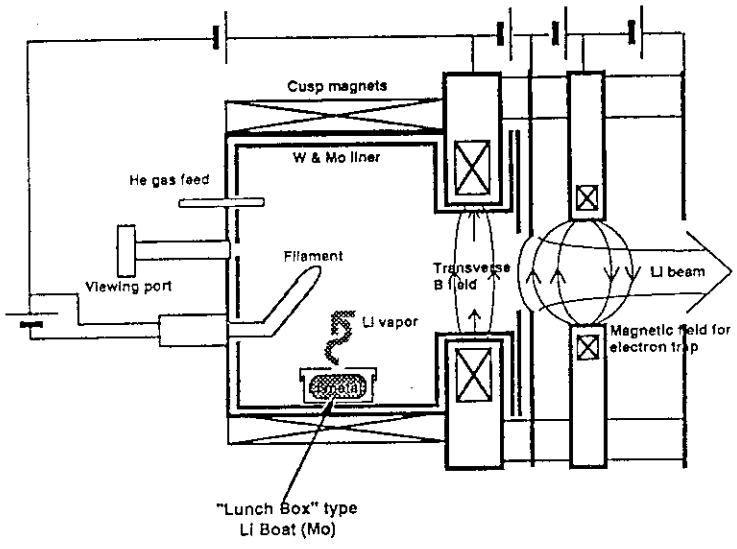

Fig. 3.8.1.1 A schematic of the lithium negative ion source.

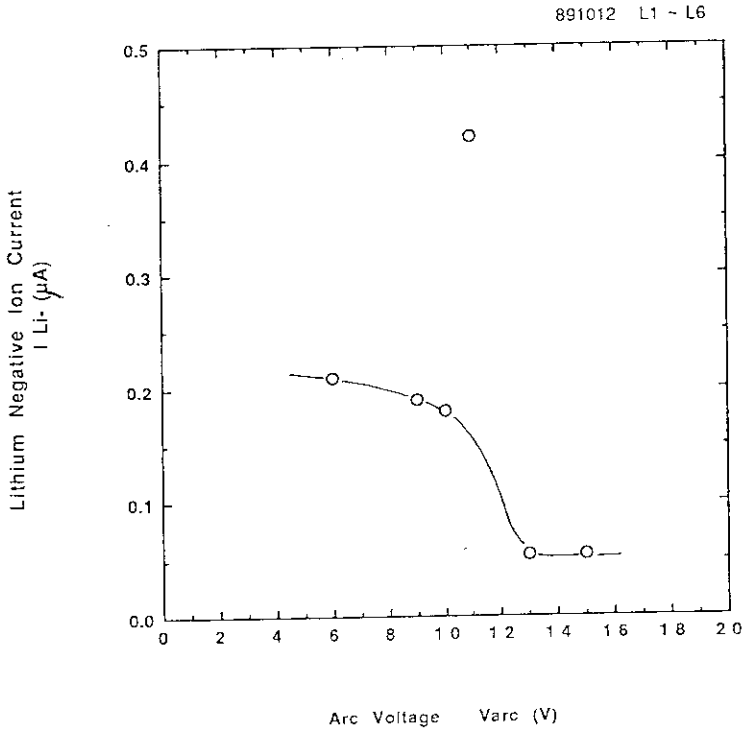

Fig. 3.8.1.2 The Li^- current as a function of the arc discharge current.

4. R&D RESULTS OF BEAMLINE COMPONENTS

4.1 Beam Dump Element

In the ITER NBI, one side of beam dump elements is exposed to intense particle beams in steady state. The heat flux on the dump surface is estimated to be around 20 MW/m^2. This heat flux is beyond the present technology. Therefore, developmental studies on high heat flux components have been done at JAERI using a particle beam engineering facility (PBEF) and an electron beam irradiation stand (JEBIS). For the first step, we have conducted burnout experiments to investigate critical heat flux of various tubes [1]. Experimental results are summarized as follows.

a. Effect of External Fins

We found that critical heat flux (CHF)* of tubes with external fins is 1.4 times higher than that of tubes without fins. Main reason is that nucleate boiling region develop widely along the inner surface of the tube because the heat flux to external fins are transported by conduction to the back side of the tube. However, we believe that both tubes have the same CHF if it is defined at the inner surface. Another merit of the external fins is that it helps to reduce thermal stress across the tube.

b. Effect of Twisted Tape Inserted

It is clear that a twisted tape enhances heat transfer because of the vortex flow. The insertion of a tape with a twist ratio of 2.5 increases the CHF as high as 1.5 times at the condition where axial flow velocity is 13 m/s and inlet water pressure is 0.9 MPa. Our CHF data for an externally-finned swirl tube obey the following equation which is a modification of Gambil correlation [2].

$$\phi_{CHF} = 1.27 \frac{V_{ri}}{(L_h/D_i)^{1/3}} + 18.3$$

$$V_{ri} = 3.28 \frac{V_a}{2Y} (4Y^2 + \pi^2)^{1/2}$$

where,

ϕ_{CHF} : critical heat flux (MW/m^2)
D_i : inner diameter of the tube (mm)
L_h : heated length (= 100 mm)
V_a : axial flow velocity (m/s)
Y : tape twist ratio (= length to 180 deg rotating/D_i)

This correlation can be applied for the condition of $4 < V_a < 15$. Figure 4.1-1 shows CHF data of the externally-finned swirl tube. The effect of tape twist ratio on CHF is found to be small compared with predicted value with the correlations.

c. Flow Velocity dependence

Figure 4.1-2 shows the CHF of various tubes as a function of flow rate for different inlet water pressures. In tubes with twisted tape inserted or internal fins, CHF linearly increased with flow velocity up to 13 m/s, which corresponds to the flow rate of 30 l/min. On the contrary, CHF in tubes without heat transfer enhancements saturated in spite of the open and closed circles and the open triangle.

Table 4.1-1 shows a summary of CHF data obtained by PBEF together with data from other laboratories. However, CHF data obtained by PBEF look lower than other data; they are attributed to long heated length, since CHF depends on heated length. For example, heated length at ORNL is less than 3 cm compared with that of 10 cm at JAERI. We have originally developed the externally-finned swirl tube for the beam dump element of the next generation NBI.

*CHF: we defined a critical heat flux on the outer surface because it is very difficult to evaluate the heat flux at the inner surface from a limited number of temperature measurements.

Reference

[1] M. Araki et al.: Fusion Engineering and design 9 (1989), vol.B, 231-236 (1989).
[2] W.R. Gambill, R.D.Bundy and R.W. Wansbrough : ORNL-2911 (1960).

Table 4.1-1 Typical Critical Heat Flux Data on Various Cooling Channel

		qCHF EXTERNAL (MW/m^2)	qCHF INTERNAL (MW/m^2)	Velocity (m/s)	Dimension OD (mm)	Dimension ID (mm)	Twist Ratio y	Pressure INLET (MPaG)	Pressure OUTLET (MPaG)	Material
SMOOTH TUBE (JAPAN: JAERI)		21	-	13	10	7	-	0.9	(0.5)	0.2%Ag + OFCu
INTERNALLY- FINNED TUBE (JAPAN: JAERI)		25	-	13	10	7	*	0.9	(0.4)	0.2%Ag + OFCu
EXTERNALLY- FINNED TUBE (JAPAN: JAERI)		30	-	13	10	7	-	0.9	0.5	0.2%Ag + OFCu
EXTERNALLY- FINNED SWIRL TUBE (JAPAN: JAERI)		41	-	13	10	7	2.5	0.9	0.2	0.2%Ag + OFCu
RECTANGULAR TUBE (JAPAN: JAERI)		20	-	11	16 X16	10 dia.	-	0.9	-	0.2%Ag + OFCu
SWIRL TUBE (US: ORNL)		>54	-	10.7	9.6	6.3	2.0	17	0.4	OFCu
HYPER- VAPOTRON (EC: JET)	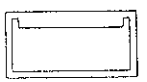	≤ 16	-	(14)	112^W X 30^H X 540^L		-	0.7	-	1%Cr + Cu
PANEL (US: LBL)	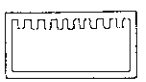	≤ 16	-	(220 l/min)	215^W x 200^L		-	17	0.7	0.2%Zr + OFCu
SWIRL TUBE		-	60	10	9.5	8	2.0	-	1.14	OFHC

Where marked * means that number of fins, fin height and herix angle are 16, 1 mm and 5°, respectively.

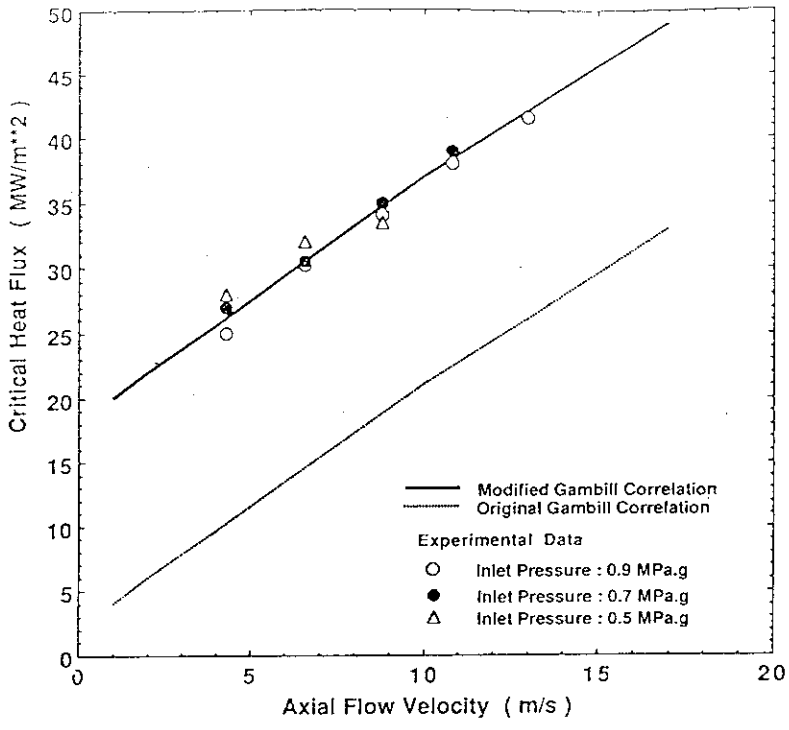

Fig. 4.1-1 CHF data of the externally-finned swirl tube.

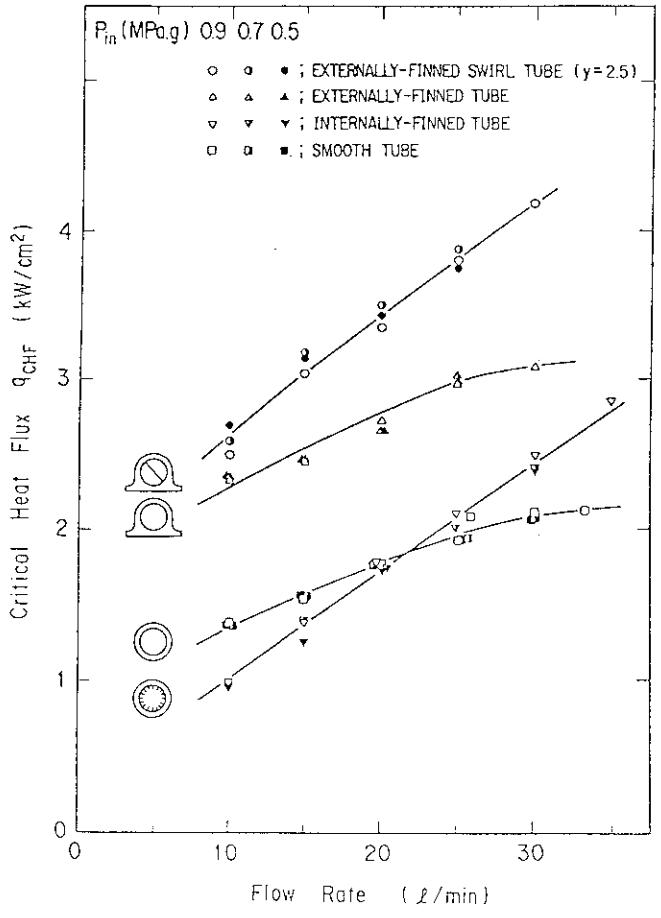

Fig. 4.1-2 CHF data of various tubes.

4.2 Plasma Neutralizer

Plasma neutralizer has a capability to offer higher neutralization efficiency (~85 %) than the conventional gas neutralizer, and to improve the system efficiency of the neutral beam injectors. For this purpose, we have tried to produce a highly-ionized, high-charge-state plasma by using a Microwave.

As a first step, a Xe plasma was produced in the ECR Plasma Generator that is described in Section 3.6.2 and shown in Fig. 3.6.2-1 [1]. Figure 4.2-1 shows the plasma parameters of the produced plasma as a function of the pressure in the plasma generator, where the microwave power is 1 kW at 2.45 GHz. A dense plasma, which has an ion saturation current density (J_{is}) of more than 100 mA/cm^2, was obtained at an extremely low operating pressure of 0.01 Pa. The average charge-state was estimated by the ratio of J_{is} to J_{es}. In order to take account of the effect of magnetic field, the ratio was compared with the ratio obtained in He plasma where it was assumed that there was no double-charge-state He ions. The plasma density, the average charge-state (Xe^{Z+}), and the ionization ratio were estimated to be 1.3 x 10^{12} cm^{-3}, z= 3.6, and 30 %, respectively. These parameters appears to be promising for the plasma neutralizer.

Then, we fabricated a multicusp ECR plasma generator for the neutalizer study. Figure 4.2-2 shows a schematic of the plasma generator. Microwave of 2.45 GHz, 5 kW is injected into the field free region of the multicusp chamber, and electron-cyclotron resonance occurs at each line cusps close to the wall. In the preliminary experiment, Xe plasma was produced at low pressures less than 0.1 Pa.

Reference

[1] Y. Matsuda et al.; Proc. 12th Symp. on Ion Source and Ion-Assisted Technology, Tokyo, 1989, p.107

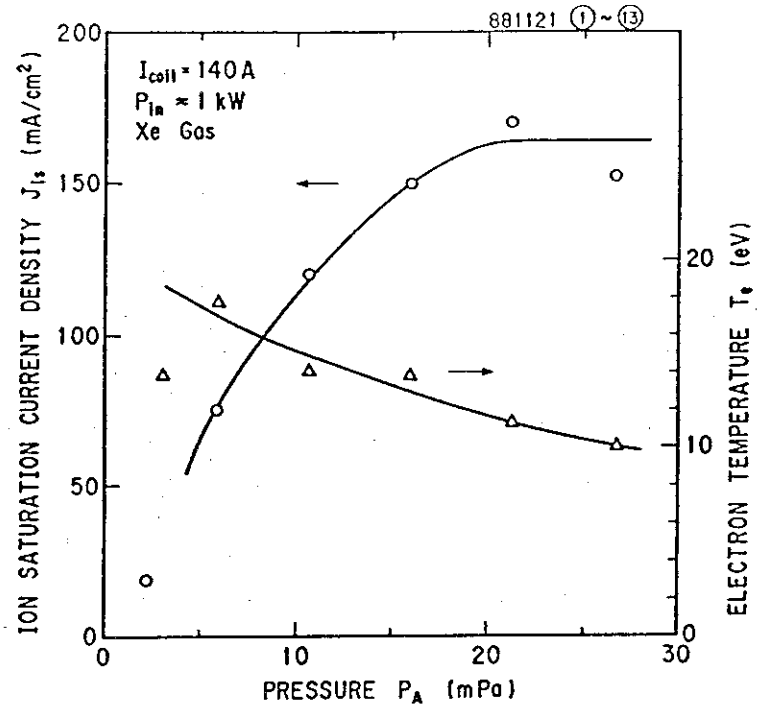

Fig. 4.2-1 Plasma parameters of the Xe plasma produced in the ECR Plasma Generator shown in Fig. 3.6.2-1. A high density plasma could be produced at a extremely low pressure of 0.01 Pa.

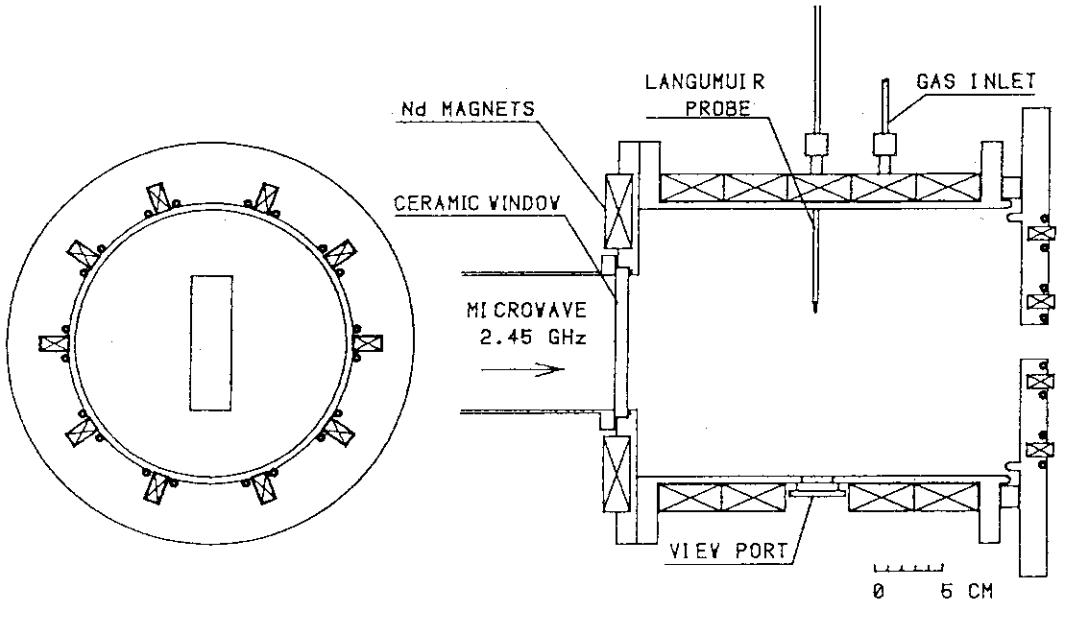

Fig. 4.2-2 A schematic of the 'ECR' multicusp plasma generator for the plsma neutralizer study. Microwave of 2.45 GHz, 5 kW is injected into the chamber from the ceramic window which is magnetically opened for the injection.

4.3 Energy Recovery System

Direct energy recovery of the residual ion beams is one of the interesting technology to improve the overall power efficiency of neutrl beam injectors and to reduce the heat flux on the beam dump surface. In the neutral beam injector based on negative ions, the residual ions are composed of negative and positive ions. Hence, we proposed an energy recovery system which can decelerate both ions. In the system, both ions are separateed by the stray magnetic field from the tokamak and guided to the collectors. Since an additional power supply is needed for positive ion recovery, the energy of positive ions is not recovered but consumed by a resistor connected to the collector, namely, the soft landing beam dump. Figure 4.3-1 shows an example of three dimensional ion trajectories in the recovery system. Both the ions are separated by the stray magnetic field and successfully guided to the negative ion collector and the soft landing beam dump[1].

As a first step to understand the energy recovery mechanism, we are conducting a collaborative experiment of the energy recovery using a JAERI high proton plasma generator[2] at Cadarache. Experimental results showed that more than 90 % of the residual full energy ions were recovered electrically and the overall power efficiency of neutral beam injector was improved by 25 % at 100 keV for deuterium ion beams using the energy recovery system[3].

To investigate an applicability of the energy recovery system to the negative-ion-based NBI system, the collaborative experiments using negative ion beams is scheduled in succession.

Reference

[1] M. Araki, Y. Ohara and Y. Okumura : Fusion Tech. 17,555 (1990).
[2] K. Watanabe, et al.: Proc. 15th Symp on Fusion Technology, Vol.1, Utrecht (1988) pp.647-651.
[3] J. Pamela, M. Araki, K. Watanabe et al.: to be published in Nuclear Instruments and Methods.

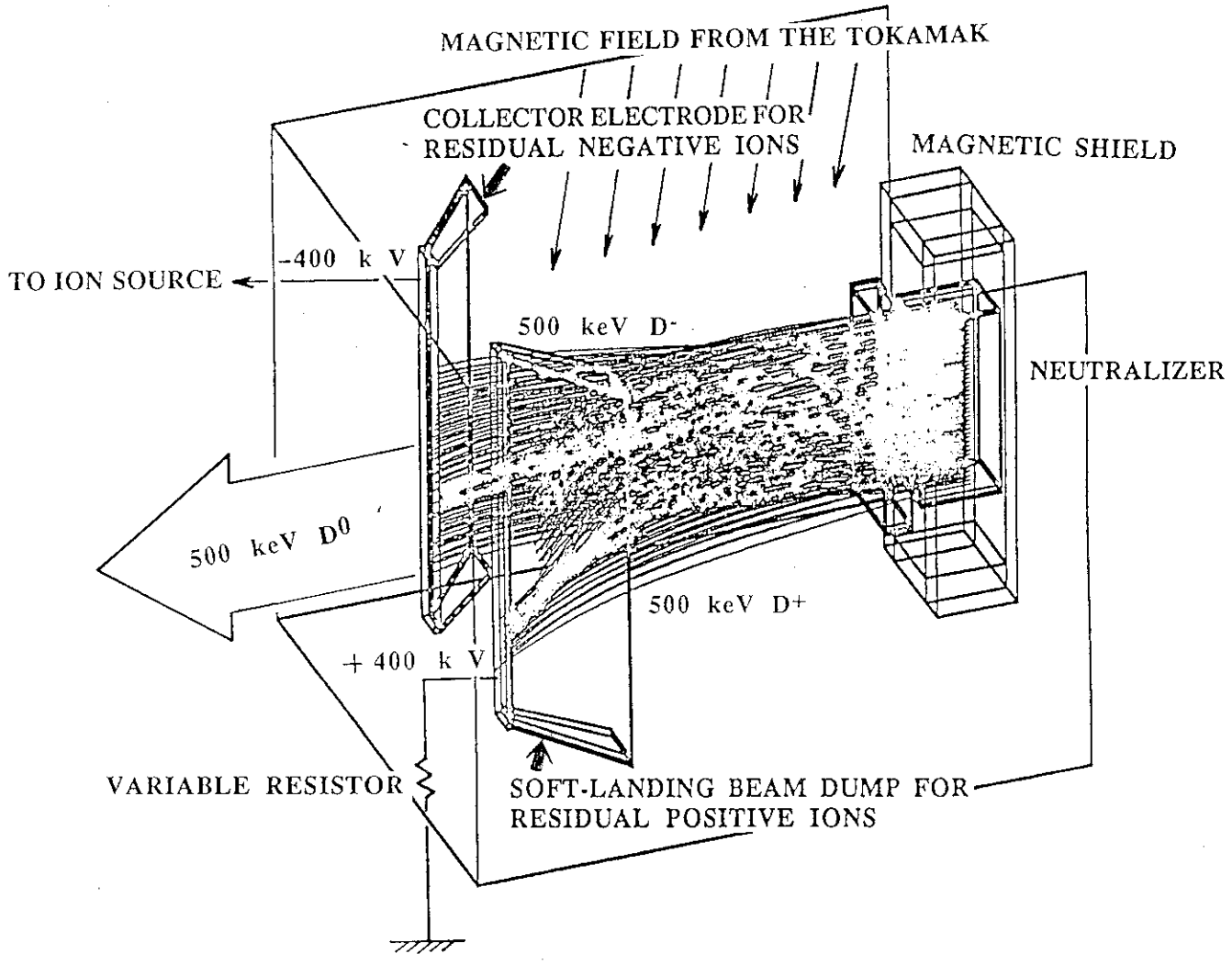

Fig. 4.3-1 An example of ion beam trajectories in the energy recovery system.

5. R&D RESULTS OF POWER SUPPLY

5.1 Inverter Type Acceleration Power Supply

In the NBI system for FER/ITER, a DC power supply of about 1 MV is required. However, DC switch can not be available from the viewpoint of reliability. Hence, we are investigating the inverter type DC power supply, that controls and cuts off the output voltage quickly by the operation of the AC low voltage circuit (Fig.5.1-1). As the first step of R&D, we adopted the inverter type DC power supply for JAERI Electron Beam Irradiation Stand (JEBIS) [1], that is the test facility for high heat flux component development.

The power supply is an electron acceleration power supply. Features are as follows [2]:

1. Output of 100 kV, 5 A, continuous rating.
2. Power supply is composed of 10 inverters, 10 rectifier-transformers and 1 converter (Fig.5.1-2).
3. Switching frequency of inverters is 5 kHz and the switching timing is shifted to reduce the ripple.
4. Output voltage is controlled by the pulse width control of the inverters.
5. Inverters cut off the output when breakdown occurs.

The results of the operation combined with an electron gun are:

1. Electron beams of 100 keV, 4 A are extracted successfully (Fig.5.1-3).
2. By turning off inverters, the breakdowns do not cause severe damage to the accelerator (Fig.5.1-4).

These results shows that the inverter type power supply has sufficient protection function for breakdowns and is applicable for the beam acceleration power supply.

Reference

[1] M. Akiba et al., " High heat flux experiments at JAERI," Proc. of 13th. Symp. on Fusion Engineering, Knoxville, Oct. 2-6, 1989, pp.529-532.

[2] M. Mizuno et al., " Inverter type high voltage DC power supply for negative-ion-based neutral beam injectors, " Proc. of 13th. Symp. on Fusion Engineering, Knoxville, Oct. 2-6, 1989, pp.574-577.

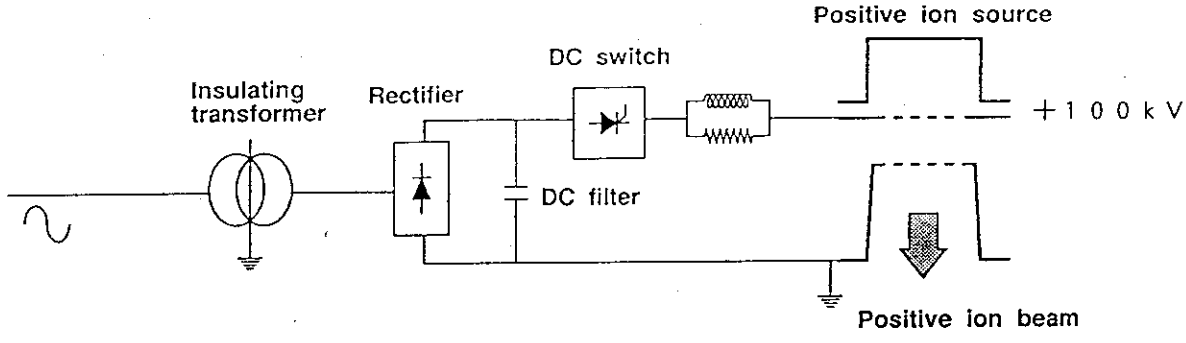

(a) DC switching system

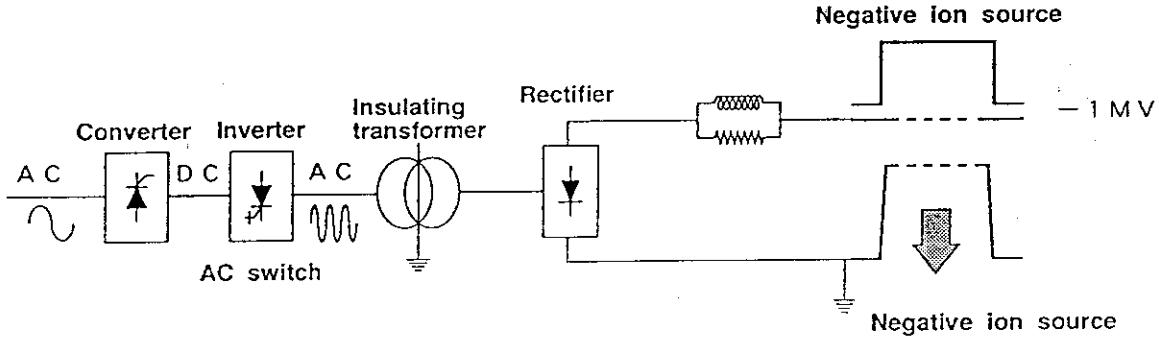

(b) AC switching sysyem

Fig.5.1-1 Comparison of DC switching system and AC switching system.

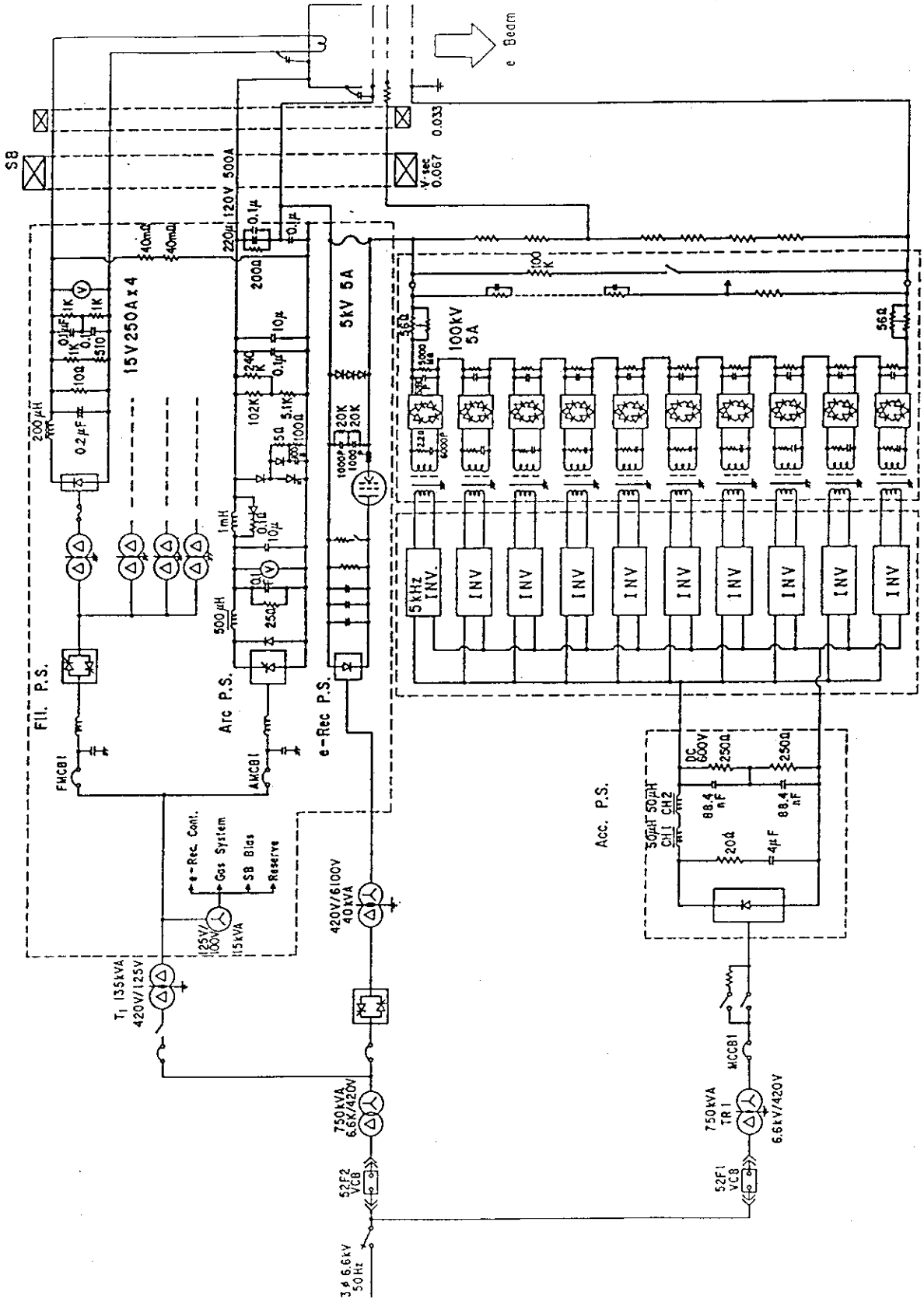

Fig.5.1-2 Schematic diagram of JEBIS power supply system

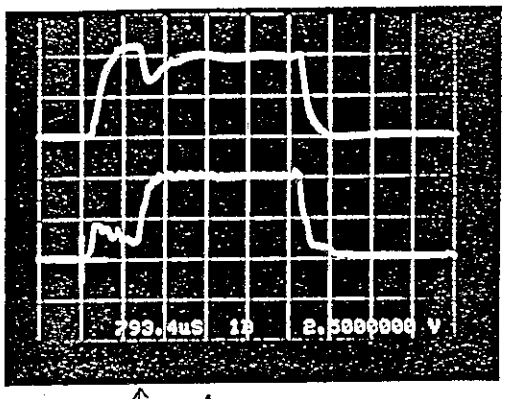

Fig.5.1-3 Waveforms of the acceleration voltage and current at 100 keV, 4 A electron beam extraction.

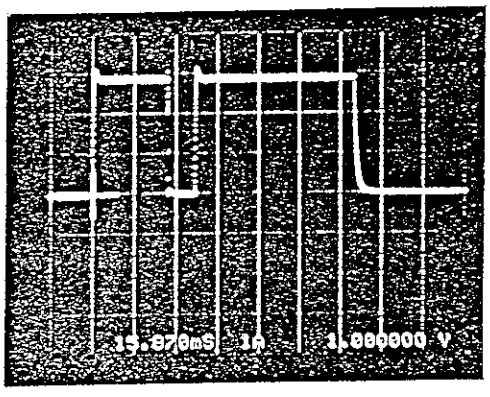

Fig.5.1-4 Waveforms of the acceleration voltage with a breakdown.

5.2 Amorphous Surge Blocker

Output voltage of the acceleration power supply for ITER/FER NBI reaches 1 MV. Energy stored in the stray capacity amounts to several hundred joules. To develop a compact surge blocker, amorphous surge blocker is investigated. An amorphous core has flexibility in shaping and has large saturation magnetic density compared to a ferrite core. Experiments by means of small amorphous cores have been carried out. Major results are summarized below;

1. Saturation magnetic flux density is about four times larger than the ferrite core at around 5 MHz.
2. Permeability at around 5 MHz is almost same as the ferrite core.
3. Amorphous core prove to be effective for surge suppression in the simulation experiments of breakdowns (Fig.5.2-1).

From the experimental data, the weight of the amorphous surge blocker is estimated about half of the ferrite core surge blocker. On a basis of the experimental results, the amorphous surge blocker of 0.05 vs for 350 kV test stand (NIAS) is under manufacturing (Fig.5.2-2).

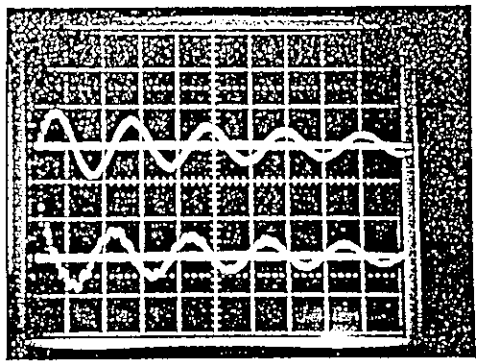

I : 1000 A / div

V : 5.63 kV / div

500 ns / div

Amorphous cores

(a) Without amorphous cores

Impulse voltage

V

I

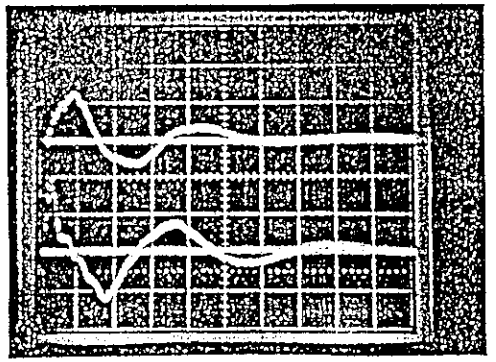

I : 500 A / div

V : 14.1 kV / div

500 ns / div

(b) With amorphous cores

Fig.5.2-1 Waveforms at breakdowns (with and without amorphous cores)

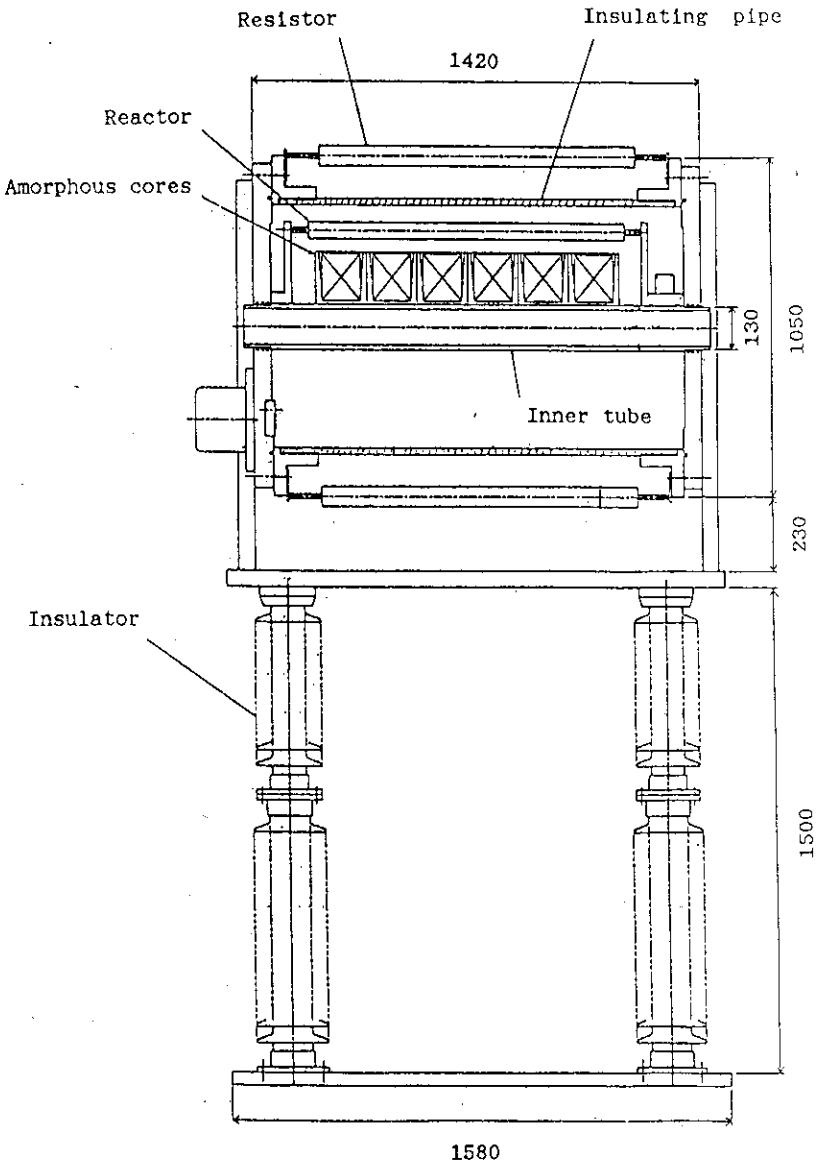

Fig.5.2-2 Amorphous core surge blocker for 350 kV system

5.3 SF_6 Cable Duct

Output of an acceleration power supply have to be transmitted through SF6 cable duct. In a DC voltage system, the effect of conductive dusts and charge up of insulators on voltage holding may be different from an AC voltage system. Experiments on these effects are carried out by means of 500 kV / 300 kV model (Fig.5.3-1). Before the experiments, the calculations of electric field distribution for AC and DC voltage were carried out (Fig.5.3-2). Maximum electric field at the surface of the insulator for DC voltage is around 10 % larger than that for AC voltage. By optimizing the shape of the insulator, conventional AC GIS (Gas Insulated Switchgear) seems to be applicable to DC voltage transmission in a steady state. Considering the calculation results, conductive dusts are attached to the insulators. Experimental results are as follows:

1. There is no difference on DC voltage holding up to 600 kV whether the dust exists or not.
2. Impulse voltage holding decreases down to around 50 % when the dust is attached on the insulators.
3. When the impulse voltage is applied after the DC voltage, the voltage holding decreases by 20 %.

From these results, it is shown that the elimination of the conductive dusts and suppression of the surge voltage are important. They may change the dimension of SF_6 cable duct by factor 2.

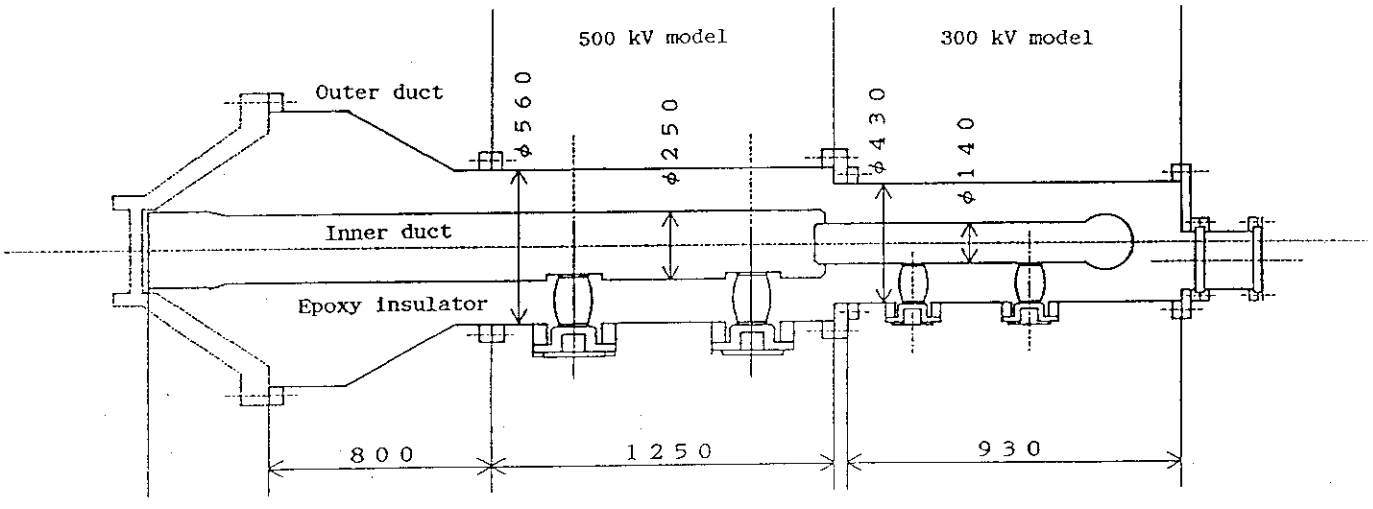

Fig.5.3-1 A SF_6 cable duct model

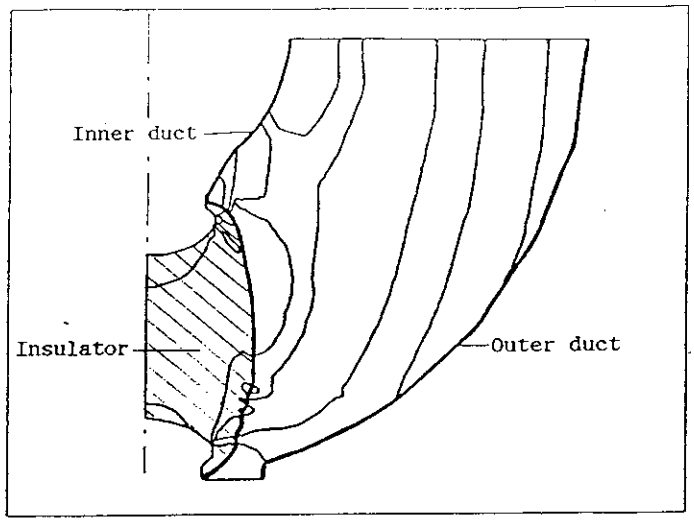

(a) AC electric field

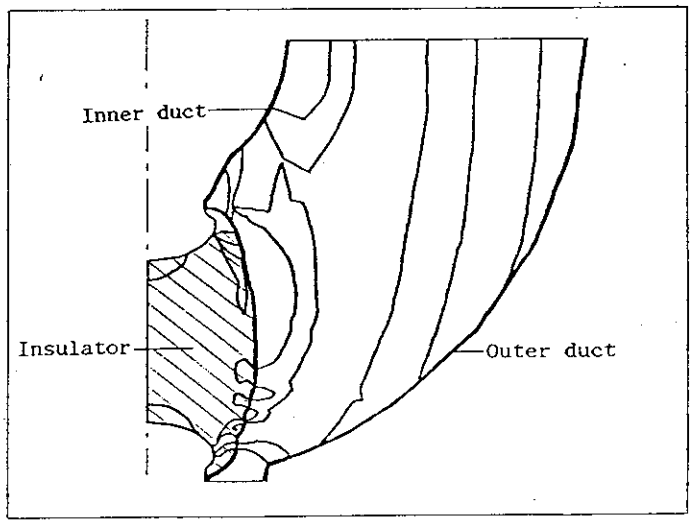

(b) DC electric field

Fig.5.3-2 Simulation of the electric field intensity distribution of the 300 kV model.

6. SUMMARY

R&D efforts to realize a negative-ion-based neutral beam injection system have been made intensively at JAERI for the past several years. Concerning a high current negative ion source, a 10 A, 50 keV negative hydrogen ion beam has been produced successfully. The negative ion beam and the current density corresponds already to the values required for the negative-ion-based NBI system. In order to increase the beam energy, a 350 keV, 0.1 A test stand has been constructed, and the test of a high energy negative ion accelerator has started.

The development of the negative ion sources at JAERI is illustrated in Fig.6-1. The negative ion beam current has reached to a level of the typical ion source for the present NBI systems based on the positive ion beams. Figure 6-2 shows the negative ion beam current and energy obtained so far together with the target values to be attained for the JT-60U and FER/ITER. The beam energy must be increased further by one order of magnitude.

An 100kV, 5A acceleration power supply, which has a high speed AC switch based on 5kHz inverters, has been developed for the JAERI electron beam irradiation stand. The reliable operation indicates that this system can be applied for a MV class acceleration power supply. As one of the promissing proposal for a beam dump element, an externally-finned swirl tube which has the burnout heat flux up to 4.1kW/cm^2 has been developed.

Due to these intensive efforts and results, construction of the 500keV class negative-ion-based NBI system has become realistic in the near future.

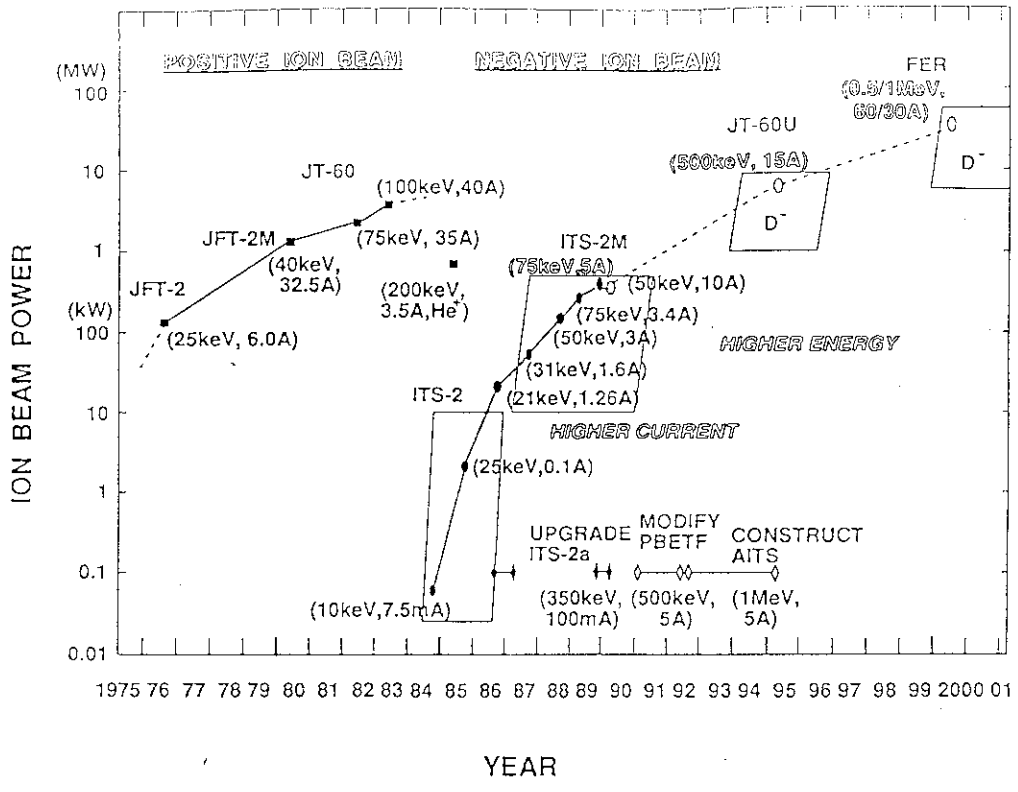

Fig. 6-1 Progress of the negative ion sources at JAERI

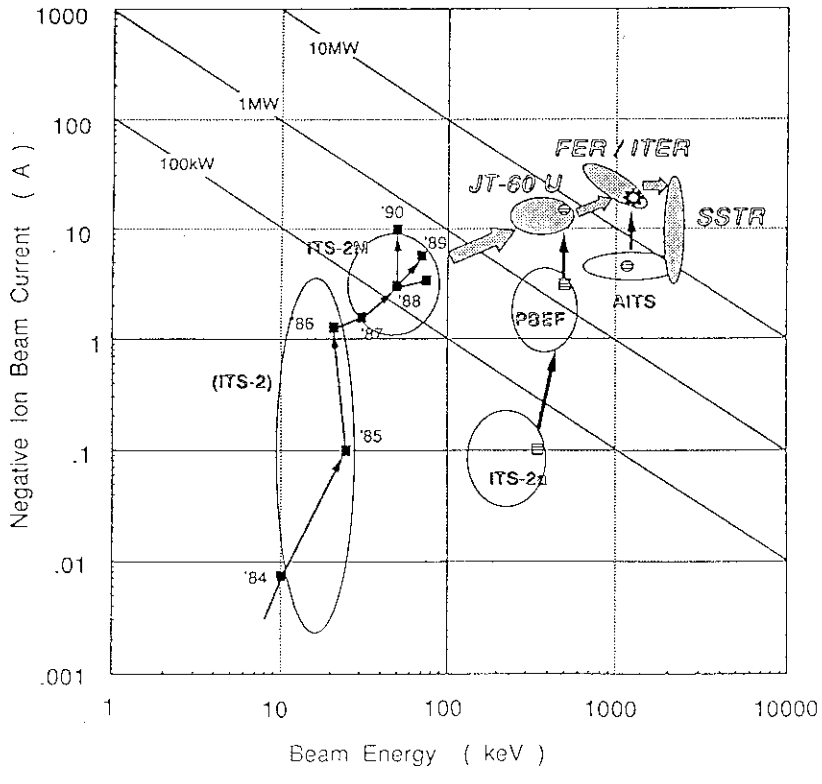

Fig. 6-2 Increase of the negative ion beam current and energy.

Acknowledgement

The authors would like to thank other members of the NBI group for their supports and encouragement in the experiments. They are indebted to Y. Yamashita and T. Uede in Hitachi Ltd., A. Ozaki in Toshiba Corporation, and K. Nakada in Nissin Electric Co. Ltd., for their participation in the R&D activities. They are also grateful to S. Matsuda and S. Simamoto for their continuous encouragement.

Appendix 1 Negative Ion Source Development in the World

Since the neutralization efficiency of the positive ions become fairly low at the energy above 100 keV/nucleon, it is impossible to realize a positive-ion-based NBI system with high system efficiency. Hence NB scientists in the world changed their scopes to negative ion source R&D after developing positive-ion-based NBIs for the existing large tokamaks such as TFTR, JET and JT-60.

In the initiation of the R&Ds, three basic processes were investigated as candidates for the high current negative ion production; i.e. charge exchange[1-3], surface production[4-7], and volume production[8-17]. Table A1-1 summarizes typical parameters achieved in some negative ion sources based on these three processes.

Throughout several years of the research, it was recognized that the volume production is the most attractive method for the future NBI systems. The reasons are summarized as follows: i)This process requires no cesium, then ii)it makes the source operation stable and reliable. In addition, iii)their structure is simple enough to scale up, and iv)the produced negative ion has good beam qualities[18,19]. Owing to these advantages, R&D of the volume negative ion sources have been progressed as a main current[20-23].

In this decade, many scientists worked on the volume production type source, especially multicusp source with magnetic filter, which is an extrapolation of the bucket type positive ion source. However, it is not successful yet to obtain high negative ion current density (more than 20 mA/cm^2) at the low operating pressure, which is a key to realize a high efficiency and compact NBI systems. Up to now, the current density obtained by the pure volume source is very low at the pressure required for future NBI systems, as shown in Fig. A1-1. R&D on the source of this type is energetically continued at Culham[24]. They proposed to overcome its defects by mounting cryopumps in the accelerator region, which will reduce the pressure in the extractor and accelerator, and subsequently the stripping loss is minimized.

Resently, a small amount of cesium vapor was seeded into the conventional multicusp source called "Multi Ampere Negative Ion Source" at JAERI[25], then the current density was improved by a factor of four at a low pressure of 0.5 Pa. In addition, the electron current extracted from the plasma was reduced to almost zero. The source could have operated stably for a week at a low Cs consumption rate. It was also confirmed that impurity content in the beam was less than 1 %.

Another cesiated source, called hydrogen-cesium plasma-volume source, is being developed at Kurchatov[26]. The source is an axi-symmetric geometry with a hollow cathode as a cesium injector. They have succeeded in extracting H^- stably at the current density of 60 mA/cm^2 (at the emission surface).

LBL[27] started to develop an advanced surface source. The source uses barium, of which vapor pressure is two orders of magnitude lower than that of Cs. This change of the coverage material on the converter may reduce problems of voltage holding and beamline contamination. They have obtained 145 mA of D^- from 6 cm diameter converter at a quite low pressure of 1.25 mTorr. They encountered a few troubles in the source operation; One is the contamination of the Ba converter, which affect negative ion production considerably. The other is high transverse ion temperature in the extracted beam, which is proportional to the converter voltage.

As described above, they are trying to improve the source performance by Cs or Ba, which was thrown away once and now being looked back with some high technology supports. Fig. A1-2 shows a summary of negative ion source R&Ds. Thus the production of the high current negative ions has become realistic for the next generation fusion reactor.

Reference

[1]C. Jacquot, P. Ludwig, J. C. Rocco and F. Zadworny: Proc. IAEA Tech. Comittee Meeting on Negative Ion Beam Heating, Grenoble (1985) 113

[2]E. B. Hooper, P. Poulsen and P.A. Pincosy: J. Appl. Phys. 52 (1981) 7027

[3]V. V. Kuznetsov, N. N. Semashko, A. I. Krylov I. A. Ilunin and P. S. Firsov: Proc. IAEA Tech. Comittee Meeting on Negative Ion Beam Heating, Grenoble (1985) 110

[4]Yu. I. Bel'chenko and G. I. Dimov: Proc. Int. Symp. on the Production and Neutralization of Negative Ions and Beams, Broolheaven (1983) 363

[5]K. Prelec, ibid.,333

[6]J. W. Kwan, G. D. Ackerman, O. A. Anderson, C. F. Chen, W. S. Cooper et.al.: Rev. Sci. Instrum.,57 (1986) 831

[7]G. Dammertz and B. Piosczyk: 4th Int. Symp. on Heating in Toroidal Plasma, Rome (1984) 1087

[8]J. W. Kwan, O. A. Anderson, C. F, Chen, W. S. Cooper, K. N. Leung et.al.: 2nd IAEA Tech. Comittee Meeting on Negative Ion Beam Heating, Culham (1987)

[9]A. J. T. Holmes, G. Dammerz, T. S. Green: Rev. Sci. Instrum. 57 (1986) 2402

[10]M. Bacal and F. Hillon: Rev. Sci. Instrum. 56 (1985) 2274

[11]J. H. Bonnie, P. J. Eenshuisstra and H. J. Hopman: Phys. Rev. Lett. 57 (1986) 3256

[12]O. Fukumasa and S. Saeki: J. Phys. D: Appl. Phys. 20 (1987) 237

[13]K. R. Kendall, M. Mcdonald, D. R. Mosscrop, P. W. Schmor, D. Yuan et.al.: Rev. Sci. Instrum. 57 (1986) 1277

[14]W. K. Dagenhart, C. C. Tsai, W. L. Stirling, P. M. Ryan, D. E. Schecher et.al.: 4th Int. Symp. on the Production and Neutralization of Negative Ions and Beams, Brookheaven (1986)

[15]J. Uramoto: Res. Report of Institute of Plasma Phys., Nagoya Univ. IPPJ-645

[16]G. Hellblom and C. Jaquot: Nucl. Instrum. Meth. in Phys Res. A243 (1986) 255

[17]Y. Okumura, H. Horiike, T. Inoue, T. Kurashima, S. Matsuda et.al.: Proc. 4th Int. Symp. on the production and Neutralization of Negative ions and Beams, Brookheaven (1986)

[18]Y. Okumura et.al.: JAERI-M 89-090 (1989)

[19]D. H. Yuan, R. Baartman, K. R. Kendal, M. McDonald, D. R. Mosscrop: Proc. 4th Int. Symp. on Production and Neutralization of Negative Ions and Beams, Brookheaven, (1986) 346

[20]K. N. Leung, K. W. Ehlers, C. A. hauck, W. B. Kunkel and A. L. Lietzke, Rev. Sci. Instrum. "A Small Multicusp Source" (1987)

[21]L. M. Lea, A. J. T. Holmes, G. O. R. Naylor, D. C. Clark and A. F. Newman: Proc. 3rd European Workshop on Production and Application of Light Negative Ions, (1988) 59

[22]A. I. Krylov, V> V> Kuznetsov, D. V. Penkin and N. N. Semashko: Proc. 5th Int. Symp. on the Production and Neutralization of Negative Ions and Beams, Brookheaven, (1989)

[23]M. Hanada et.al.: Rev. Sci. instrum. 61/1 (1990) 499

[24]A. J. T. Holmes et.al.: reported at ITER NB Specialists Metting, Garching, July (1990)

[25]S. P. Antipov, L. I. Elizarov, M. I. Martynov, V. M. Chesnokov: Proc. 5th Int. Symp. on the Production and Neutralization of Negative Ions and Beams, Brookheaven, (1990)

[26]Y. Okumura et.al.: Proc. 5th Int. Symp. on the Production and Neutralization of Negative Ions and Beams, Brookheaven, (1990)

[27]W. S. Cooper et.al.: roported at ITER NB Specialists Meeting, Garching, July (1990)

Table A1-1 Negative Ion Source Development in the World

Method	Laboratory	Current (A)	Beam Energy (keV)	Pulse length (s)	Current Density (mA/cm^2)
Charge Exchange	LBL[2]	2.2	10.5	70	12
	Kurchatov[3]	5.5	80	0.01	26
Surface Production	Novosibirsk[4]	11	25	$0.2 - 0.8 \times 10^{-3}$	180
	BNL[5]	0.2 - 0.3	7.5	DC	40 - 100
	LBL[6]	1.25	80	DC	10
	LBL(w. Ba)[27]	0.145	0.3	DC	5 (12 @centre)
Volume Production	Ecole Poly.[10]	0.1×10^{-3}	1	DC	0.3
	TRIUMF[11]	0.004	25	DC	29
	ORNL[12]	0.08	16.4	0.1	27
	LBL[8]	0.017	80	0.25	17
	LBL[20]	0.002	-	0.001	250
	Culham[9]	0.13	83	30	30
	Culham[21]	-	9.5	-	12
	Kurchatov(w. Cs)[26]	3.3	0.38 (?)	-	100
	JAERI[23]	3.4	50	0.1	13
	JAER(w. Cs)I[25]	10.2	50	0.1	36

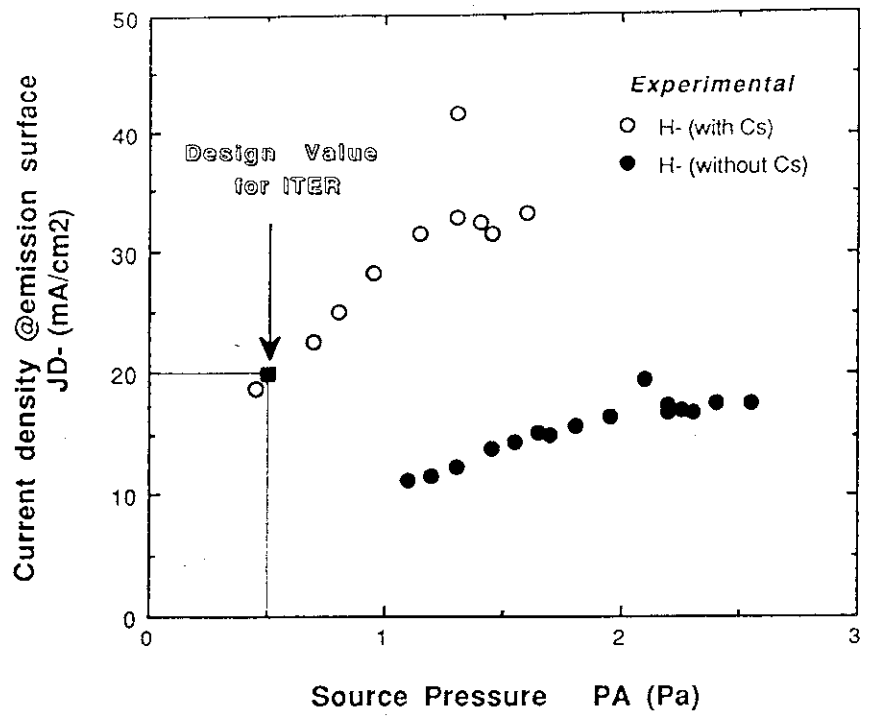

Fig. A1-1 Performance of Cs seeded source and ITER design value

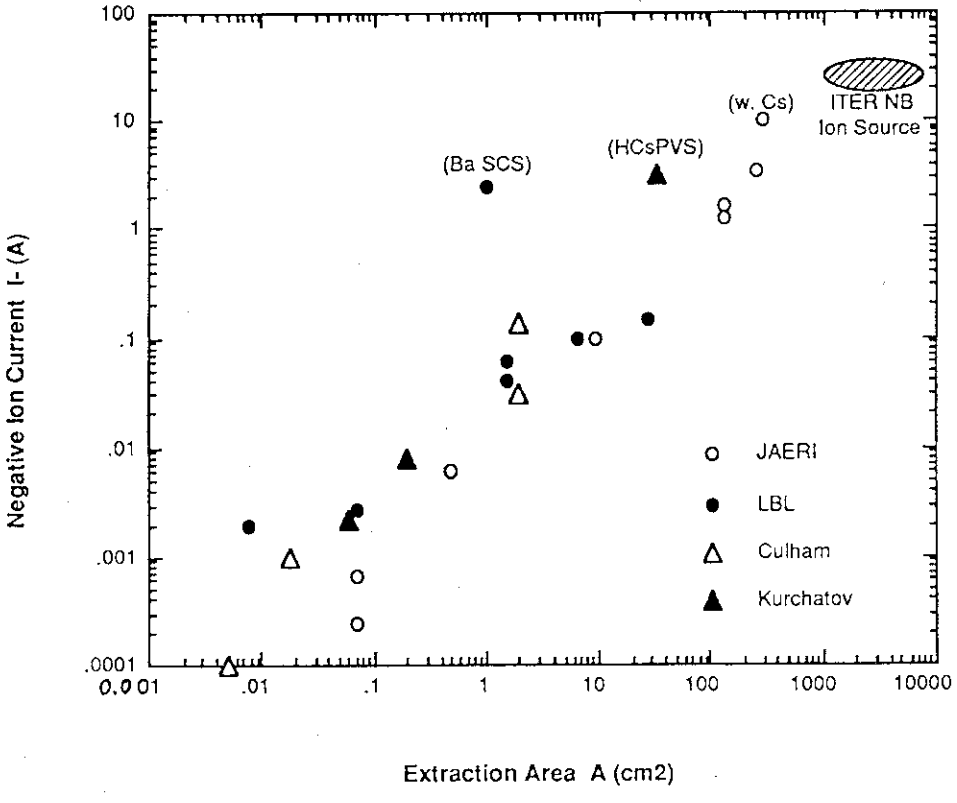

Fig. A1-2 Progress of negative ion source development in the world

Appendix 2 Types of Negative Ion Sources for the NBI systems

Various types of the negative ion sources and accelerators for the ITER NBI are illustrated according to the articles presented at the ITER specialist meeting held in 1989-1991.

(1) JAERI Design

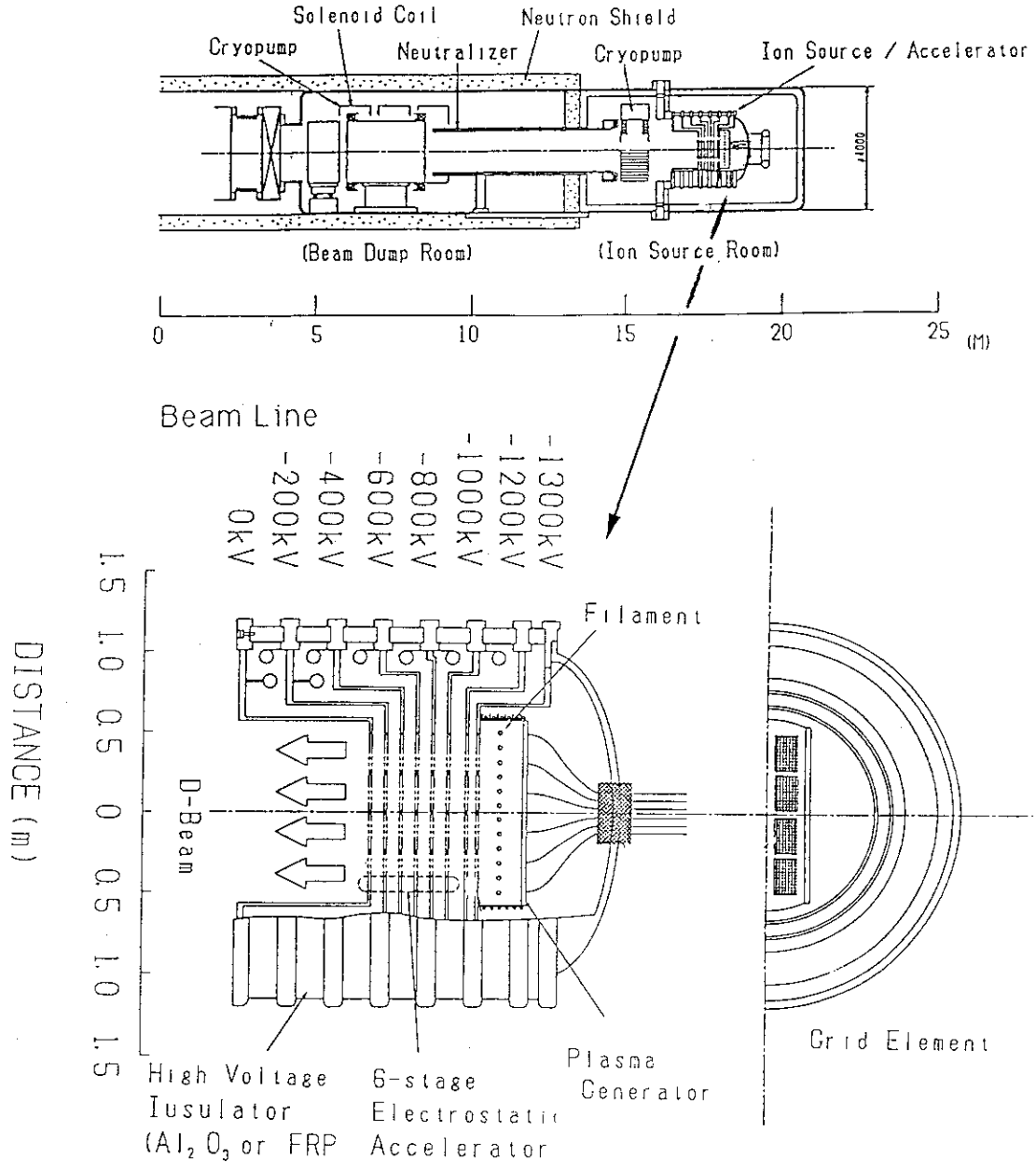

Electro Static Accelerator Cs-seeded Volume Source

(2) EC Design

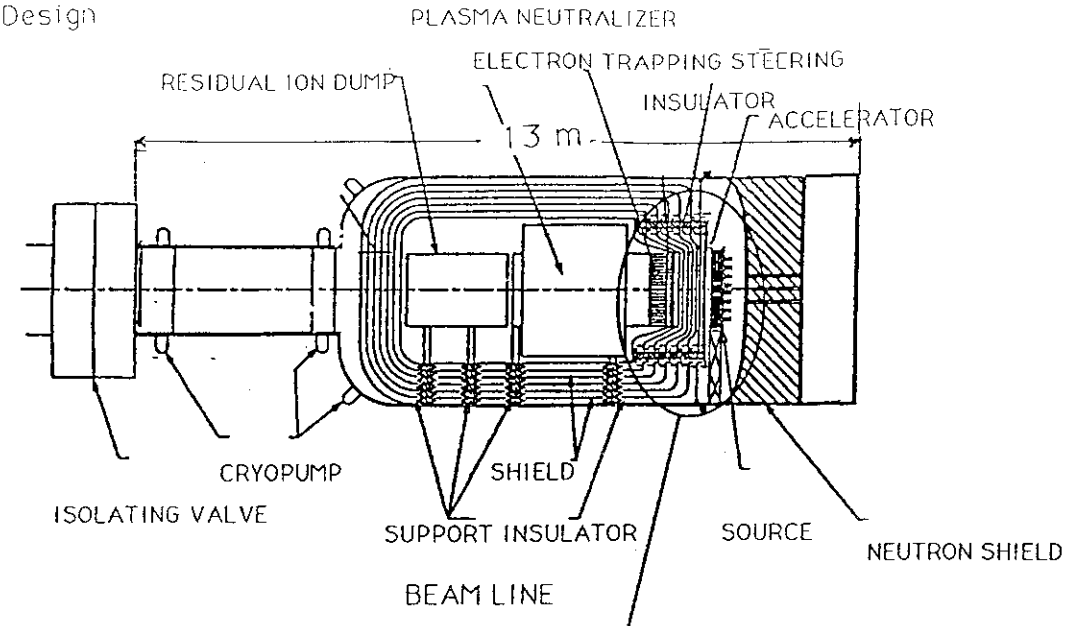

BEAM LINE

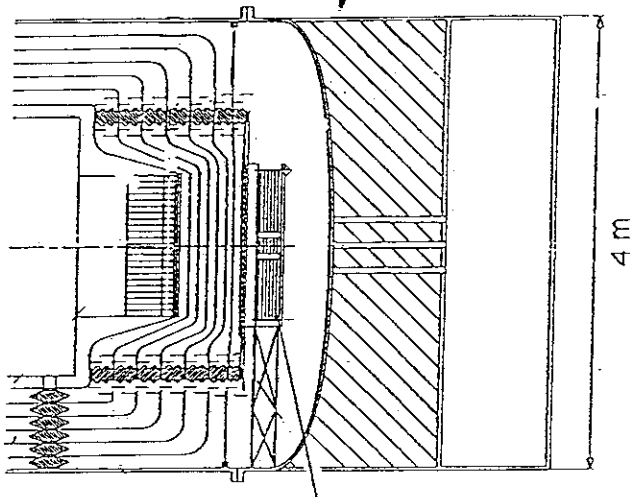

SOURCE & ACCELERATOR

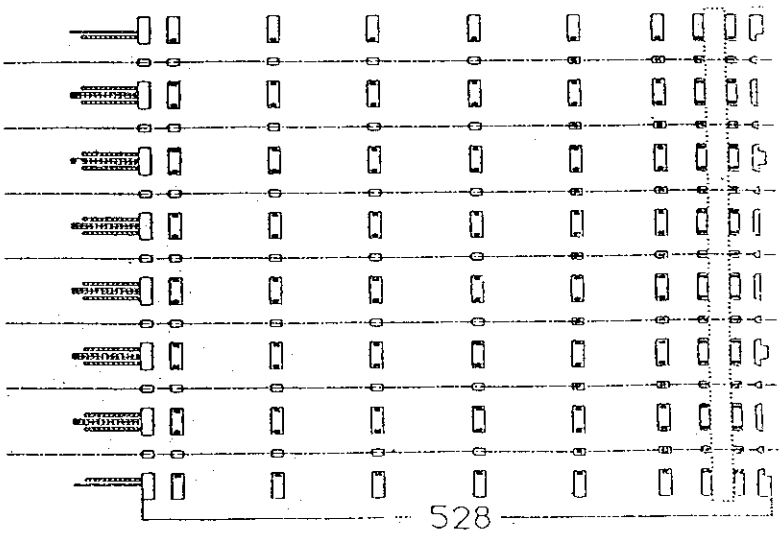

ELECTRO STATIC ACCELERATOR

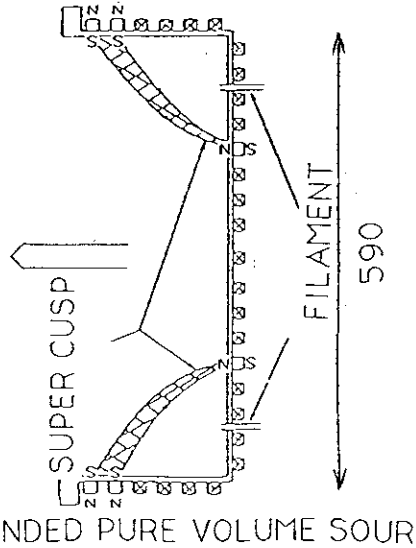

GROUNDED PURE VOLUME SOURCE

(3) US Design

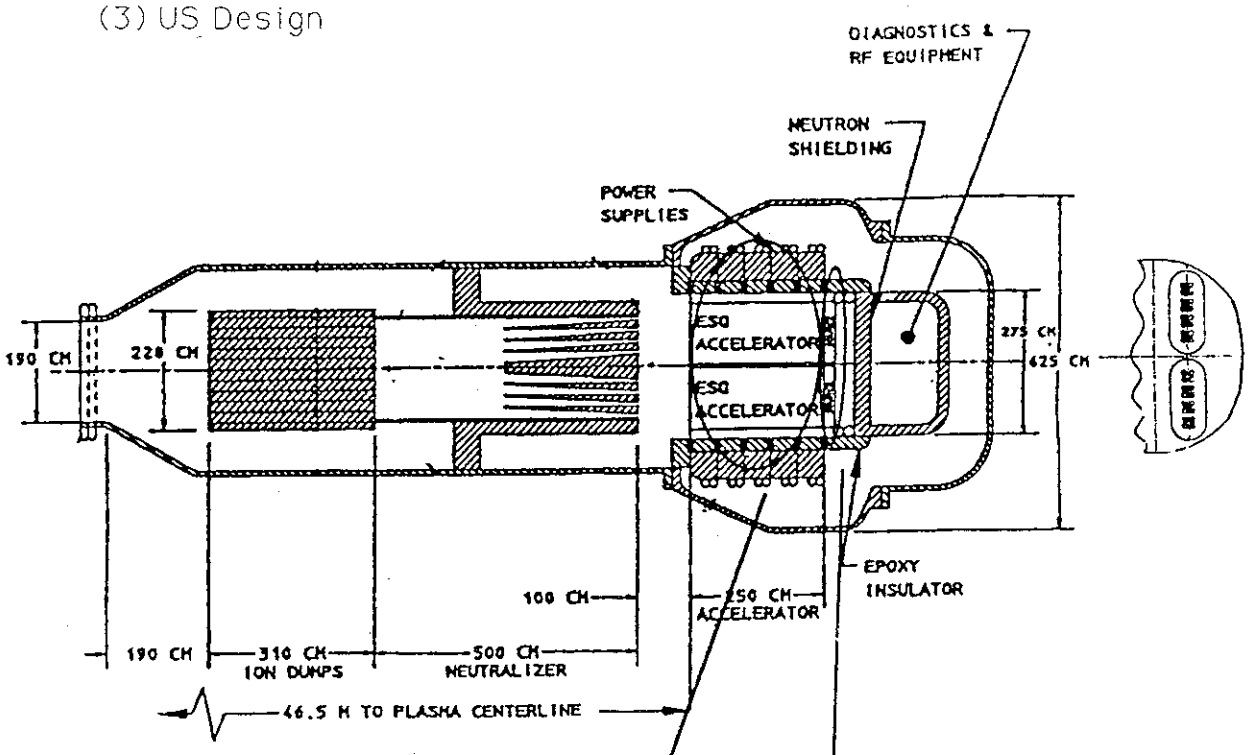

Beam Line

Ba Surface Source

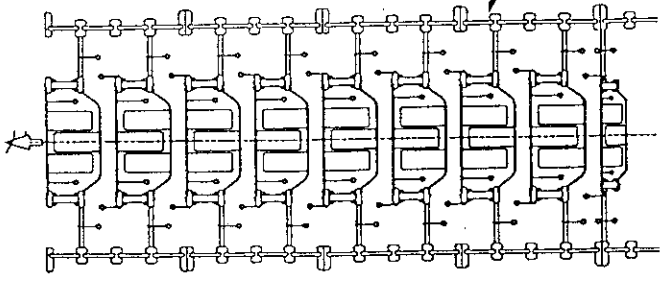

Electro Static Quadrupole Accelerator
(ESQ)

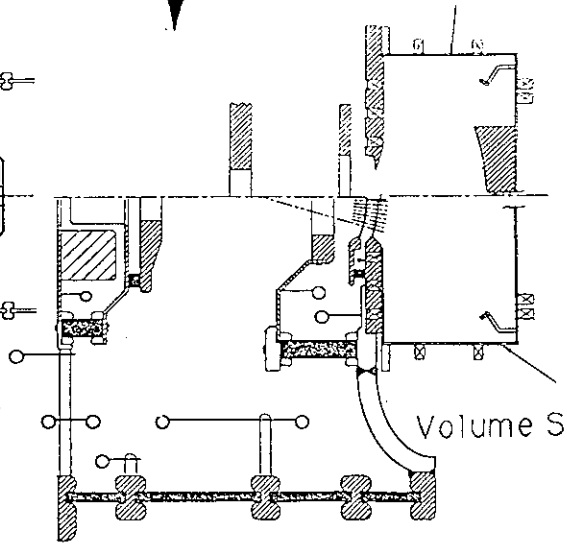

Volume Source

Ba Surface Sourcce
Pure Volume Source
1A/channel

(4) Soviet Union

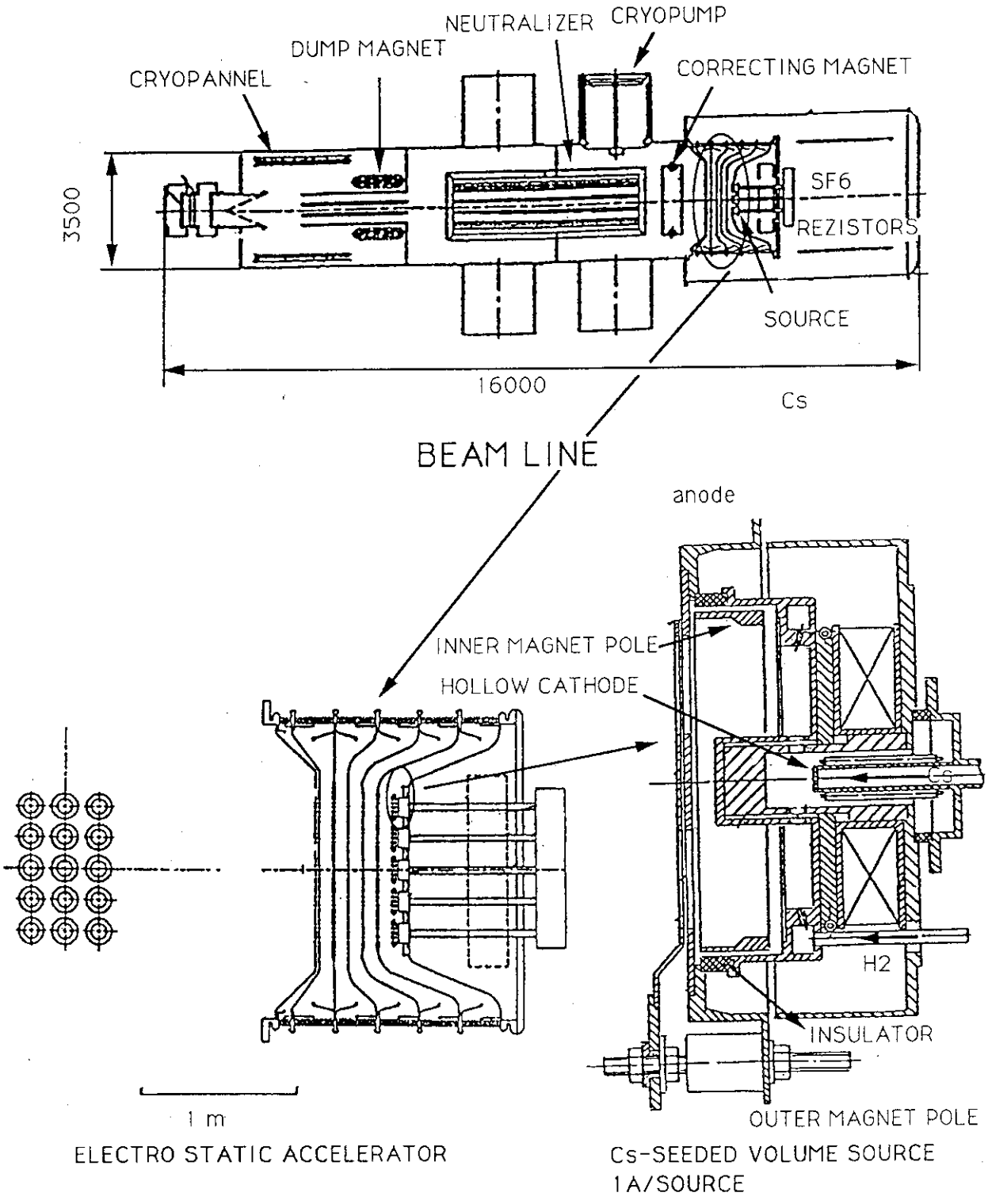

Major Computer Codes Developed for the Design of the NBI Systems

	Code Name	Purpose	Basic Equations	Numerical Method	Examples	References
1	IONORBIT	Calculation of 2D axisymmetric ion Orbits in the X-Y, or R-Z coordinates $E \neq 0$ $\rho \neq 0$ $B = 0$	Poisson's Equation Equation of Motion	Finite-Difference Calculus	Ion Source Extractor / Accelerator Electron Gun	Y. Ohara : JAERI-M 6757 (1976) [in Japanese].
2	BEAMXY	Calculation of 2D non-axisymmetric sheet ion beam orbits (X-Y) in a magnetic field Bz $E \neq 0$ $\rho \neq 0$ $B_z \neq 0$	Poisson's Equation Equation of Motion	Finite-Difference Calculus	Ion Source Extractor / Accelerator Electron Gun	Y. Ohara : JAERI-M 6757 (1976) [in Japanese].
3	BEAM3D	Calculation of 3D ion beam orbits in a 3D magnetic field $E \neq 0$ $\rho \neq 0$ $B \neq 0$ $\mu = 1$	Poisson's Equation Equation of Motion	Finite-Element Calculus	Ion Source Extractor / Accelerator Aperture Displacement	Original code is developed by K. Ohta ; Thesis of Faculty of Engineering, University of Tokyo (1983), and modified by Y. Ohara
4	ELEORBIT	Calculation of electron orbits in a 3D magnetic field $E = 0$ $\rho = 0$ $B \neq 0$ $\mu = 1$	Equation of Motion	Runge-Kutta	Ion Source Plasma Generator 1. Magnetic field distribution 2. Primary electron orbits Backstream Electron Orbits	Y. Ohara and H. Inami et al. : J. Appl. Phys. 61 (4), 1323 (1987).
5	DENSIT3D	Calculation of gas density spatial distribution in a molecular flow with temperature gradient		Monte Carlo	Gas density distribution in an ion source accelerator	Developed by M. Hanada, Y. Okumura and K. Shibanuma.
6	BEAMPROF	Calculation of beam intensity profile in a beamline	Integration of gaussian-like beamlet profile		Geometric transmission efficiency Heat flux distribution in the beam-line and on the torus far wall	Y. Ohara and M. Kuriyama: JAERI-M 82-066 (1982) [in Japanese]
7	NBI3DGF	Calculation of charged particle orbits in a 3D magnetic field, where each particle is weightened according to their power $E = 0$ $\rho = 0$ $B \neq 0$ $\mu \neq 1$	Equation of Motion	Runge-Kutta	Beam profile controller Relonized ion orbits Beam dump Bending magnet	Developed by Y. Ohara
8	DCON2D	Calculation of 2D axisymmetric ion beamm orbits in X-Y, and R-Z coordinates $E \neq 0$ $\rho \neq 0$ $B = 0$	Poisson's Equation Equation of Motion	Finite-Difference Calculus Runge-Kutta	Direct energy recovery	Developed by H. Horiike
9	DCON3D	Calculation of 3D ion beam orbits in a 3D magnetic field $E \neq 0$ $\rho \neq 0$ $B \neq 0$ $\mu = 1$	Poisson's Equation Equation of Motion	Finite-Element Calculus	Direct energy recovery	Original code is developed by H. Watanabe : Thesis of Department of Electrical Engineering II, Kyoto University (1986), and modified by M. Araki.
10	COMPAS	Calculation of neutralization efficiency of the ion beam in a gas cell			Neutralization efficiency of H+ and H- ion beams	Developed by Y. Okumura

Types of the Acceleration Power Supply

TYPE	PRESENT STATUS	PROSPECTS
Rectifier-Transformer (DC - switch)	Low voltage (~ 200 kV) Large current (~ 100 A) Output can be cut off in less than 10 μs by DC switch. Commonly used in the present NBI systems.	Difficult to increase the voltage up to MV region. Current of more than 100 A may be possible.
Rectifier-Transformer (AC - switch)	Low voltage (0.1 MV) Medium current (5 A) Output can be cut off in less than ~ 100 μs by AC switch.	Possible to increase the voltage up to MV region and the current up to 100 A.
Cockcroft-Walton (Schenkel)	High voltage (< 5 MV) Small current (~ few 100s mA) Protection by series resistors.	Current of more than 1 A may be possible by high frequency operation.
Electrostatic generator (Van de Graaff, Pelletron)	High voltage (~ several10s MV) Small current (~ several mA)	Difficult to increase current. Require mechanical maintainance.

Typical Operational Region of the Acceleration Power Supply

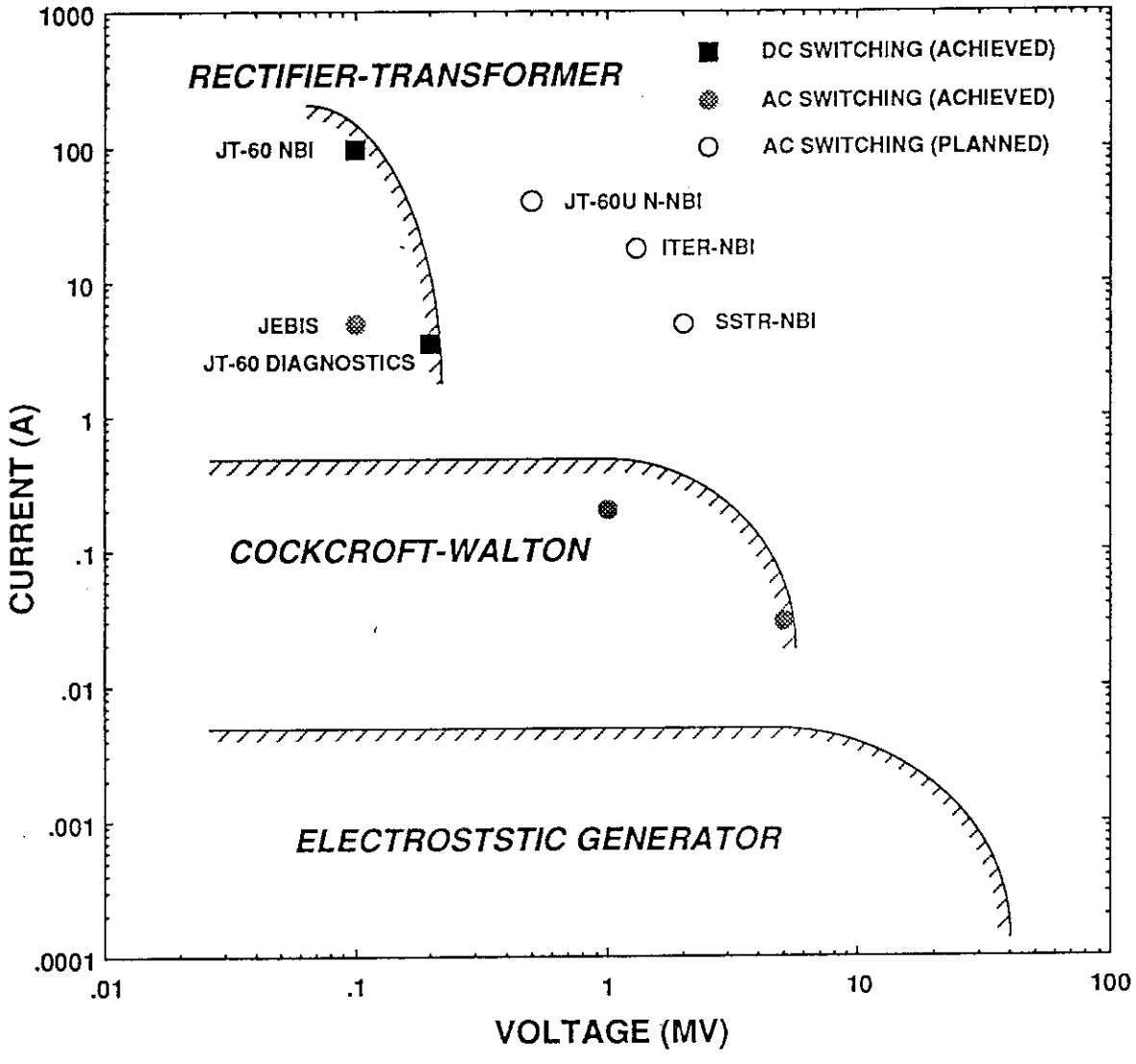

A4 - 2

Appendix 5 List of Papers Concerning the JAERI R&D Activities on the Negative-ion-based NBI System

List of the Papers Concerning the JAERI R&D Activities on the Negative - Ion - Based NBI System

	TITLE	AUTHORS	PUBLICATION	YEAR
OVERALL				
1	Negative - Ion - Based Neutral Beam Injector for steady State Operation of Tokamak Fusion Reactor	S. Tanaka	Journal of the Atomic Energy Society of Japan, 33 (7), pp. 573 - 579 [in Japanese]	1986
2	Development of 20 MW Neutral Hydrogen Beam Injector and the Plan for Developing Next Step Intense Neutral Beam for Fusion Research	S. Matsuda and M. Akiba	Proc. of the 11th Symp. on Ion Sources and Ion-Assisted Technology, Tokyo, June 1 - 3, pp. 95 - 104.	1987
3	Recent Activities on Negative Ion Beams at JAERI	Y. Ohara, M. Akiba, M. Araki, M. Hanada, T. Inoue, H. Kojima, M. Kuriyama, M. Matsuoka, M. Mizuno, Y. Matsuda, Y. Okumura, M. Seki, S. Tanaka, and K. Watanabe	Proc. of the 13th Symp. on Fusion Engineering, Knoxville, Oct. 2 - 6, pp. 284 - 287	1989
4	Negative Ion Beam Programs at JAERI	Y. Ohara	Proc. of the 5th Int. Symp. on the Production and Neutralization of Negative Ions and Beams, Brookhaven, Oct. 30 - Nov. 3	1989
5	Fusion Reactor Development Using High Power Particle Beams	Y. Ohara	Proc. of the 2nd Int. Symp. on Advanced Nuclear Energy Research -- Evolusion by Accelerators -- Mito, Japan, Jan. 24 - 26, pp. 120 - 125	1990
R&Ds on Ion Sources				
1	Development of a Volume H - Ion Source for Neutral Beam Injector	Y. Okumura, Y. Ohara, H. Horiike and T. Shibata	Japan Atomic Energy Research Institute Report JAERI - M 84 - 098	1984
2	H - Production in Large Bucket Source at JAERI	T. Shibata, H. Horiike, H. Inami, S. Matsuda, Y. Ohara, Y. Okumura, and S. Tanaka	Proc. of the IAEA Technical Committee Meeting on Negative Ion Beam Heating, Grenoble	1985
3	Development of a Volume Produced H - Ion Source	Y. Okumura, H. Horiike, H. Inami, Y. Ohara, and T. Shibata	Proc. of the 9th Symp. on Ion Sources and Ion-Assisted Technology, Tokyo, June 3 - 5, pp. 121 - 124.	1985

List of the Papers Concerning the JAERI R&D Activities on the Negative - Ion - Based NBI System

	TITLE	AUTHORS	PUBLICATION	YEAR
4	Development of a Volume H - Ion Source st JAERI	Y. Okumura, H. Horiike, H. Inami, S. Matsuda Y. Ohara, T. Shibata, and S. Tanaka	Proc. of the 11th Symp. on Fusion Engineering, Austin, Texas, Nov. 18 -22, pp. 113 - 117.	1985
5	A High Current Volume H - Ion Source with Multi-Aperture Extractor	Y. Okumura, H. Horiike, T. Inoue, T. Kurashima, S. Matsuda, Y. Ohara, and S. Tanaka	Proc. of the 4th International Symp. on the Production and Neutralization of Negative Ions and Beams, Brookhaven Nat. Lab., Oct. 26 - 31, pp. 309 - 318.	1986
6	Steady - State H - Ion Production in a Magnetically Filtered Multicusp Plasma Generator	T. Inoue, M. Araki, T. Kurashima, Y. Ohara, Y. Okumura, and S. Tanaka	Proc. of the 11th Symp. on Ion Sources and Ion-Assisted Technology, Tokyo, June 1 - 3, pp. 173 - 176.	1987
7	Development of High Intensity Negative Ion Source for Neutral Beam Injectors	Y. Okumura	ibid. pp. 267 - 276.	1987
8	One Ampere Volume H - Ion Source with Multi-Aperture Extractor	Y. Okumura, M. Araki, M. Hanada, H. Horiike, T. Inoue, T. Kurashima, S. Matsuda, Y. Matsuda, Y. Ohara, S. Tanaka, and K. Watanabe	Proc. of the IAEA Technical Committee Meeting on Negative Ion Beam Heating, Culham Lab., July 15 - 17.	1987
9	Multi-Ampere H - Beam Production in a Volume Ion Source	K. Watanabe, M. Araki, M. Hanada, H. Horiike, T. Inoue, T. Kurashima, S. Matsuda, Y. Matsuda, Y. Ohara, Y. Okumura, and S. Tanaka	Proc. of the 12th Symp. on Fusion Engineering, Monterey, California, Oct. 12 - 16, pp. 302 - 305	1987
10	Multi - Ampere Negative Hydrogen Ion Source for Fusion Application	T. Inoue, M. Araki, M. Hanada, T. Kurashima, S. Matsuda, Y. Matsuda, Y. Ohara, Y. Okumura, s. Tanaka, and K. Watanabe	The 7th Int. Conf. on Ion Implantation Technology - ITT'88, Kyoto, June 7 - 10 [Nuclear Instruments and Methods in Physics Research B37 / 38, 111 - 115, 1989.]	1988
11	Development of a High Current Negative Ion Source for Fusion Application	Y. Okumura	Kakuyugo Kenkyu 60, 329 [in Japanese].	1988
12	Measurement of Impurities in a Volume Produced H - Ion Beam	Y. Okumura, M. Hanada, H. Kojima, Y. Matsuda, and H. Oohara	Japan Atomic Energy Research Institute Report JAERI - M 89 - 090 [in Japanese].	1989

List of the Papers Concerning the JAERI R&D Activities on the Negative - Ion - Based NBI System

	TITLE	AUTHORS	PUBLICATION	YEAR
13	Multi-Ampere Negative Ion Source	M. Hanada, T. Inoue, H. Kojima, Y. Matsuda, Y. Ohara, Y. Okumura, and K. Watanabe	Proc. of the 12th Symp. on Ion Sources and Ion-Assisted Technology, Tokyo, June 5 - 7, pp. 17 - 22.	1989
14	High Density ECR Plasma for Negative Ion Source	Y. Matsuda, M. Hanada, T. Inoue, H. Kojima, Y. Ohara, Y. Okumura, and K. Watanabe	ibid. pp. 107 - 110.	1989
15	Beam Optics of a Multi-Single Type Negative Ion Beam Acceleration	Y. Ohara, Y. Matsuda, Y. Okumura, and K. Watanabe	ibid. pp. 143 - 146.	1989
16	Comparison of H - and D - Production in a Magnetically Filtered Multicusp Source	T. Inoue, G. D. Ackerman, W. S. Cooper, M. Hanada, J. W. Kwan, Y. Ohara, Y. Okumura, and M. Seki	Int. Conf. on Ion Sources, Berkeley, 10 - 14 July. [Rev. Sci. Instrum. 61 (1), 496 - 498, 1990]	1989
17	A 14cm x 36cm Volume Negative Ion Source Producing Multi-Ampere H - Ion Beams	M. Hanada, T. Inoue, H. Kojima, Y. Matsuda, Y. Ohara, Y. Okumura, K. Watanabe, and M. Seki	ibid. [Rev. Sci. Instrum. 61 (1), 499 - 501, 1990]	1989
18	Cesium Mixing in the Multi-Ampere Volume H - Ion Siurce	Y. Okumura, M. Hanada, T. Inoue, H. Kojima, Y. Matsuda, Y. Ohara, M. Seki, and K. Watanabe	Proc. of the 5th Int. Symp. on the Production and Neutralization of Negative Ions and Beams, Brookhaven, Oct. 30 - Nov. 3	1989
19	Development of a Large Current H - Ion Source	K. Watanabe, M. Hanada, T. Inoue, H. Kojima, Y. Matsuda, Y. Ohara, Y. Okumura, and M. Seki	Proc. of the 2nd Int. Symp. on Advanced Nuclear Energy Research, Mito, Japan, Jan. 24 - 26, pp. 447 - 452.	1990
20	A Large Multicusp Source Producing a 10 A, 50 keV, 0.1 s H - Ion Beam	H. Kojima, M. Hanada, T. Inoue, Y. Matsuda, Y. Ohara, Y. Okumura, H. Oohara, K. Watanabe, and M. Seki	Proc. of the 13th Symp. on Ion Sources and Ion-Assisted Technology, Tokyo, June 4 - 6, pp. 145 - 148.	1990
21	Effect of Cesium Vapor Injection in a Large Volume H - Ion Source	Y. Okumura, M. Hanada, T. Inoue, H. Kojima, Y. Matsuda, and K. Watanabe	ibid. pp. 149 - 152.	1990
22	Beam Optics of a Multi-Ampere Negative Ion Source	K. Watanabe, M. Hanada, T. Inoue, H. Kojima, Y. Hanada, Y. Ohara, and Y. Okumura	ibid. pp. 153 - 156.	1990

List of the Papers Concerning the JAERI R&D Activities on the Negative - Ion - Based NBI System

	TITLE	AUTHORS	PUBLICATION	YEAR
R&Ds on Beamline Components				
1	Burnout Experiments on the Externally - Finned Swirl Tube for Steady - State and High - Heat Flux Beam Stops	M. Araki, M. Dairaku, T. Inoue, M. Komata, M. Kuriyama, S. Matsuda, M. Ogawa, Y. Ohara, M. Seki, and K. Yokoyama	Fusion Engineering and Design, 9, 231 - 236	1989
R&Ds on Power Supply System				
1	Inverter Type High Voltage DC Power Supply for Negative - Ion - Based Neutral Beam Injectors	M. Mizuno, M. Dairaku, Y. Ohara, A. Ozaki, S. Tanaka, T. Uede, K. Watanabe, Y. Yamashita, and K. Yokoyama	Proc. of the 13th Symp. on Fusion Engineering, Knoxville, Oct. 2 - 6, pp. 574 - 577	1989
Design				
1	Conceptual Design of a 500 keV, 20 MW Negative - Ion - Based Neutral Beam Injector for FER	T. Shibata, H. Horiike, S. Matsuda, Y. Ohara, Y. Okumura, and S. Tanaka	Kakuyugo Kenkyu 56 (2), 124 - 133 [In Japanese].	1986
2	Conceptual Design of Negative-Ion-Based 500 keV 20 MW Neutral Beam Injector	H. Horiike, Y. Ohara, Y. Okumura, T. Shibata, and S. Tanaka	Japan Atomic Energy Research Institute Report JAERI - M 86 -064 [in Japanese].	1986
3	Tokamak Reactor Operation Scinario Based on Plasma Heating and Current Drive by Negative - Ion - Based Neutral beam Injector	S. Yamamoto, K. Okano, S. Nishio, M. Sugihara, R. Saito, T. Uede, T. Kobayashi N. Fujisawa, T. Tone. Y. Ohara, S. Tanaka, H. Horiike, Y. Okumura, T. Shibata, S. Matsuda. K. Tani, T. Hirayama, M. Azumi.	Proc. of the 11th International Conf. on Plasma Physics and Controlled Nuclear Fusion Research, Kyoto, IAEA-CN-47 / H - I - 3, pp267 - 277.	1986
4	Design of a 500 keV, 20 MW Negative - Ion - Based Neutral beam injection system for Fusion Experimental Reactor	Y. Ohara, M. Akiba, M. Araki, H. Horiike, T. Inoue, S. Matsuda, M. Matsuoka, K. Mizuhashi, M. Mizuno, K. Nakashima, y. Okumura, K. Shibanuma, S. Tanaka, T. Uede, K. Watanabe, and S. Yamamoto	Proc. of the 12th Symp. on Fusion Engineering, Monterey, California, Oct.12-16, pp. 298 - 301.	1987

List of the Papers Concerning the JAERI R&D Activities on the Negative - Ion - Based NBI System

	TITLE	AUTHORS	PUBLICATION	YEAR
5	Conceptual Design Study of Fusion Experimental Reactor (FY86FER) – NBI Heating and Current Drive System Design –	K. Nakashima, S. Yamamoto, T. Uede, K. Okano, Y. Ohara, K. Watanabe, M. Mizuno, and M. Araki	Japan Atomic Energy Research Institute Report JAERI - M 87 - 145 [in Japanese].	1987
6	NAVIGATOR (FER) - Negative - Ion - Grounded Advanced Tokamak Reactor -	S. Yamamoto, Y. Ohara, M. Azumi, N. Fujisawa, T. Horie, H. Iida, S. Nishio, Y. Seki, Y. Shimomura, M. Sugihara, S. Tanaka, K. Tachikawa, K. Tani, Y. Okumura, K. Shibanuma, S. Matsuda, and FER Team	Proc. of the 15th Symp. on Fusion Technology, Utrecht, The Netherlands, Sep. 19 - 23	1988
7	Study on Negative-Ion-Based Neutral Beam Injection System for JT - 60 Upgrade	M. Matsuoka, H. Kamada, M. Kikuchi, M. Kuriyama, Y. Kusama, H. Ninomiya, Y. Ohara, and S. Yamamoto	Japan Atomic Energy Research Institute Report JAERI - M 89 - 117 [in Japanese].	1989
8	Proposal of Confined Fast Alpha-Particle Measurement Using 2 MeV Li - Beam on JT - 60	Y. Kusama, K. Tobita, Y. Ohara, Y. Okumura, M. Nemoto, H. Kimura, H. Takeuchi, and JT-60 Team	Proc. of the IAEA Technical Committee Meeting on Alpha Particle Confinement and Heating, Kiev, Oct. 23 - 26.	1989
9	Non - Inductive Current Drive In Toroidal System 5. Prospect for Nuclear Fusion Reactor	M. Mori, H. Kimura, and S. Tanaka	Kakuyugo Kenkyu 62 (3) 161 - 176.	1990
10	Design Study of a Beam Energy Recovery System for a Negative - Ion - Based Neutral Beam Injector	M. Araki, Y. Ohara, and Y. Okumura	Fusion Technology 17, 555	1990
11	Beam Profile Controller in Neutral Beam System	S. Tanaka, Y. Ohara, and S. Yamamoto	Submitted to Fusion Technology	1990